Experimental study of a reduced scale model seismically base isolated with Rubber-Layer Roller Bearings (RLRB)

D. Foti
J.M. Kelly

CIMNE Monograph IS-18 1996

Monograph Series in Earthquake Engineering

Edited by A. H. Barbat

Experimental study of a reduced scale model seismically base isolated with Rubber-Layer Roller Bearings (RLRB)

D. Foti
Researcher, Department of Structural Engineering
Technical University of Bari, Italy

J.M. Kelly
Professor, Earthquake Engineering Research Center
University of California at Berkeley, USA

CIMNE Monograph IS-18 1996

INTERNATIONAL CENTER FOR NUMERICAL METHODS IN ENGINEERING
Edificio C1, Campus Norte UPC
C/ Gran Capitán, s/n
08034 Barcelona, España.

MONOGRAPH SERIES IN EARTHQUAKE ENGINEERING
Edited by A.H. Barbat

ISSN: 1134-3249

EXPERIMENTAL STUDY OF A REDUCED SCALE MODEL SEISMICALLY BASE ISOLATED WITH RUBBER-LAYER ROLLER BEARINGS (RLRB)
Monografía CIMNE IS-18

ISBN: 84-87867-82-0
Depósito Legal: B-31009-96

IMPRESO EN ESPAÑA - PRINTED IN SPAIN

acknowledgements

This research was completed when the first author visited the Earthquake Engineering Research Center (EERC) of the University of California at Berkeley as Visiting Scholar from March 1993 to October 1993 with financial support from the National Reasearch Council (CNR) of Italy. The collaborative research effort was made possible through the organization and facilities of the Earthquake Engineering Research Center and of the Department of Civil Engineering of the University of California at Berkeley. authors very much appreciate the support and cooperation of EERC, CNR and the Department of Civil Engineering of the University of California at Berkeley.

The authors are also grateful to the Malaysian Rubber Producers' Reasearch Association for furnishing the rubber for the isolation device and, in particular, to Professor A. G. Thomas as the inventor of the concept of isolation with rubber and rollers.

INDEX

CHAPTER 1

INTRODUCTION

1.1 INTRODUCTION

Seismic events sometimes have devastating effects on structures due to the emmission of energy from the ground to the structures. The acceleration transmitted to the upper stories by the earthquake motion depends on the input accelerations, the stiffness of the structure and the dynamic response characteristics of the structure itself.

The traditional design approach for the fixed base building is to retain the structure response in the elastic range for a moderate eathquake and to make it sufficiently safe when the earthquake energy is very strong. In this approach the superstructure is coupled to the ground movement so that the damaging horizontal components of the earthquake are transmitted into the building.

In this view passive control methods of vibrations are rapidly gaining acceptance in aseismic design. The aim is to reduce the energy input in the superstructure through devices which minimize the damage and prevent the collapse of the whole system. Base isolation is one of the methods used to reduce the seismic vibrations of the structures.

This strategy is based on the concept that a structure can be partially protected from seismic vibrations by uncoupling it from the ground. Seismic effects are mitigated both improving the capacity of a structure to absorb energy and shifting the system natural frequencies towards values far from the range of maximum response accelerations. In this way the effect of the seismic load is reduced.

To obtain the shifting of the system natural frequencies implies a realization of a very

low horizontal stiffness isolation system. Unfortunately this effect is accompanied by a sensible increment of the relative displacements between the superstructure and the ground. This problem can be overcome increasing the isolator capacity to absorb seismic energy. In this way the structural displacements are lower because the energy quantity transmitted to the superstructure is lower.

The input energy is kept low not only by an absorbing capacity to dissipate energy with a non-linear behaviour which is activated also at low frequencies.

Usually base isolation is applied to every kind of structure realised in the field of civil engineering: tall buildings, bridges, thin towers and any other system subjected to dynamic forces. The benefits of this design approach can also be applied to the protection of equipment and machines. The desired result of this design is to require that certain sensitive equipment and machines could remain functional after an earthquake of a certain magnitude.

The main purpose of the research reported here is to investigate the behaviour of Rubber-Layer Roller Bearings (RLRB) used to base isolate a low-rise structure during horizontal ground motions. The isolation system consists of high damping natural rubber pads and steel balls. In order to study the behaviour of this kind of base isolation device, a theoretical approach of the problem has been conducted, followed and completed by a series of experimental shaking table tests performed on a scaled model of the entire structure.

REFERENCES

[1] J.M. Kelly, "Aseismic Base Isolation: Review and Bibliography", *Soil Dynamics and Earthquake Engineering*, Vol.5, N.3, 1986, pp. 202-216.

[2] I.G. Buckle, R.L. Mayes, "Seismic Isolation: History, Application and Performance - A World View", *Earthquake Spectra*, Vol. 6, N. 2, 1990, pp. 161-201.

[3] J.M. Kelly, "Base Isolation: Linear Theory and Design", *Earthquake Spectra*, Vol. 6, N. 2, 1990, pp. 223-244.

CHAPTER 2

THE ISOLATION SYSTEM

2.1 THE ISOLATION SYSTEM

The devices utilized to base isolate the superstructue were rubber-layer roller bearings (RLRB). Each of them consists of two 6"x12"x0.08" high damping natural rubber pads and 28 steel balls devided in 4 rows. The balls roll between the two rubber pads, as shown in Figures 1a, 1b.

The idea was originally proposed by research at the Malaysian Rubber Producers' Research Association (MRPRA) who also supplied the rubber pads used for the isolation system for the test program.

The 1" diameter steel balls were furnished by SKF Industries.

These devices uncouple the ground motion when the rollers start to move, exceeding the rolling friction between rubber and steel.

Based on the same concept, a similar isolation device was previously analysed. It consists of steel balls rolling on steel surfaces. These devices were utilized to base isolate the same frame tested in the present experimental study.

Shaking table tests were performed, but the results were not as satisfactory as in the case of RLRB isolation system. In fact the damping properties and dissipation capacities of the rubber considerably contribute in mitigating the response of the whole system to ground vibrations.

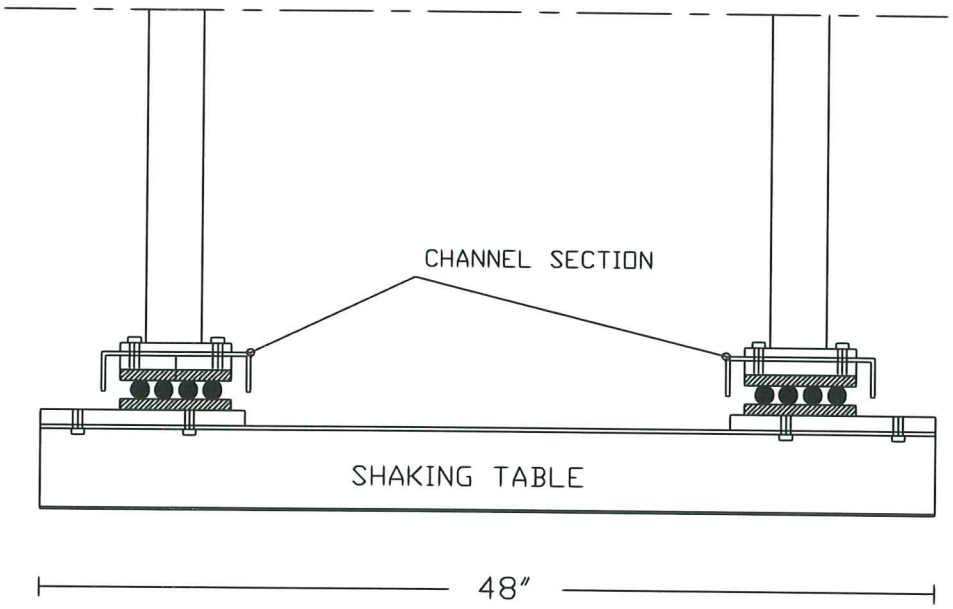

Fig. 1a. Longitudinal section of the isolation system.

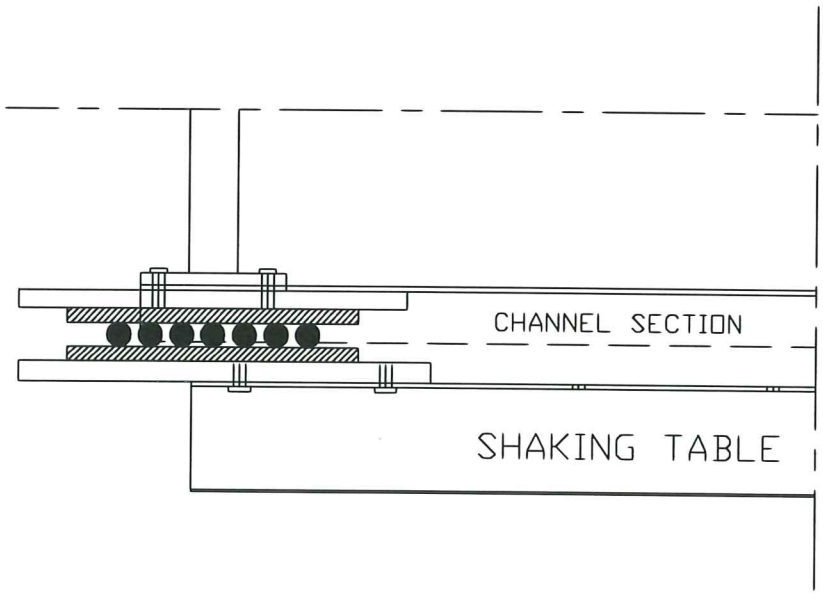

Fig. 1b. Transversal section of the isolation system.

CHAPTER 3

THEORETICAL ANALYSIS

3.1 THEORETICAL ANALYSIS

A rigid cylinder rolling on the surface of a viscoelastic material was assumed as a simplified theoretical model for an RLRB isolation system. As shown in Figure 2, 'a' and 'b' are the two portions of the contact area respect to the centre of the cylinder, Q is the vertical load, F is the horizontal force under which the cylinder is moving on the rubber with a stationary velocity V.

For a viscoelastic material, the pressure distribution under the contact area is not symmetric as in the case of an elastic material. The eccentricity of the resultant of the pressure generates a moment which opposes to the rolling of the cylinder.

The solution is determined assuming a Kelvin-type model for the viscoelastic medium and neglecting the inertial forces.

In this assumption, the pressure under the contact area between the cylinder and the layer is

$$q = Kv + K\tau\dot{v} \qquad (1)$$

where K is the stiffness of the material, τ is a constant of the material, v is the displacement in the rubber.

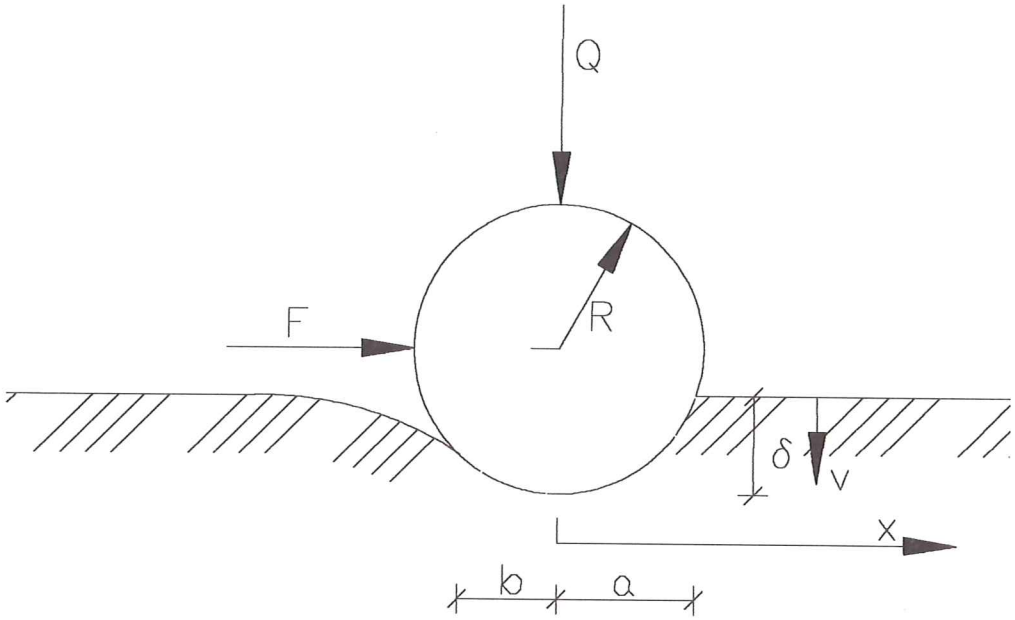

Fig. 2. Simplyfied model of a cylinder rolling on a rubber layer.

The model assumed for the rubber layer is a spring and a dashpot connected in parallel. The local spring takes into account the elastic effects and the local dashpot models the viscous behaviour. In this model the reaction that occurs in a point subjected to the local conditions v=0, $\dot{v}\neq 0$, is due to the viscous properties of the medium. In other words v=0 can give a pressure different from zero, if the local velocity is not zero.

The expression for v is derived from the deformed configuration of the rubber corresponding to the contact area of the rolling cylinder. At a certain instant v has the following law:

$$v(x) = \phi - x^2/2R \qquad (2)$$

where δ is the maximum vertical displacement of the deformed rubber under the cylinder, R is the radius of the cylinder, x is the coordinate position of the points on the deformed surface measured from the contact point at the maximum displacement of the rubber.

Substituting (2) in equation (1), the pressure results:

$$q(x) = K(\delta - x^2/2R) - K\tau Vx/R \qquad -b \leq 0 \leq a \qquad (3)$$

$$a \leq 0 \qquad b \leq 0$$

For an elastic material the expression for the pressure is:

$$q(x) = Kv = K(\delta - x^2/2R), \qquad 0 \le x \le a \tag{4}$$

It is evident that the symmetry associated with this problem is destroyed by the introduction of viscoelastic effects.

From the boundary conditions:

$$x=-b \qquad q(-b)=0,$$
$$x=a \qquad q(a)=0,$$

$$Q=\int_{-b}^{a} q(x)dx\,, \tag{5}$$

it is possible to obtain the following expressions for the total pressure Q and the moment M:

$$Q = K\left[\frac{a^3}{3R}+\frac{a^4}{4Rb}+\frac{b^3}{12R}\right] \tag{6}$$

$$M=K\left[\frac{a^4}{8R}+\frac{a^5}{6Rb}-\frac{a^2b^2}{12R}-\frac{a^3b}{6R}-\frac{b^4}{24R}\right] \tag{7}$$

M is the moment of the horizontal force respect to the contact point at the maximum displacement of the rubber: M=FR.

It is interesting to investigate the results in terms of the following dimensionless quantities:

$$\Gamma_1 = \tau V/R\,, \quad \Gamma_2 = 12\ Q/KR^2\,, \quad \Gamma_3 = 24\ M/KR^3$$

The diagram (Γ_1 , Γ_3) shows the relation between the rolling velocity V and the horizontal force F applied to the steel roller, as shown in Figure 3a. The curve is determined for a vertical load Q=50 Pounds. This is the maximum admissible load for each ball utilized in the experimental analysis. It presents a very steep behaviour in the first part starting from zero up to a maximum value of the force F. Beyond this value, the curve gradually decreases. In fact the horizontal applied force is a maximum for a certain value of the velocity V. For higher values of the velocity, the horizontal force necessary to mantain this velocity is lower. In fact the moment arising from the asymmetric distribution of the pressure becomes smaller as the velocity increases.

This behaviour is also shown in the diagrams of the pressure distribution in Figure 4: the distance of the centre of gravity of the area under each pressure distribution curve from the centre of the cylinder increases up to a certain value of Γ_1 and then decreases for higher values of Γ_1 . In fact, for a viscoelastic material, contrary to the elastic behaviour, the resultant pressure is no longer directed through the center of gravity of the cylinder. For this reason a resisting moment M should be opposed by a horizontal force F to mantain the cylinder rolling at the same constant speed.

Figure 3b shows the diagrams (Γ_1 , Γ_3) for different values of Γ_2 , which depends on Q.

The diagrams (Γ_2 , Γ_3) in Figure 5 show the relation between Q and F when the velocity V is fixed at different values. It is important to notice that each curve presents a local slope which is almost constant. This is the typical behaviour of a friction system: when the load Q increases, the force F increases with an almost linear behaviour.

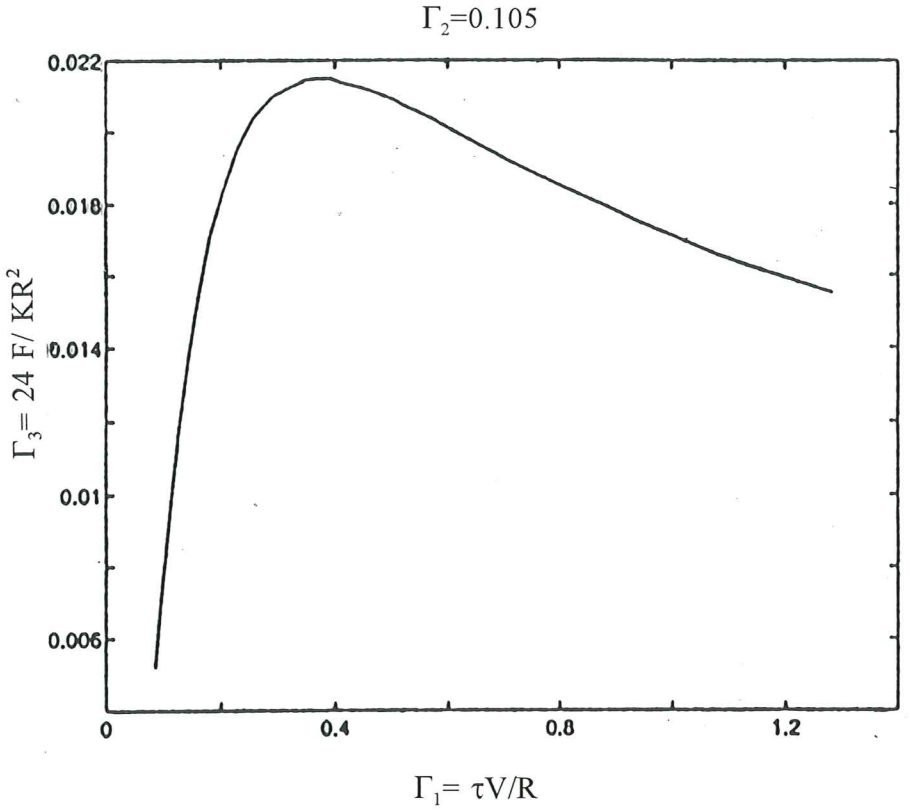

Fig. 3a. Dimensionless velocity V-Force F diagram for a fixed vertical load Q=50 pounds.

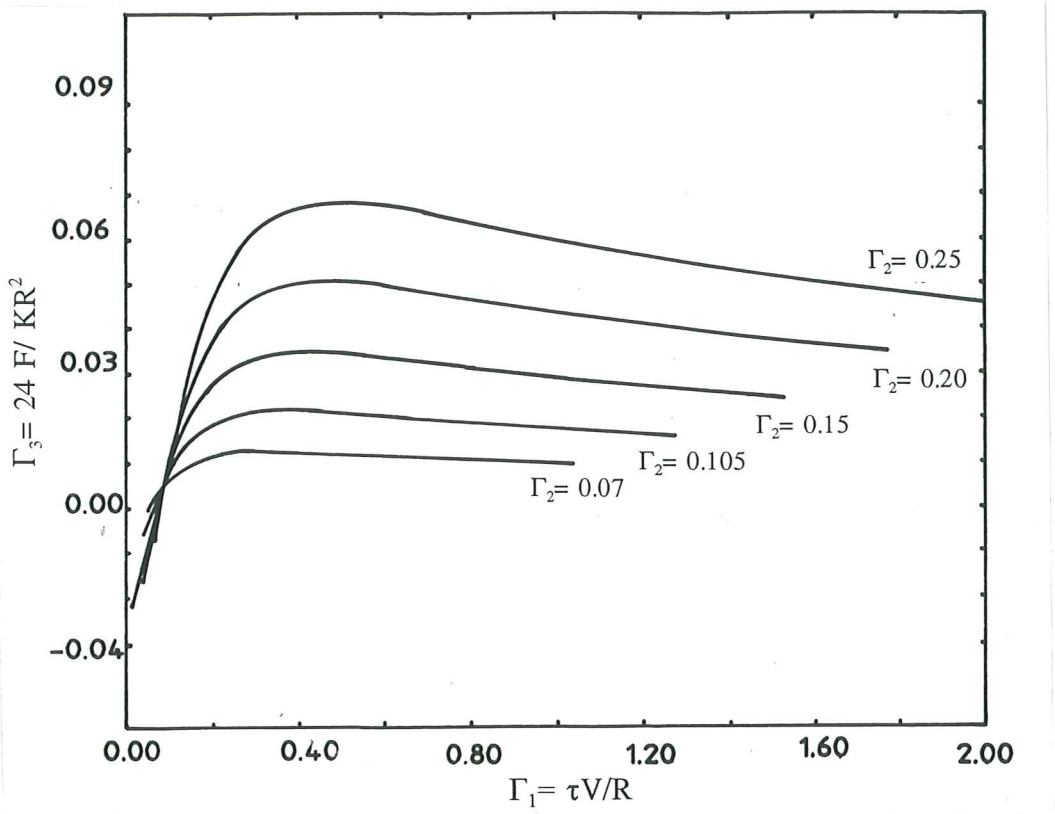

Fg. 3b. Dimensionless velocity V-Force F diagrams for different values of the vertical load Q.

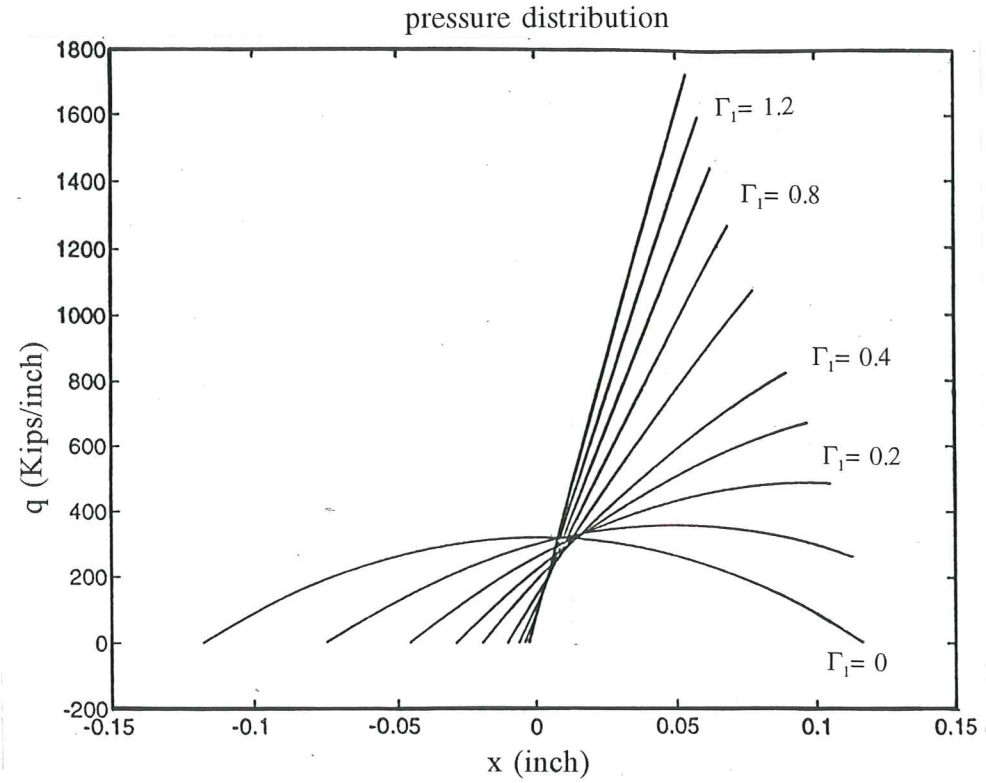

Fig. 4. Pressure distribution under a vertical load Q=50 pounds, for different values of Γ_1.

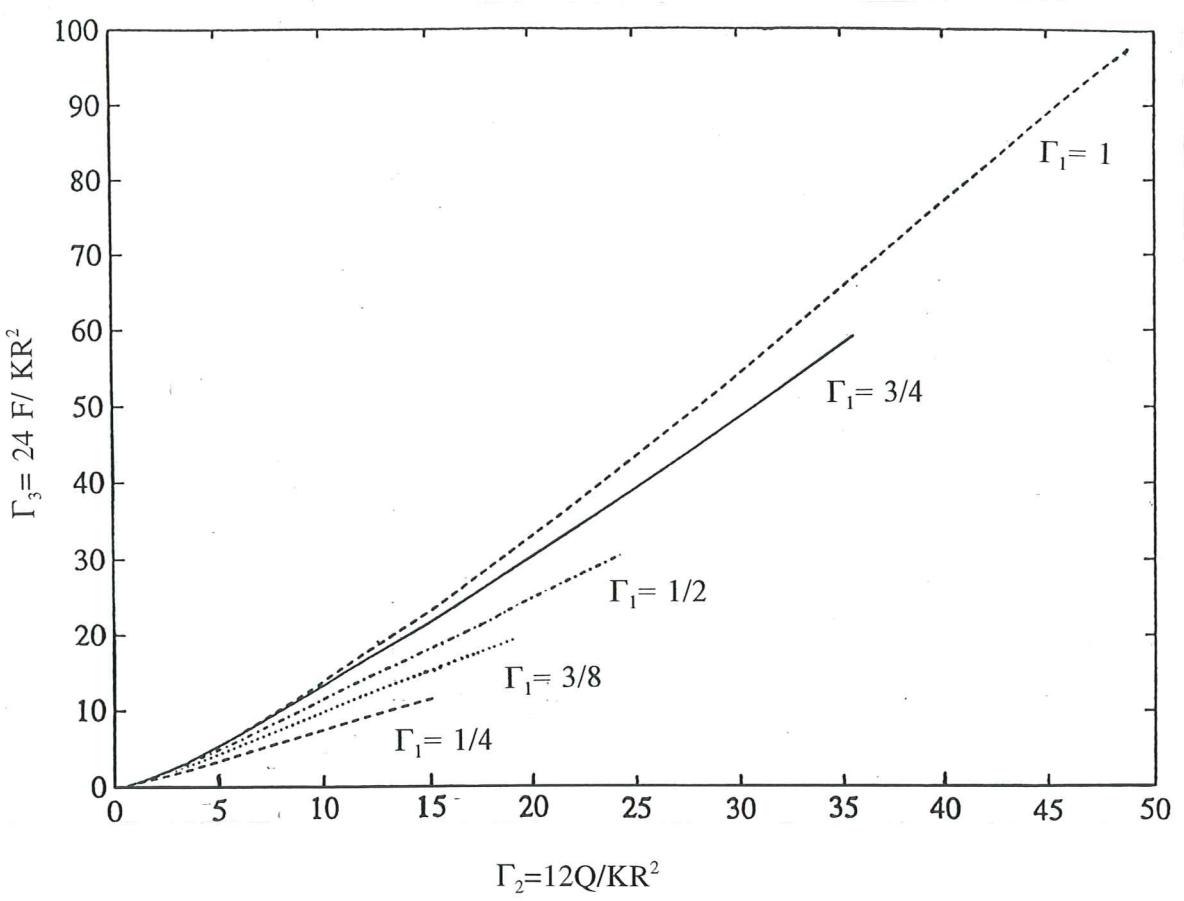

Fig. 5. Dimensionless vertical load Q-Force F diagram for different values of the velocity V.

REFERENCES

[1] S.C. Hunter, "The Hertz Problem for a Rigid Spherical Indenter and a Viscoelastic Half-Space", Journal of Mech. Phy. Solids, 1960, Vol. 8, pp. 219-234.

[2] J.A. Greenwood, H. Minshall, D. Tabor, "Hysteresis Losses in Rolling and Sliding Friction", Proceedings of the Royal Society, 1960, Vol. 259 A, pp. 480-507.

[3] S.C. Hunter, "The Rolling Contact of a Rigid Cylinder with a Viscoelastic Half Space", ASME Journal of Applied Mechanics, 1961, Vol. 28, N. 4, pp. 611-617.

[4] I.G. Goriacheva, "Contact Problem of Rolling of a Viscoelastic Cylinder on a Base of the Same Material", PMM, Vol. 37, 1973, N. 5, pp. 925-933.

[5] J.M. Golden, "The Problem of a Rigid Punch Sliding on an Elastic or a Viscoelastic Layer", Acta Mechanica, 1982, Vol. 43, pp. 201-221.

[6] J.A. Greenwood, D. Tabor, "The Friction of Hard Sliders on Lubricated Rubber: The Importance of Deformation Losses", Proceeding of Phisics Society, 1958, Vol. 71, pp. 989-1001.

[7] W. Flugge, "Viscoelasticity", Springer-Verlag, New York-Heidelberg-Berlin, 1975.

[8] C. Bapat, R. C. Batra, "Identation of a Viscoelastic Rubber Covered by a Rigid Plane Surface", Mechanics Research Communications, 1982, Vol. 9, N. 4, pp. 265-278.

[9] G. Wang, K. Knothe, "The Influence of Inertial Forces on Steady-State Rolling Contact", Acta Mechanica, 1988, Vol. 79, pp. 221-232.

CHAPTER 4

THE EXPERIMENTAL MODEL

4.1 BASE ISOLATED MODEL

Shaking table tests were carried out on a four-storey one-bay welded steel model, (Fig. 6). The base isolation system consisted of four RLRB with an RLRB located under each column of the model structure. The model was placed on a shaking table which produced unidirectional motion.

A series of system identification tests and simulated earthquake motions were performed. The results of these experiments were compared with those obtained from tests on the same model with fixed base.

All tests were conducted in the Laboratory of the Department of Civil Engineering, Davis Hall, University of California at Berkeley.

4.2 THE SUPERSTRUCTURE

The superstructure was a steel-welded four storey moment-resisting frame, 3ft x 4ft in plan and 6ft high with story heights of 2ft.

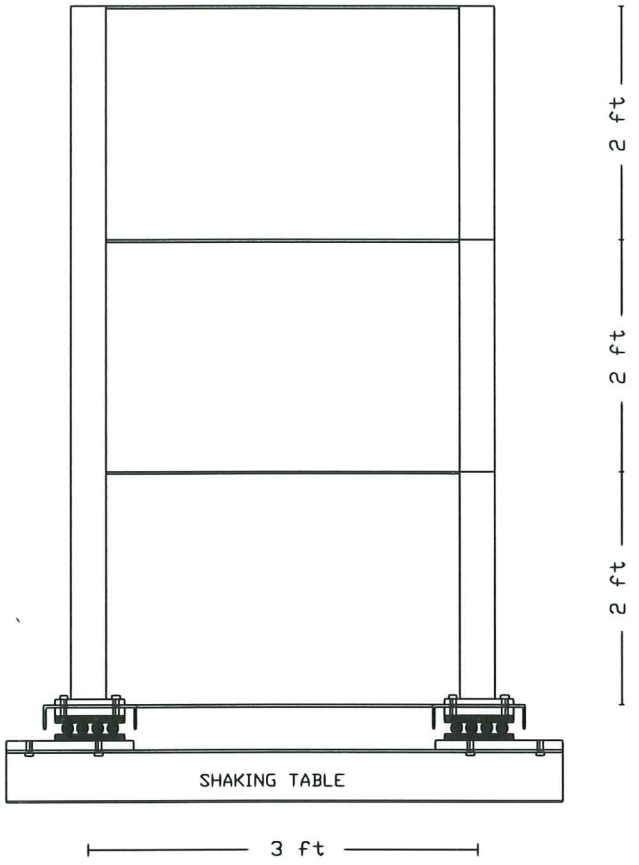

Fig. 6. The base isolated model

The floors were 1/2" steel plates and the columns continuous angles. There were base plates at the foot of each column. Each couple of base plates was bolted to the channels of the base which we will refer to as basement of the structure.

Approximately one thousand pounds of lead weight were added to the four floors. The weights were composed of one hundred pound lead billets. The billets were ganged together into groups of five with steel straps and rods. Then two gangs were bolted to each floor of the model. The gangs of lead added some stiffness to the structure positively influencing the flexure of the floor plates when subjected to lateral load.

A further series of tests were also performed for the base isolated model with smaller values of the added weight.

A special restraint was located between the model and the shaking table, to keep the steel balls and the frame in place.

4.3 ELASTOMERIC PADS

The elastomeric pads used in the RLRB isolation system were constitued by a 0.08" thick rubber layer vulcanized to a steel plate, (Figure 7). The rubber is basically the soft high damping natural rubber (HDNR) MRPRA formulation. It was bonded to steel plates via the Henkel 205 primer and 220 top coat chemlok system . The dimensions of each steel plate were 6"x15"x0.2".

The characteristics of this compound and of the test machine are shown in Table T-1. These results are derived from test pieces cured at 110°C whereas the plates were cured at 140°C. The higher cure temperature leads to the compound being slightly softer and looser.

Fig. 7. A scheme of the elastomeric pad.

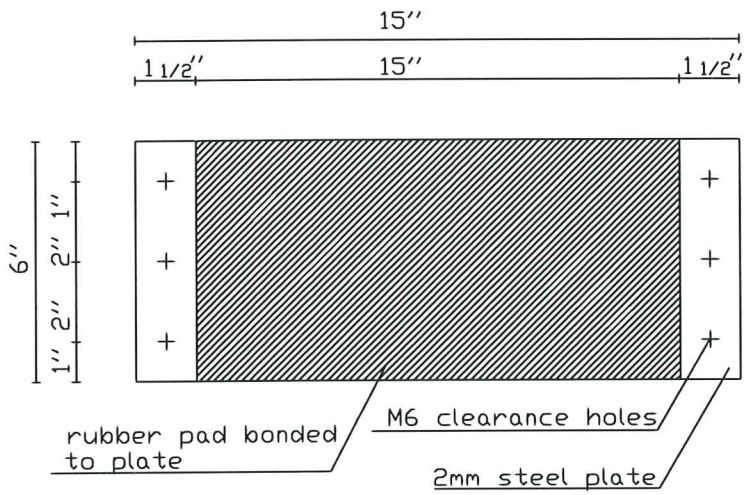

Rubber: 22-15-009-06	Moduling Date: July - 93
Metal: B61	
Rubber Diameter(mm): 25-3	Rubber Thickness (mm): 5-87
Cure time and temperature:	300 at 110°C
Test Date: 1 July 1993	Tested by: Jhon Cook
Test Machine: DARTEC	
Load Range: 5KN	Displ. Range: 25mm
Frequency: 0.5 Hz	Temperature: 23°C
Measuring Conditions:	Dynamic 6th Cycle

Table T-1. Characteristics of the rubber.

Strain %	Comments	Shear Modulus [MPa]	Loss Angle	tan Loss Angle
1	FIRST RUN (SAMPLE UNWORKED)	1.99	12.34	0.2188
2		1.60	13.91	0.2476
5		1.11	14.54	0.2593
10		0.87	13.17	0.2340
20		0.68	11.41	0.2018
50		0.50	9.34	0.1644
100		0.41	8.19	0.1439
150		0.38	7.42	0.1303
200		0.38	6.87	0.1204

Table T-2a. Dynamic shear properties of the rubber. First run.

Strain %	Comments	Shear Modulus [MPa]	Loss Angle	tan Loss Angle
1	SECOND RUN (SAMPLE WORKED)	1.26	12.49	0.2215
2		1.07	14.37	0.2562
5		0.80	14.63	0.2611
10		0.68	13.56	0.2411
20		0.57	11.83	0.2094
50		0.45	9.73	0.1715
100		0.37	8.59	0.1510
150		0.34	7.75	0.1361
200		0.37	6.79	0.1191

Table T-2b. Dynamic shear properties of the rubber. Second run.

4.4 RESTORING SPRINGS

Four steel springs were utilized to provide a restoring force for the position of the frame during the shaking tests . These springs were disposed parallel to the table movement in number of two on each side. They have a length of 16 3/8" and they were installed with an elongation of 4" each to avoid compression during the shaking tests where a maximum displacement of the table of 2" was assumed. Their stiffnesses were measured from empirical load-displacement tests using a Universal Testing Machine in the Material Testing Laboratory of the Department of Civil Engineering, University of California at Berkeley.

The results are shown in the F-δ diagrams in Figure 8. For each value of the load it was possible to measure the elongation of the spring. The stiffness of each spring was quite high at first due to settlement phenomena. In the following stages, the stiffness was almost constant around a value of 27 Pounds/inch.

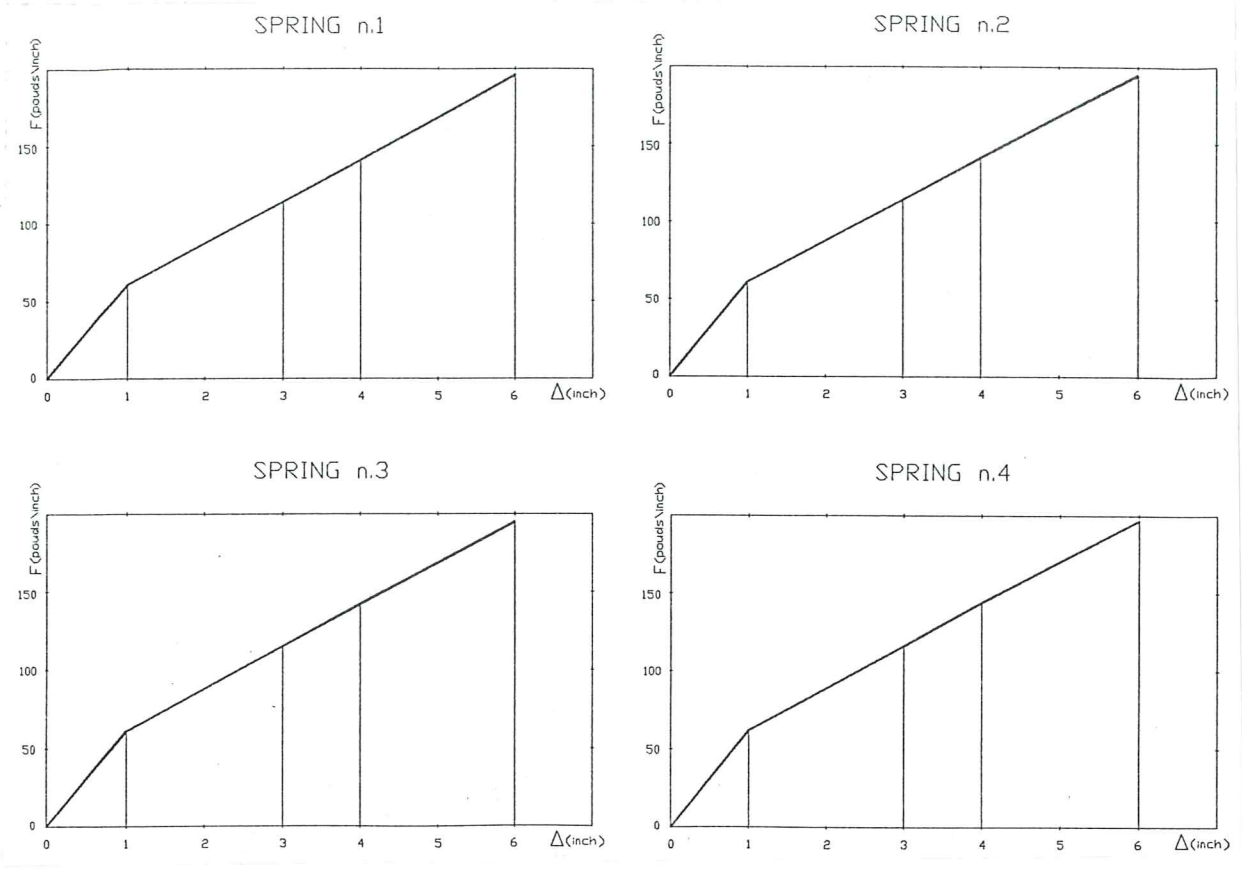

Fig. 8. Stiffnesses of the springs. Experimental F-δ diagrams.

REFERENCES

[1] I. Aiken, J:M: Kelly, "Earthquake Simulator Testing and Analytical Studies of Two Energy-Absorbing Systems for Multistory Structures"; *Report N. UCB/EERC-90/03, Earthquake Engineering Research Center*, University of California atBerkeley, October 1990.

CHAPTER 5

TEST FACILITIES

5.1 SHAKING TABLE

The present tests were conducted at the Structural Dynamics Laboratory of the Department of Civil Engineering, Davis Hall, Univeristy of California at Berkeley.

The main facility utilized is a small shaking table with a 4'8" by 4' testbed. It was constructed of stiffened 3/8 inch steel plates and weighted approximately 500 lb

The table was supported by four tapered roller bearings which slide on steel bars. The table had one horizontal degree of freedom and was driven by a single horizontal actuator. The capacity of the table was 10 kips with a total allowable displacement of 6" and a peak acceleration greater than 1G.

5.2 INPUT SIGNALS

The signals used can be devided in external and internal signals. The external ones are harmonic and white noise input signals. The internal signals are sweep frequencies and earthquake inputs. The last ones are derived from previously recorded earthquakes available at U.C. Berkeley, stored as digitized accelerations.

Since the table is displacements controlled, these accelerations are double integrated and converted from digital to analog before being applied to the table actuators through the

MTS 406 table controller.

Some work has previously been done to adapte these signals for the shaking table tests starting with an increasing motion up to the significative values for the signals and ending with a decreasing motion up to zero.

5.3 DATA ACQUISITION SYSTEM AND ANALYSIS

The data acquisition and control system consisted of a Metabyte DAS 1601 card installed in a 50 Mhz 486 PC running under the QNX operating system. The Autonet software system was programmed to collect the experimental data, convert the readings into appropriate engineering units, and send the displacement command signal to a servo-hydraulic actuator connected to the shaking table.

All data was saved in binary (Autonet LDF) format. The experimental data were converted from binary to text (ASCII) format and transferred to a DOS-based 486 PC. The S-plus command language was used to process the recorded information.

A script was prepared to read all measurements from the text file, remove the initial offset, and generate plots of acceleration and displacement responses in the time and frequency domains.

5.4 ACTUATOR

A servo-hydraulic actuator was installed to control the displacements of the table. It was connected to the shaking table.

The actuator was driven by a 25 GPM electro-hydraulic servovalve. The pressure applied to the servo-hydraulic actuator was 3000 psi.

5.5 INSTRUMENTATION

Accelerometers and displacement transducers were attached to each floor and to the base for data acquisition and for state determination. The displacement at each level of the superstructure were measured by temposonic linear displacement transducers.

For measuring the accelerations, Statham Strain Gage Type accelerometers were utilized and placed at each level of the superstructure.

The reference frame was fixed to the base of the shaking table.

CHAPTER 6

PRELIMINARY TESTS

6.1 GENERAL

A set of quasi-static experiments were carried out by "The Malaysian Rubber Producers' Research Association" in the Tun Abdul Razak Laboratory. These preliminary tests were performed using a biaxial testing frame.

All tests were carried out on the same set-up using a 0.08" thick pads with 16 (nominal 1 inch) balls in each pad set in a 4x4 array.
Figure 13 shows a schematic model of the experimental set-up.

6.2 TEST SEQUENCE

The preliminary tests consist of three series of tests named as Exp.1, Exp.2 and Exp.3.

The three sets of tests carried out one after the other without any changes to the setup; i.e. Exp. 1A was carried out on virgin pads whilst Exp.2 and Exp.3 were following ones.

The test sequence is as follows:
Exp.1: harmonic input test with a sinewave of 0.1 Hz frequency and ±50mm amplitude;
Exp.2: harmonic input test with a sinewave of 0.5 Hz frequency and ±50mm amplitude;
Exp.3: harmonic input test with a sinewave of 0.1 Hz frequency and ±100mm amplitude.

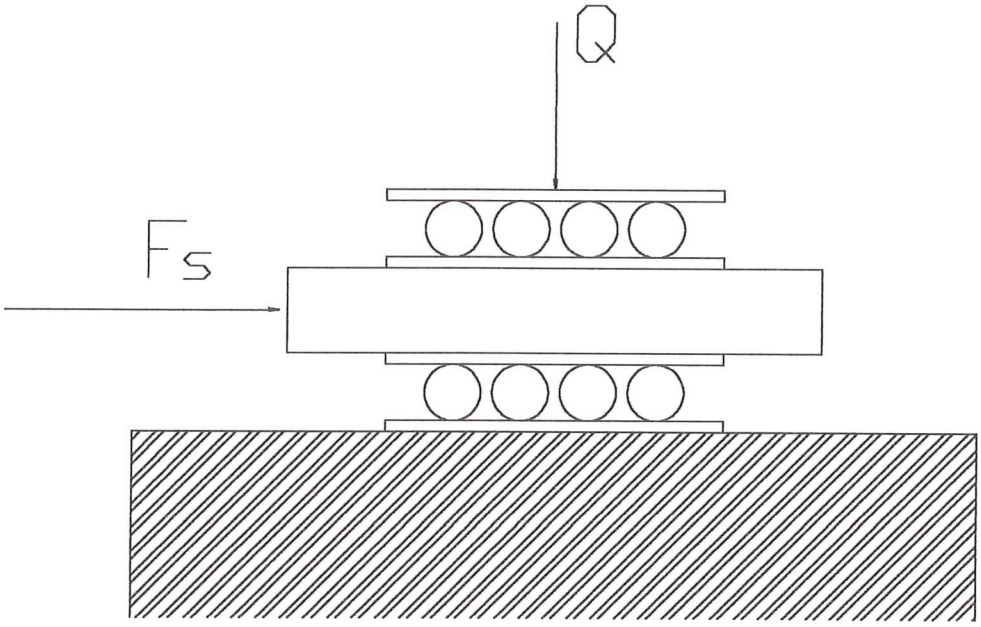

Fig. 9. Experimental set-up for the preliminary tests.

6.3 TEST RESULTS

The results of these preliminary tests can be deducted from the diagrams in figures 10, 11, 12. They show:

Exp. 1

A) Ramp to -50mm;
B) 2nd loop of 5 loops - sinewave of 0.1 Hz ± 50mm;
C) 4th loop of 5 loops - sinewave of 0.1 Hz ± 50mm.

Exp. 2

A) Ramp to -50mm;
B) 2nd loop of 5 loops - sinewave of 0.5 Hz ± 50mm;
C) 4th loop of 5 loops - sinewave of 0.5 Hz ± 50mm.

Exp. 3

A) Ramp to -100mm;
B) 2nd loop of 5 loops - sinewave of 0.1 Hz ± 100mm;
C) 4th loop of 5 loops - sinewave of 0.1 Hz ± 100mm.

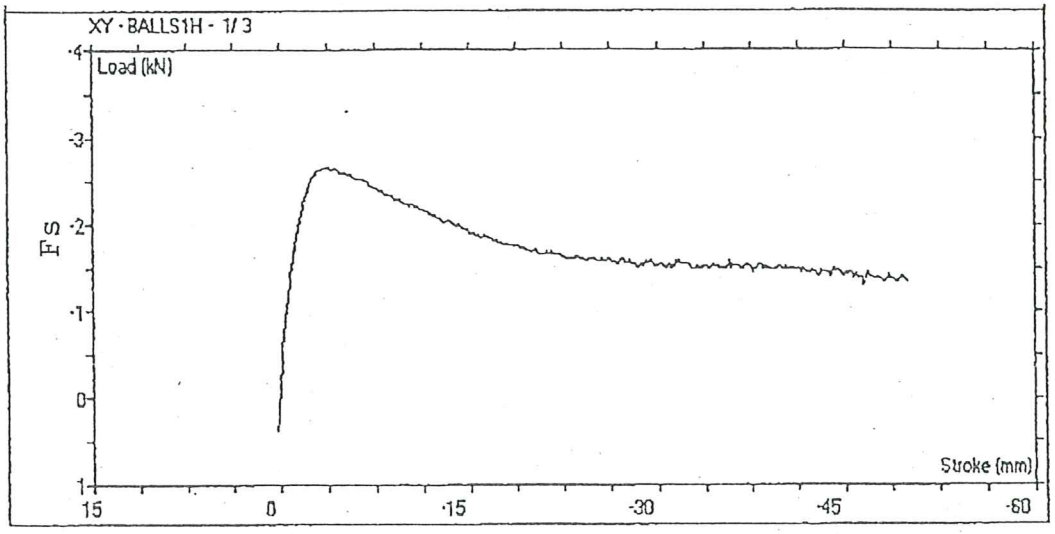

Fig. 10a. Exp. 1. Ramp to -50mm.

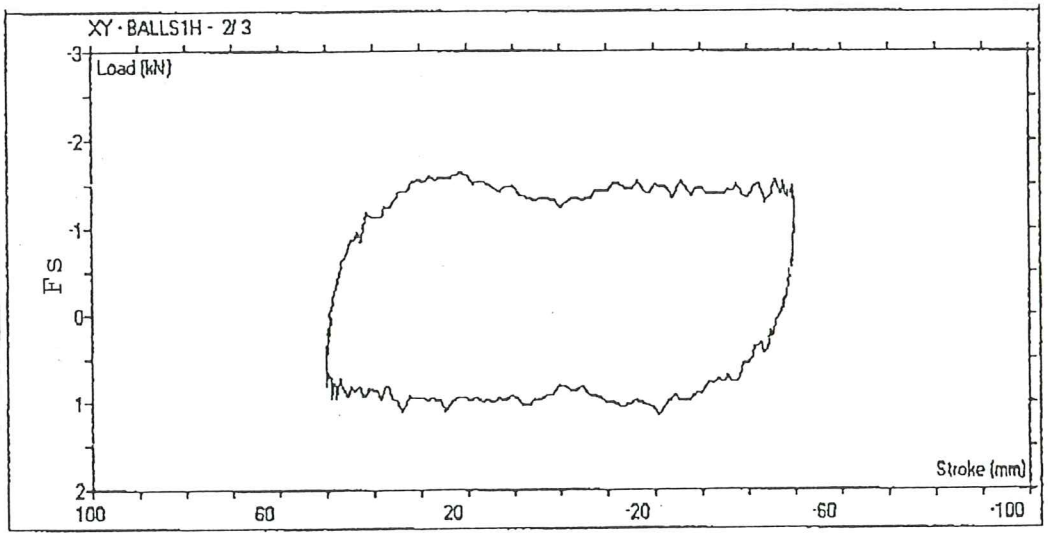

Fig. 10b. Exp.1. 2nd loop of 5 loops - sinewave of 0.1 Hz ± 50mm.

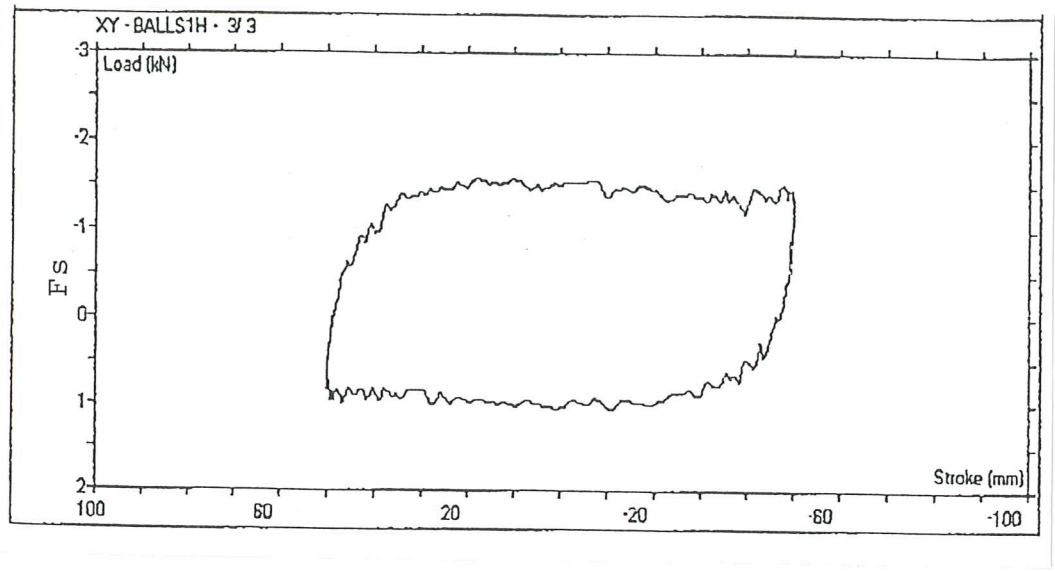

Fig. 10c. Exp.1. 4th loop of 5 loops - sinewave of 0.1 Hz ± 50mm.

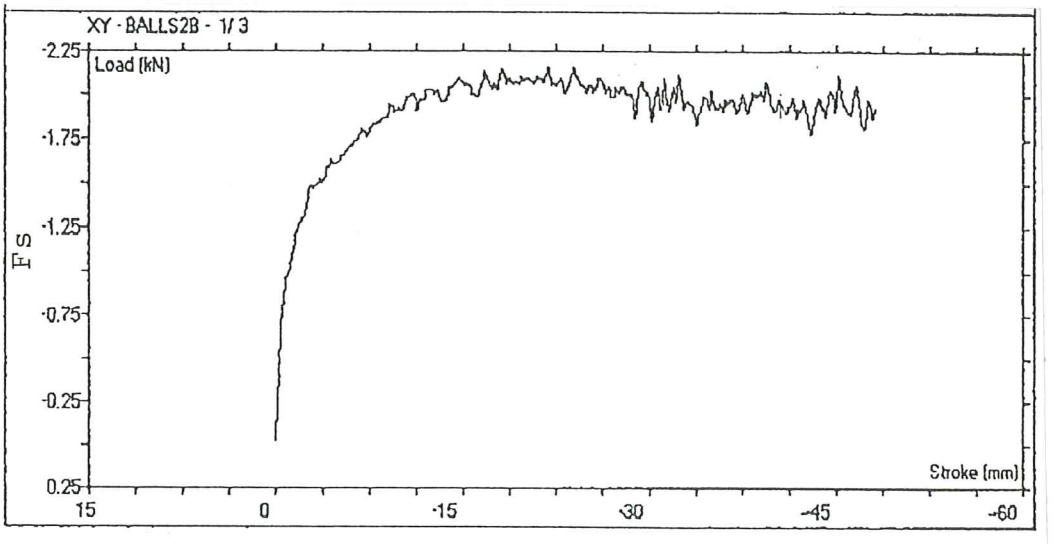

Fig. 11a. Exp. 1. Ramp to -50mm.

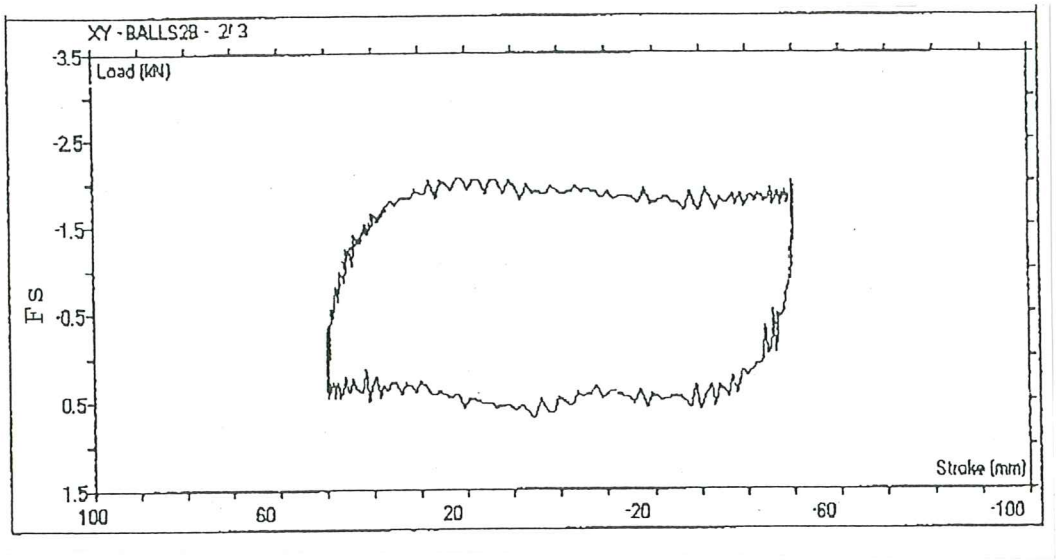

Fig. 11b. Exp.1. 2nd loop of 5 loops - sinewave of 0.5 Hz ± 50mm.

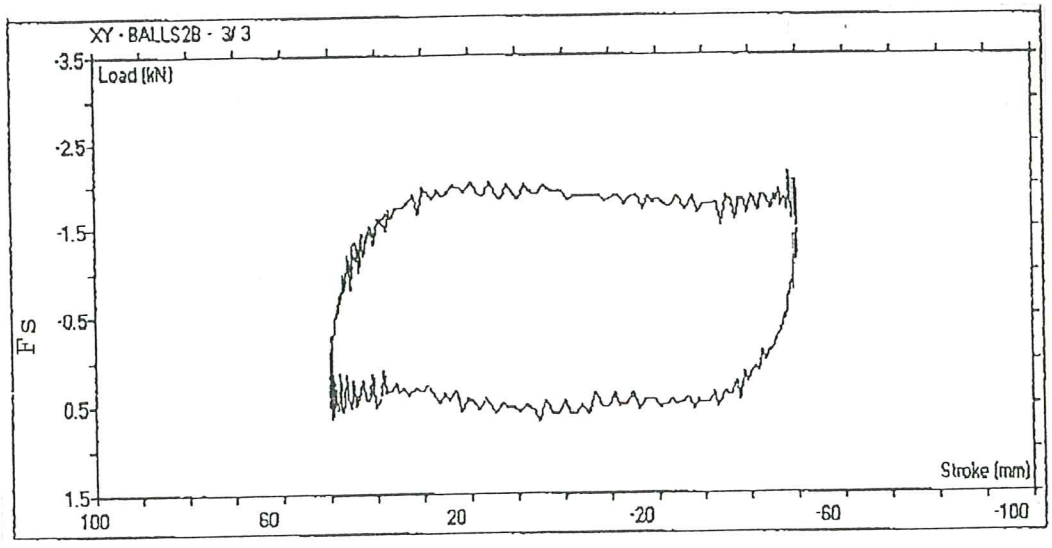

Fig. 11c. Exp.1. 4th loop of 5 loops - sinewave of 0.5 Hz ± 50mm.

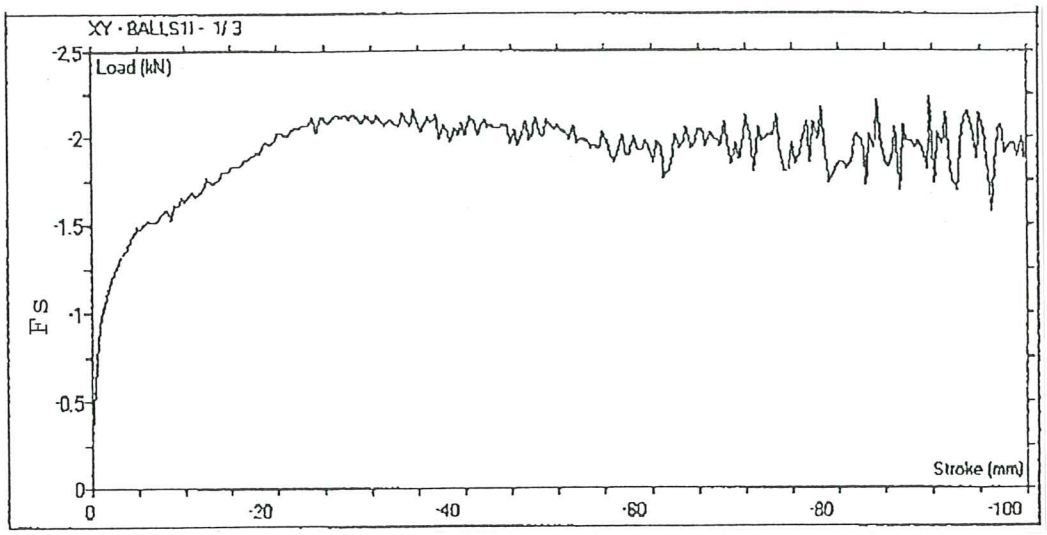

Fig. 12a. Exp. 1. Ramp to -100mm.

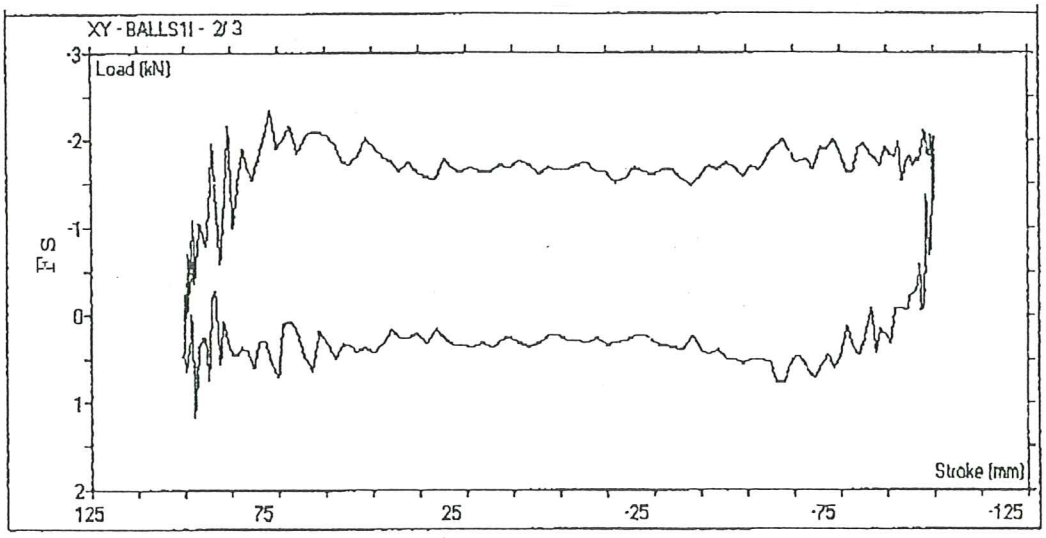

Fig. 12b. Exp.1. 2nd loop of 5 loops - sinewave of 0.1 Hz ± 100mm.

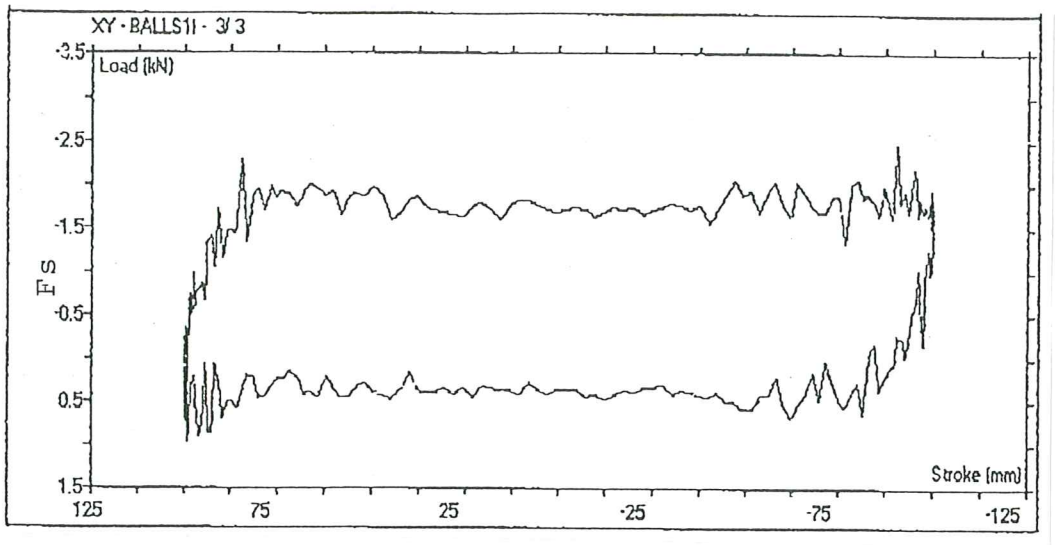

Fig. 12c. Exp.1. 4th loop of 5 loops - sinewave of 0.1 Hz ± 100mm.

From test A) in Figure 10a, the force-displacement law for Exp.1 is performed in a quasi-static way and the behaviour is assimilable to a bilinear one. It is possible to notice a slight softening for values of the displacement higher than the one corresponding to the maximum force. This behaviour shows a decrease of the horizontal force soon after the rolling phase.

In Figures 10b and 10c it is possible to notice that the system presents a typical hysteretic behaviour. The upper and lower limits are almost horizontal. Moreover there are no degradation phenomena in the loops following the first ones.

Figures 11 and 12 show the results of Exp. 2 and Exp. 3 preliminary tests. Exp.2 and Exp.3 present the same results as in Exp.1 and the hysteresis loops are almost rectangular with a high energy dissipation.

From all these considerations an extremely simplified model to assume for the system is the elastic-friction model.

CHAPTER 7

DYNAMIC TEST PROGRAM

7.1 THE TEST PROGRAM

The test program for the model structure consisted of harmonic base input tests, sweep frequency input tests, white noise input tests, and earthquake input tests. The first three types of tests were performed to determine the dynamic characteristics of the model and to evaluate the effectiveness of existing analytical methods for predicting these quantities.

The earthquake input tests consisted of three simulated ground motions. The types of earthquake varied from those with predominantly high frequency content to those with mainly low frequency content.

1) El Centro, 1940, S00W component;
2) Parkfield, 1966, N65 component;
3) Dumbarton, 1989, 267 Degrees.

Only the strong part of the motion of each earthquake was used and the amplitude of the motion was scaled such that the maximum relative displacement at the isolator level was less than 1.5".

Figures 13a, 13b, 13c show the Fourier spectra of the signals. These diagrams represent the Fourier spectra of the ground displacements of the three input earthquakes utilized in the test program.

EL CENTRO

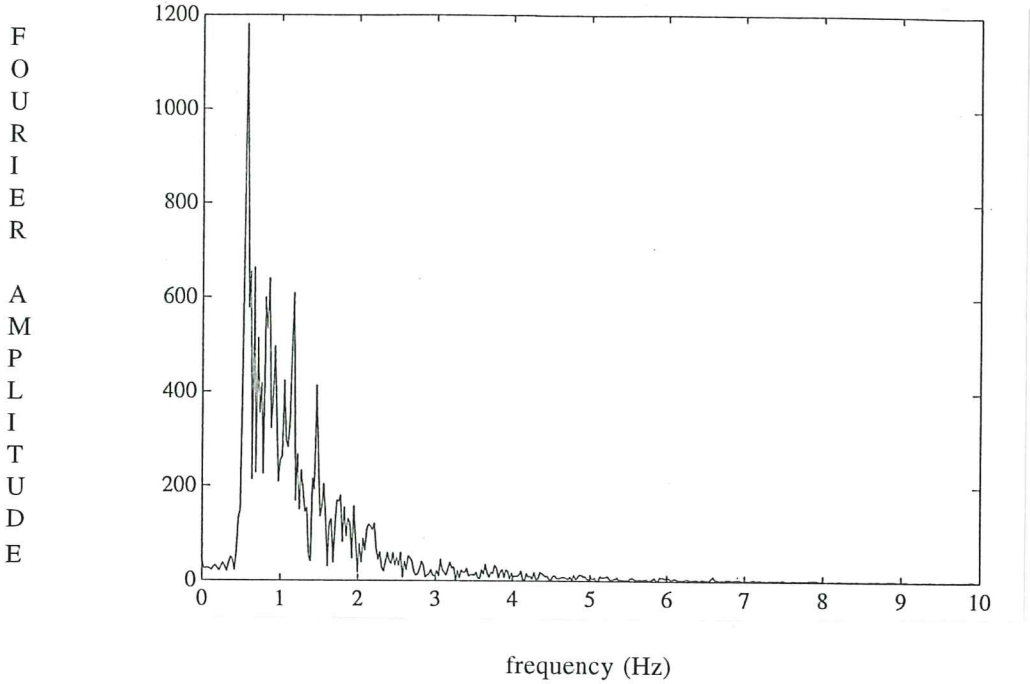

Fig. 13a. Fourier spectra. El Centro 1940, S00W component.

DUMBARTON

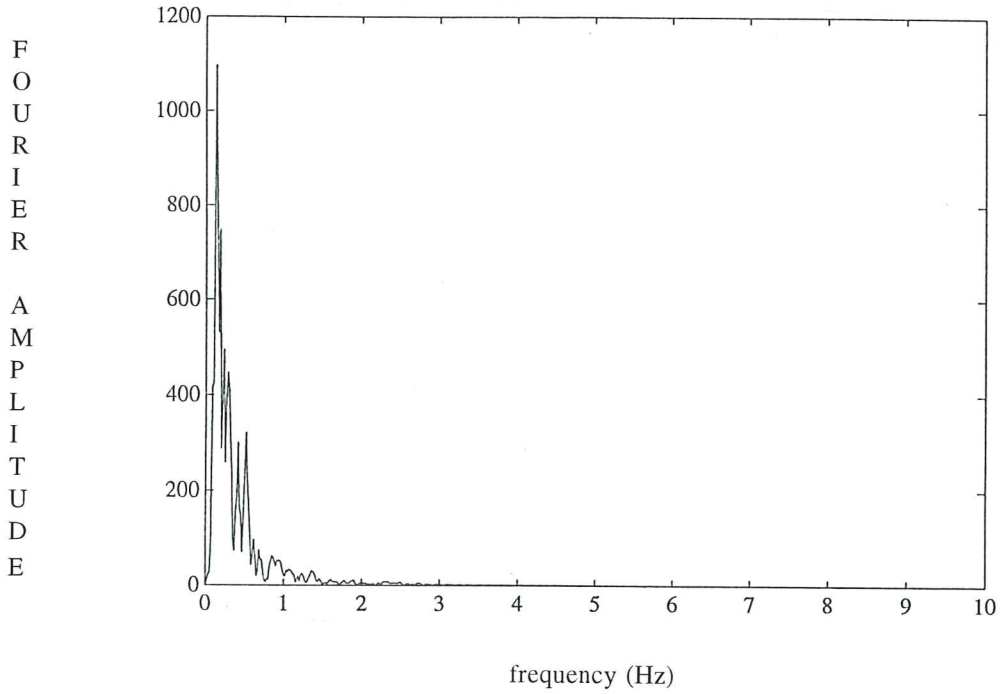

Fig. 13b. Fourier spectra. Dumbarton 1989, 267 Degrees.

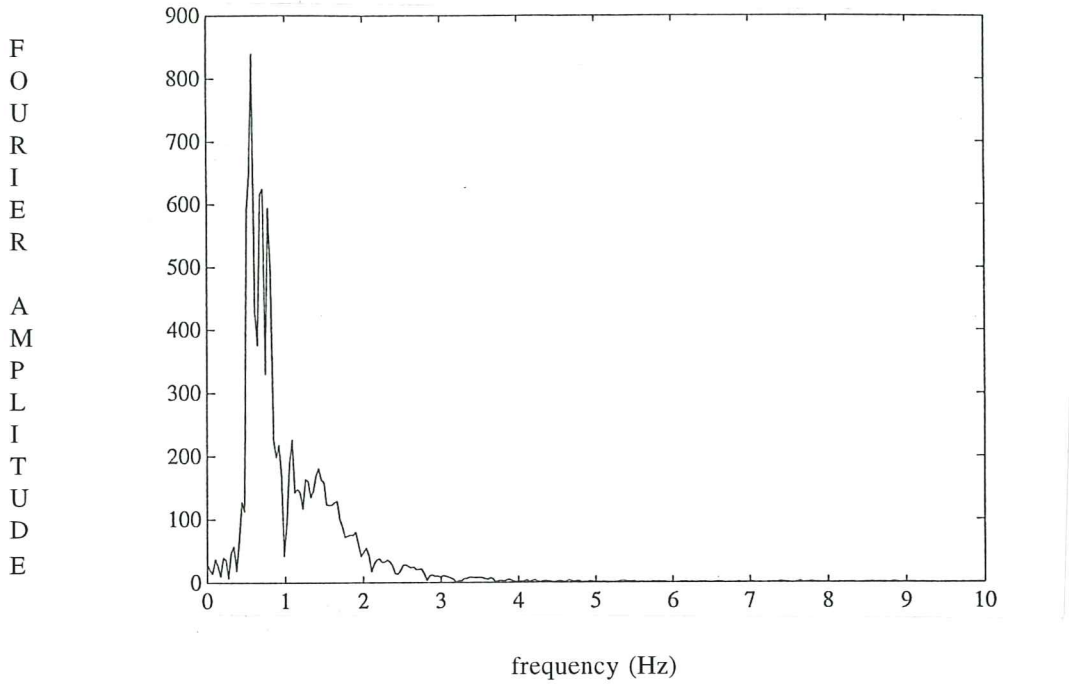

Fig. 13c. Fourier spectra. Parkfield 1966, N65 component.

In the diagram referring to El Centro earthquake it is possible to notice that the frequency content of this signal is spread over a wide range of values. In fact the reason to adopt such a seismic input lies on its broad frequency range. Dumbarton earthquake was chosen to analyse the behaviour of the whole system to low frequencies. In fact the Fourier spectra of the ground displacements of Dumbarton signal shows a low frequency content range. On the contrary Parkfield earthquake was chosen for its high frequency content.

Tables T-3 show a chronological listing of the tests. They are identified by filenames, a brief description of the kind of tests, maximum displacements and spans. The last column is occupied by Log Data File (LDT) of each test.

FILENAME	DESCRIPTION	MAX DISPL.	SPAN
d1sf01.txs	forward sweep	0.05	050
d1sf02.txs	forward sweep	0.10	100
d1sf03.txs	forward sweep	0.15	150
d1sb01.txs	backward sweep	0.05	050
d1sb02.txs	backward sweep	0.10	100
d1sb03.txs	backward sweep	0.15	150
d1ec01.txs	elcentro	0.10	100
d1ec02.txs	elcentro	0.30	300
d1ec03.txs	elcentro	0.50	500
d1du01.txs	dumbarton	0.50	500
d1pk01.txs	parkfield	0.50	500

Table T-3a. Test sequence on the base isolated frame. No restoring springs at the base. W = 5400 lb.

FILENAME	DESCRIPTION	MAX DISPL.	SPAN
d2sf01.txs	forward sweep	0.05	050
d2sf02.txs	forward sweep	0.10	100
d2sf02.txs	elcentro	0.50	150
d2ec03.txs	elcentro	0.50	500
d2du01.txs	dumbarton	0.50	500
d2pk01.txs	parkfield	0.50	500

Table T-3b. Test sequence on the base isolated frame. No restoring springs at the base. W = 3800 lb.

FILENAME	DESCRIPTION	MAX DISPL.	SPAN
d3sf01.txs	forward sweep	0.15	150
d3sf02.txs	forward sweep	0.30	300
d3sf03.txs	forward sweep	0.50	500
d3ec01.txs	elcentro	0.50	500
d3ec02.txs	elcentro	1.00	1000
d3ec03.txs	elcentro	1.50	1000
d3du01.txs	dumbarton	1.50	1000
d3pk01.txs	parkfield	0.50	333
d4si01.txs	sine f=2Hz	0.10	20
d4si02.txs	sine f=7Hz	0.10	20
d4rn01.txs	random	0.10	30

Table T-3c. Test sequence on the base isolated frame. Restoring springs at the base. W = 5360 lb.

FILENAME	DESCRIPTION	MAX DISPL.	SPAN
d5sf01.txs	forward sweep	0.15	150
d5sf02.txs	forward sweep	0.30	300
d5ec01.txs	elcentro	0.50	500
d5ec02.txs	elcentro	1.00	1000
d5du01.txs	dumbarton	1.50	1000
d5pk01.txs	parkfield	0.50	333
d5si01.txs	sine f=2Hz	0.10	20
d5si02.txs	sine f=7Hz	0.10	20
d5rn01.txs	random	0.10	30

Table T-3d. Test sequence on the fixed base frame. Weight = 5360 lb.

CHAPTER 8

TEST RESULTS

In Figures from 14 to 28 the Fourier Amplitudes of the responses are plotted in function of the frequencies. In each figure the upper diagrams show the Fourier Amplitudes of the absolute displacements of the third floor. They are followed by the plots referred to the same Fourier amplitudes for the second and first floors, the base and the shaking table.

8.1 SWEEP FREQUENCY TEST RESULTS

A set of sweep frequency tests were performed on the steel model. The frequencies vary from 0Hz to 10Hz. Forward and backward sweep signals with different amplitudes were utilized during preliminary tests on the model without the restoring springs, and loading was at the maximum capacity of the 1" steel balls. Comparisons with the results on the same model but at lower loads show that the range of predominant frequencies is slightly shifted towards higher values and the peaks are lower.

For this reason, as the differences are not very significative, the following sweep frequency tests were performed on the complete fully loaded model using the entire load capacity of the steel balls.

The responses of the base isolated model and the fixed base model were analysed and compared (Figures 14, 15). For the last model it was not possible to utilize amplitudes higher than 0.50" because of the high resonance effect around the first natural frequency (2.5Hz) of the fixed base model.

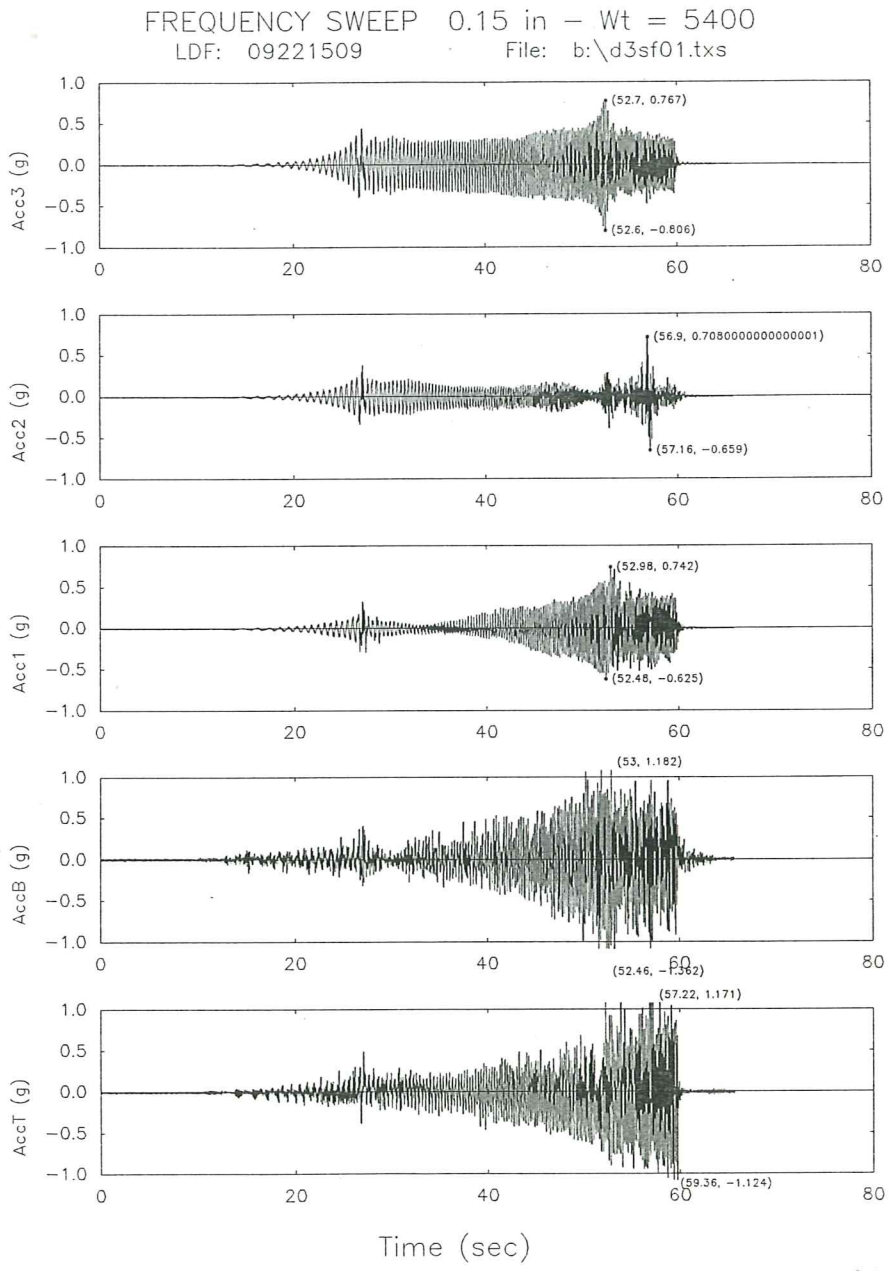

Fig. 14a. Acceleration time response for the base isolated model subjected to a sweep frequency signal.

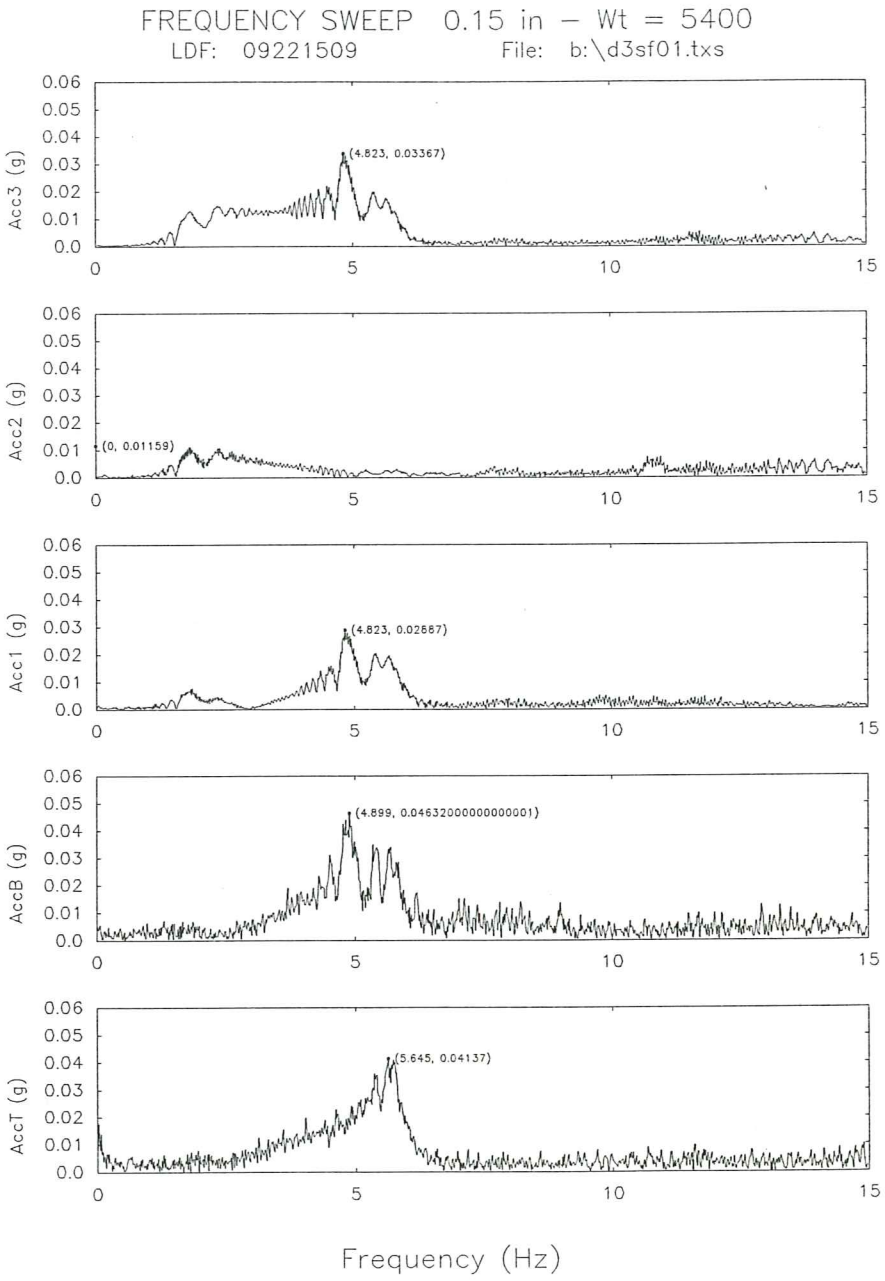

Fig. 14b. Fourier spectra of the accelerations for the base isolated model subjected to a sweep frequency signal.

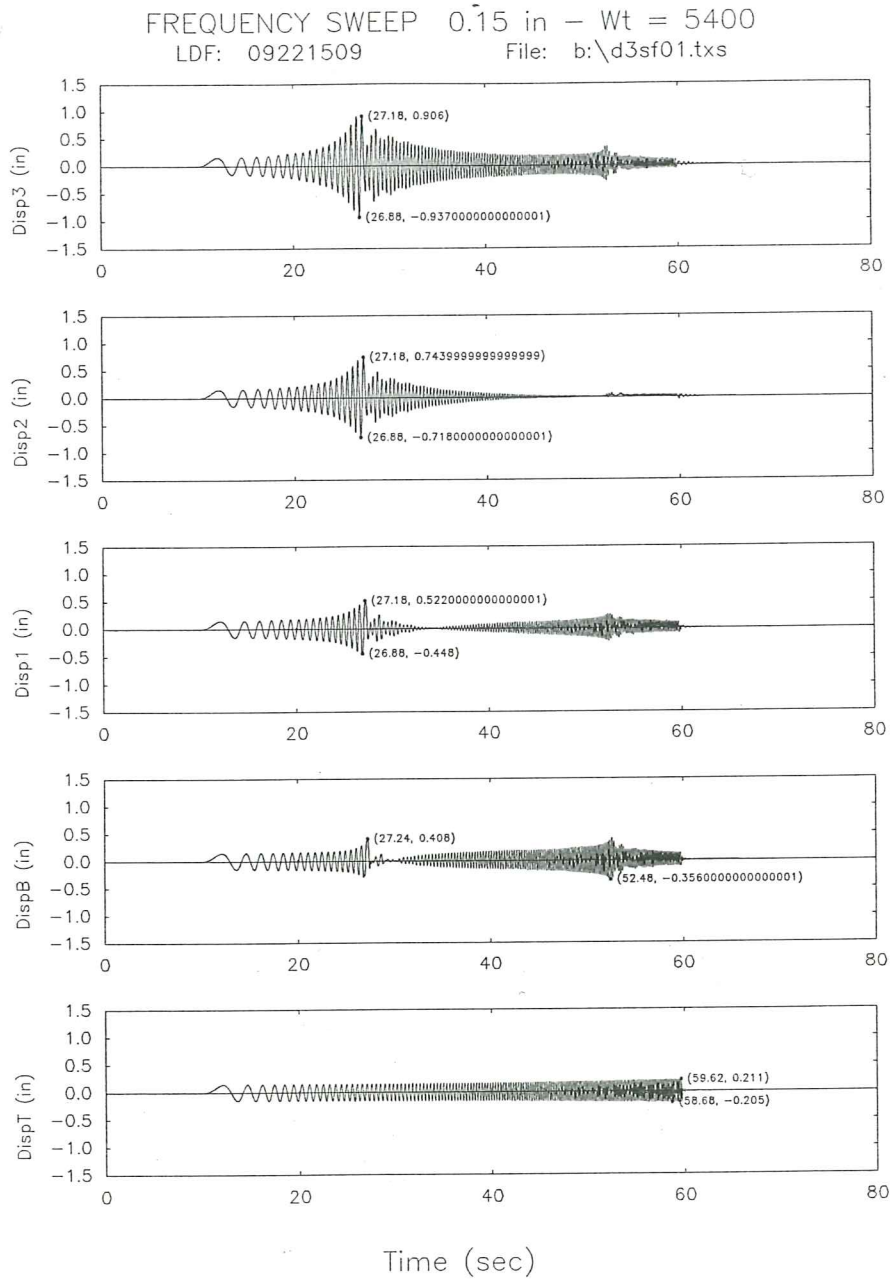

Fig. 14c. Displacement time responses for the base isolated model subjected to a sweep frequency signal.

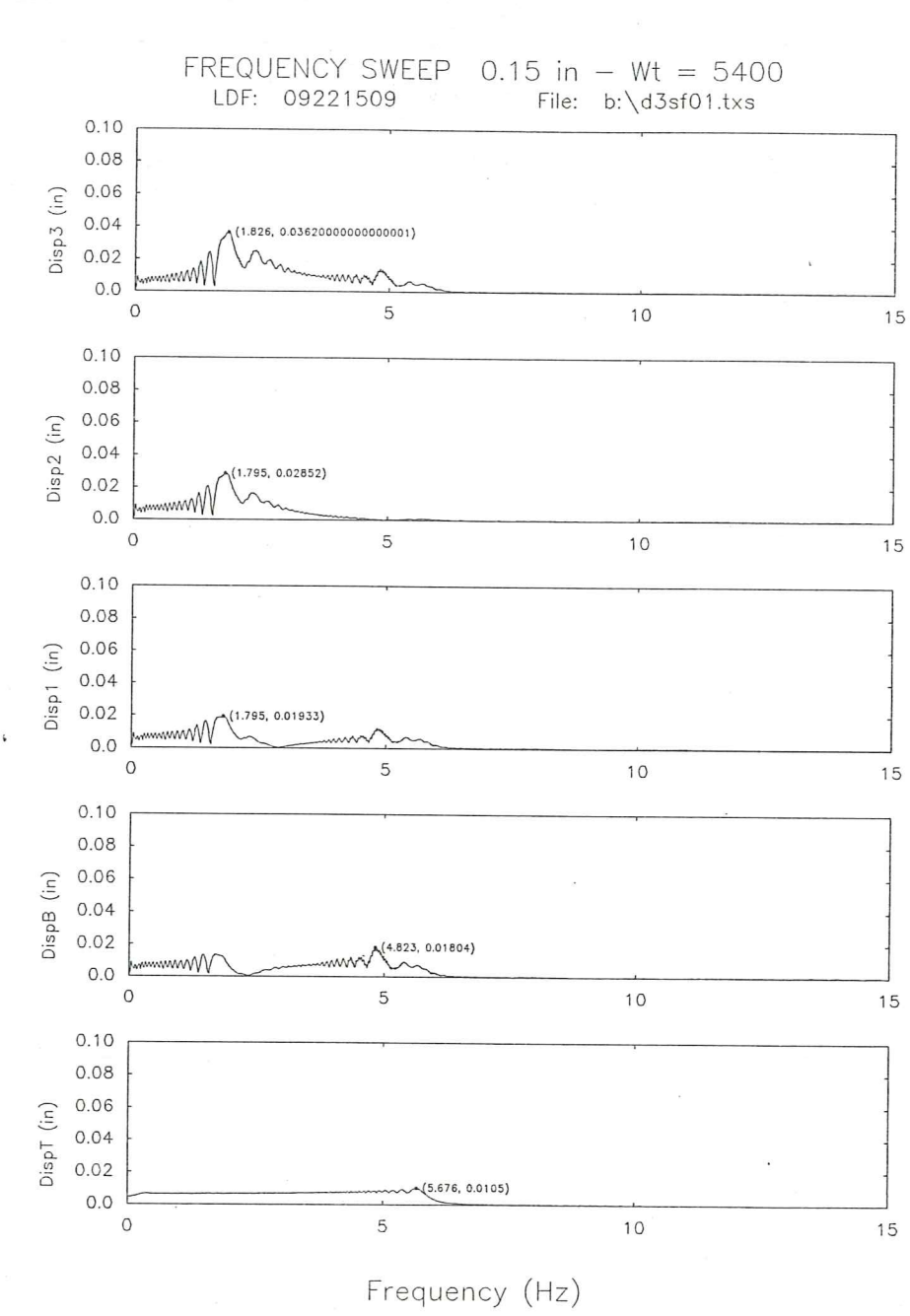

Fig. 14d. Fourier spectra of the displacements for the base isolated model subjected to a sweep frequency signal.

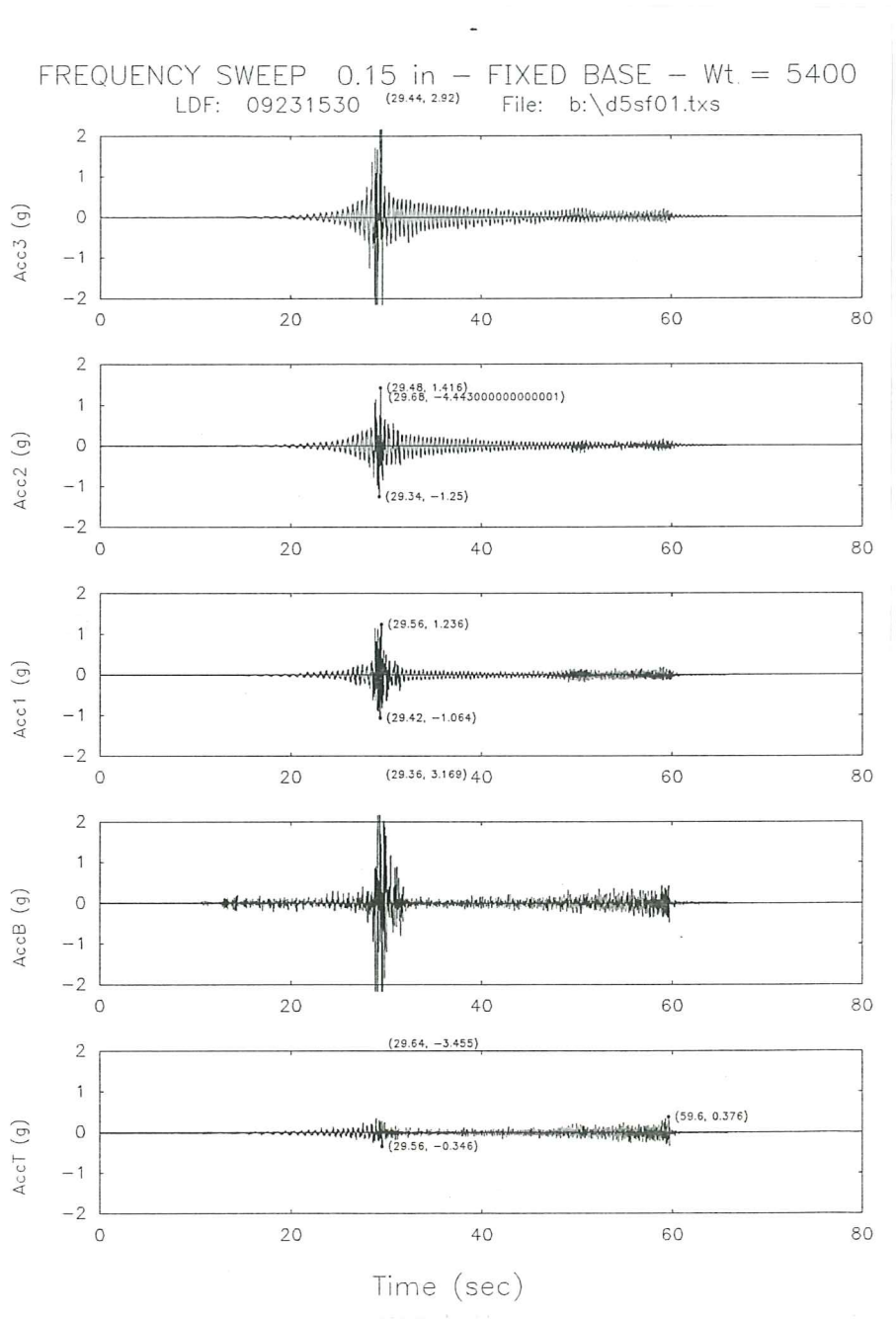

Fig. 15a. Acceleration time response for the fixed base model subected to a sweep frequency signal.

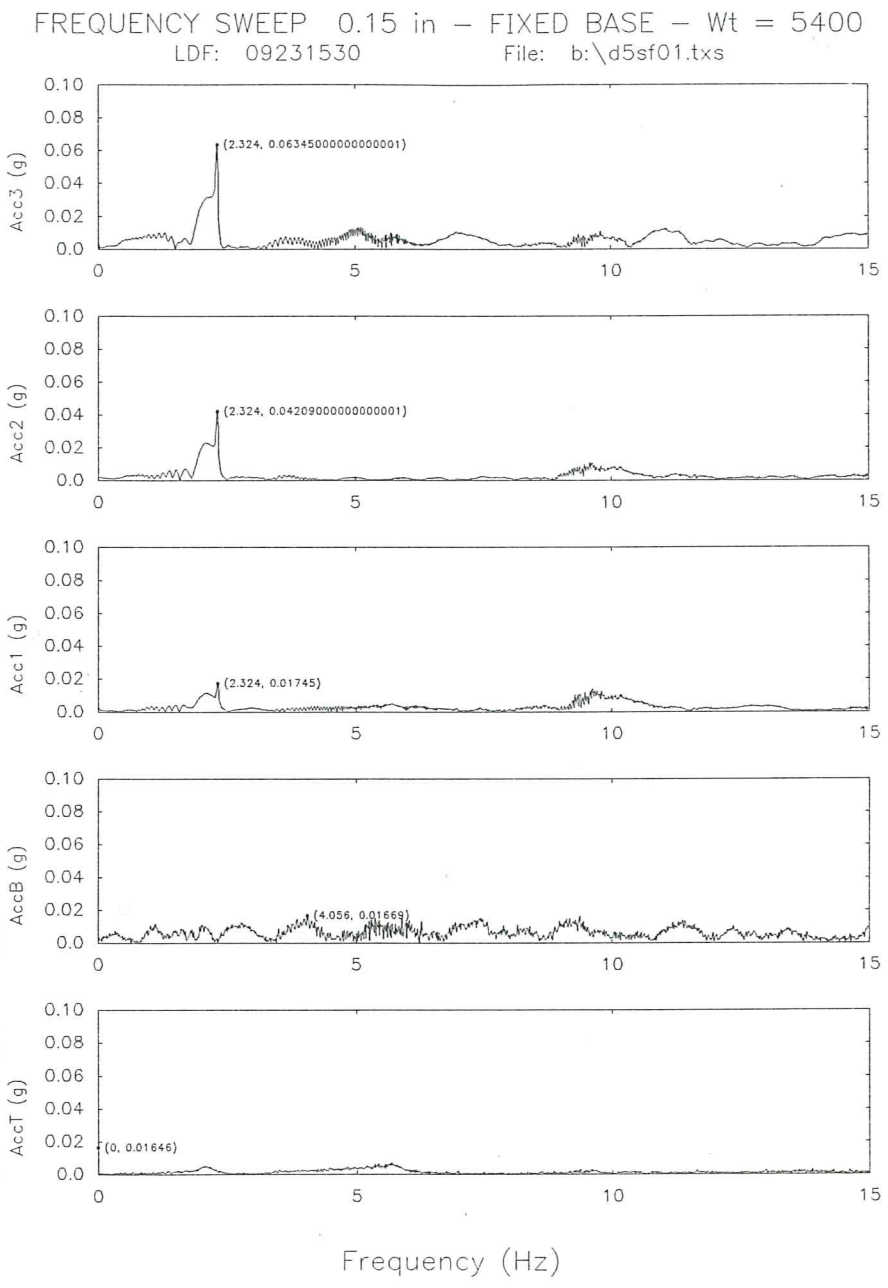

Fig. 15b. Fourier spectra of the accelerations for the fixed base model subjected to a sweep frequency signal.

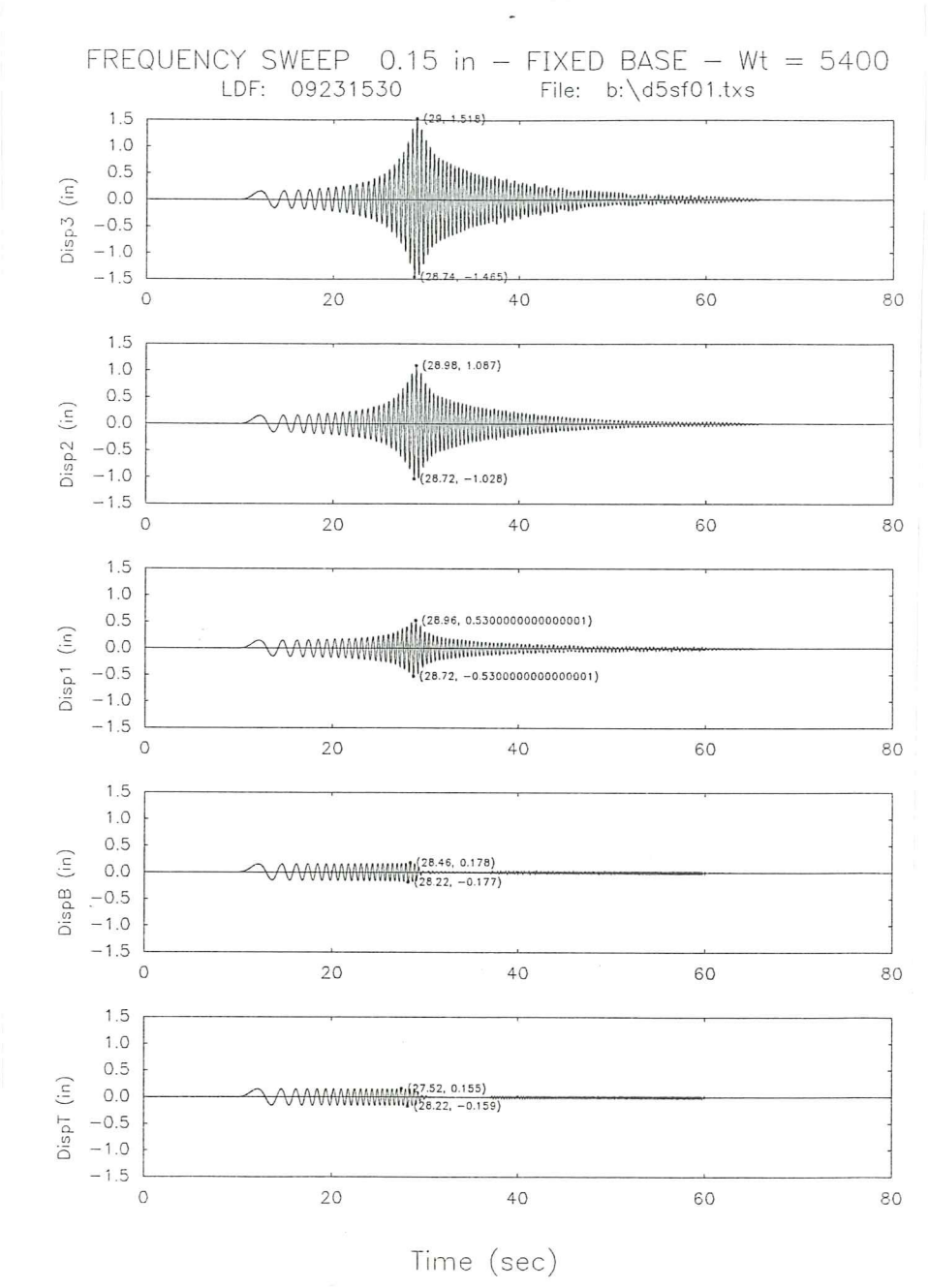

Fig. 15c. Displacement time responses for the fixed base model subjected to a sweep frequency signal.

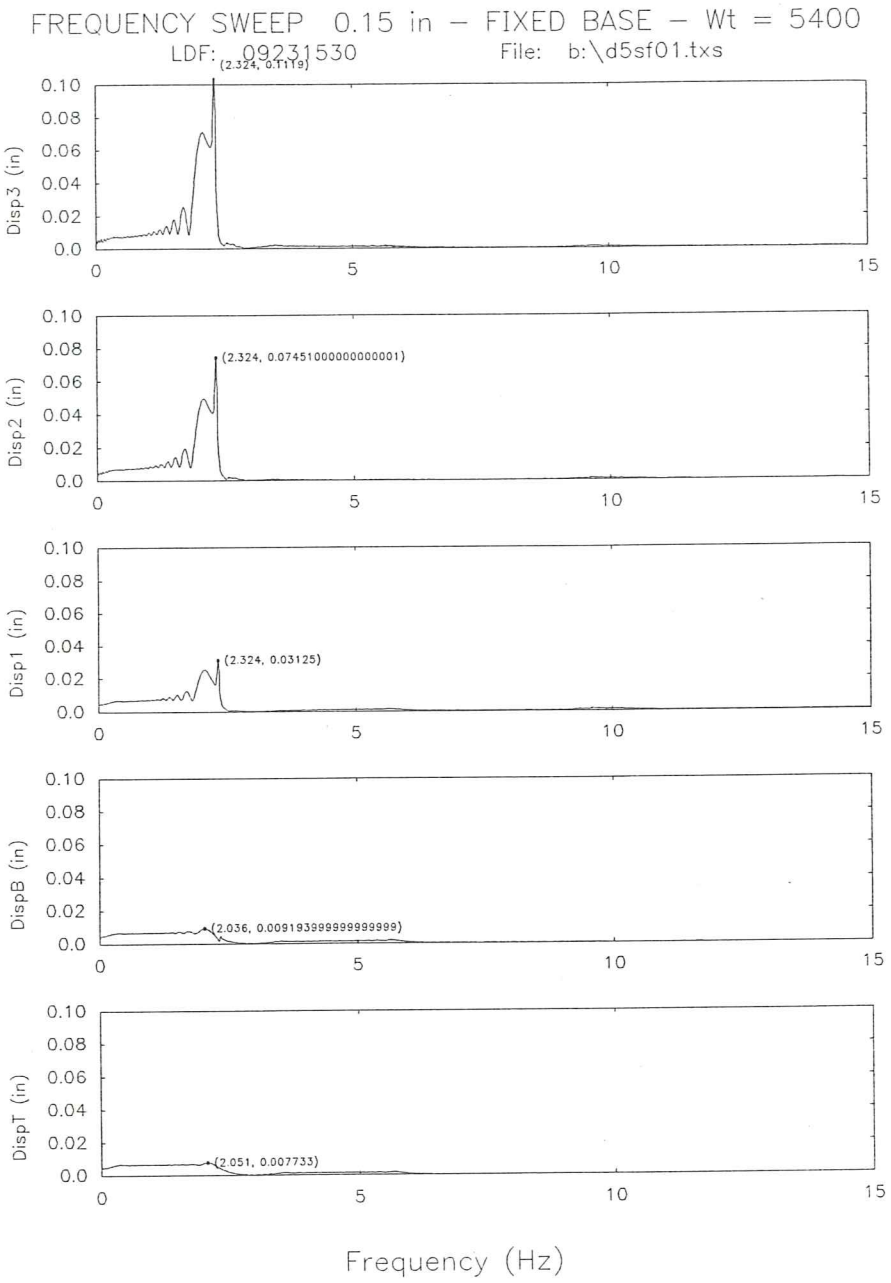

Fig. 15d. Fourier spectra of the displacements for the fixed base model subjected to a sweep frequency signal.

From a numerical calculation. hypotizing a shear type behaviour, the natural frequencies have the values:

1st mode : f_1 = 14.94 Hz
2nd mode : f_2 = 41.87 Hz
3rd mode : f_3 = 60.50 Hz

related to the following mass and stiffness matrices:

$$\mathbf{m} = \begin{pmatrix} 1.29 & 0 & 1.29 \\ 0 & 1.29 & 0 \\ 0 & 0 & 1.29 \end{pmatrix}$$

$$\mathbf{k} = \begin{pmatrix} 109200 & -54600 & 0 \\ -54600 & 109200 & -54600 \\ 0 & -546000 & 54600 \end{pmatrix}$$

If it is supposed that the connecting joints at each floor can rotate, the stiffness matrix assumes the form:

$$\mathbf{k} = \begin{pmatrix} 42000 & -24150 & 6300 \\ -24150 & 23100 & -8400 \\ 6300 & -8400 & 3675 \end{pmatrix}$$

and the natural frequencies become:

1st mode : f_1 = 2.77 Hz
2nd mode : f_2 = 18.10 Hz
3rd mode : f_3 = 48.64 Hz

During the sweep frequency tests it was noticed that the isolators became effective for frequency ranges around 2.5Hz, That is the natural frequency of the fixed base system supposed with rotating joints at each floor. For this reason it is possible to affirm that the real behaviour of the model is closer to the second hypotesis of zero stiffness of the floors. It was also noticed that when the isolation system started to work, the shear base forces suddenly decrease. The immediate effect of this decrease was a decrease of the accelerations and absolute displacements measured at each floor of the base isolated system.

8.2 RANDOM AND SINUSOIDAL SIGNAL RESULTS

These inputs were utilized only for tests on the complete model.

From these tests it was possible to obtain some information about the dynamic characteristics of the model. As for the previous sweep frequency tests the acceleration and absolute displacement response peaks were higher for the fixed base model. The results for the random signal showed two natural frequencies of the fixed base system for values around 2.5Hz and 9.5Hz (Figures 17). For the base isolation system, due to its non-linearity, it was possible only to define some regions with higher frequency content around 2Hz ÷ 3Hz, 6Hz ÷ 8Hz, 12Hz ÷ 13Hz (Figures 16). In fact in the last case the acceleration and absolute displacement values are lower and more widely spread.

The effects of non-linearity of the isolation devices are ahown also in the results of sinusoidal inputs (Figures 18, 19, 20, 21). Especially at the constant frequency of 7 Hz, it is possible to notice in the FFT plots for the accelerations that the amplification at 7 Hz is sharp for the fixed base model and is wider around this frequency for the isolated frame.

Other kind of sinusoidal tests were performed on the whole system, increasing the amplitude at a fixed frequency. In this way it is possible to determine the amplitude at which the devices start to work, that is when the steel balls start to roll. For frequencies around 2 Hz and 7 Hz, the amplitude at rolling is very small, as shown in Figure 22.

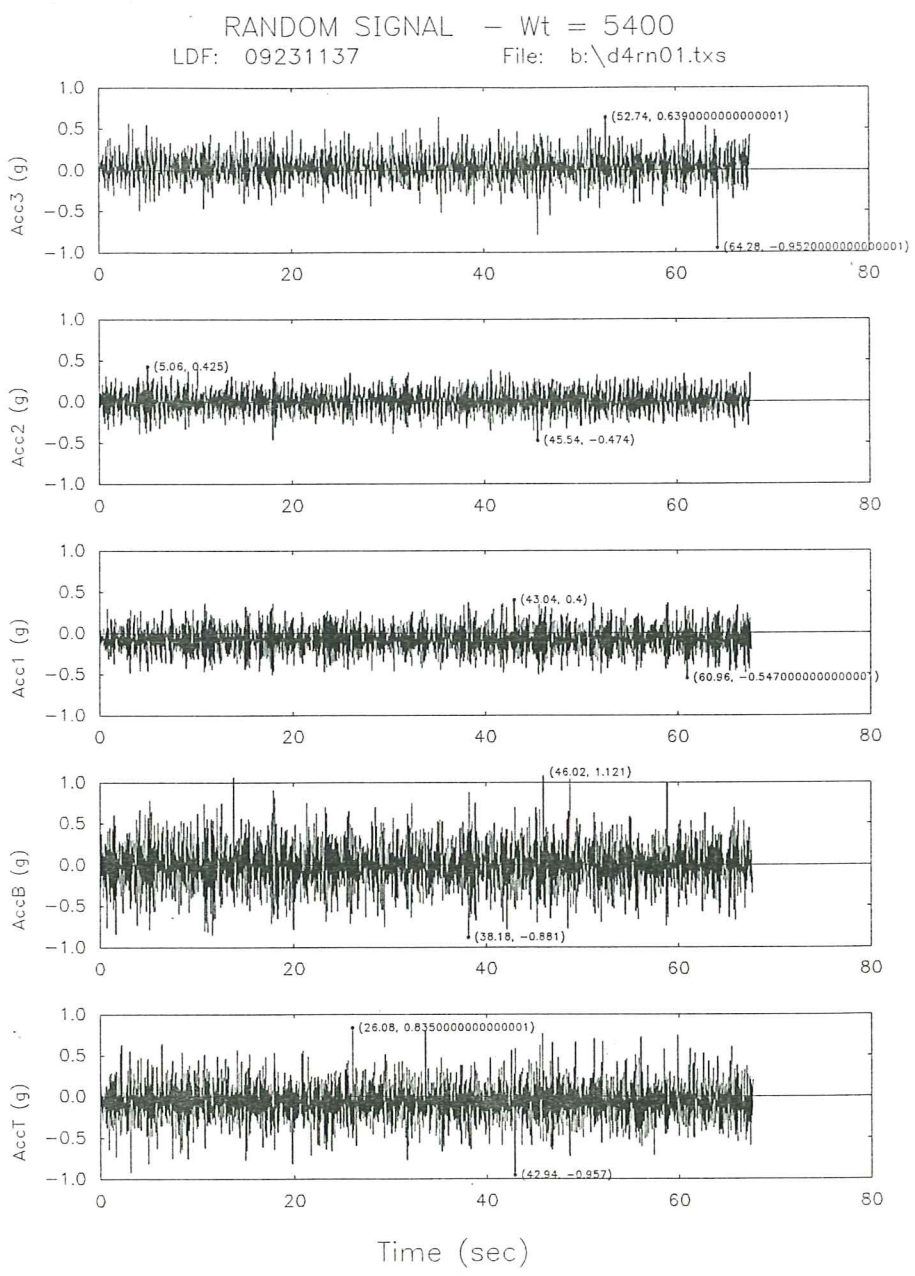

Fig. 16a. Acceleration time response for the base isolated model subjected to a random signal.

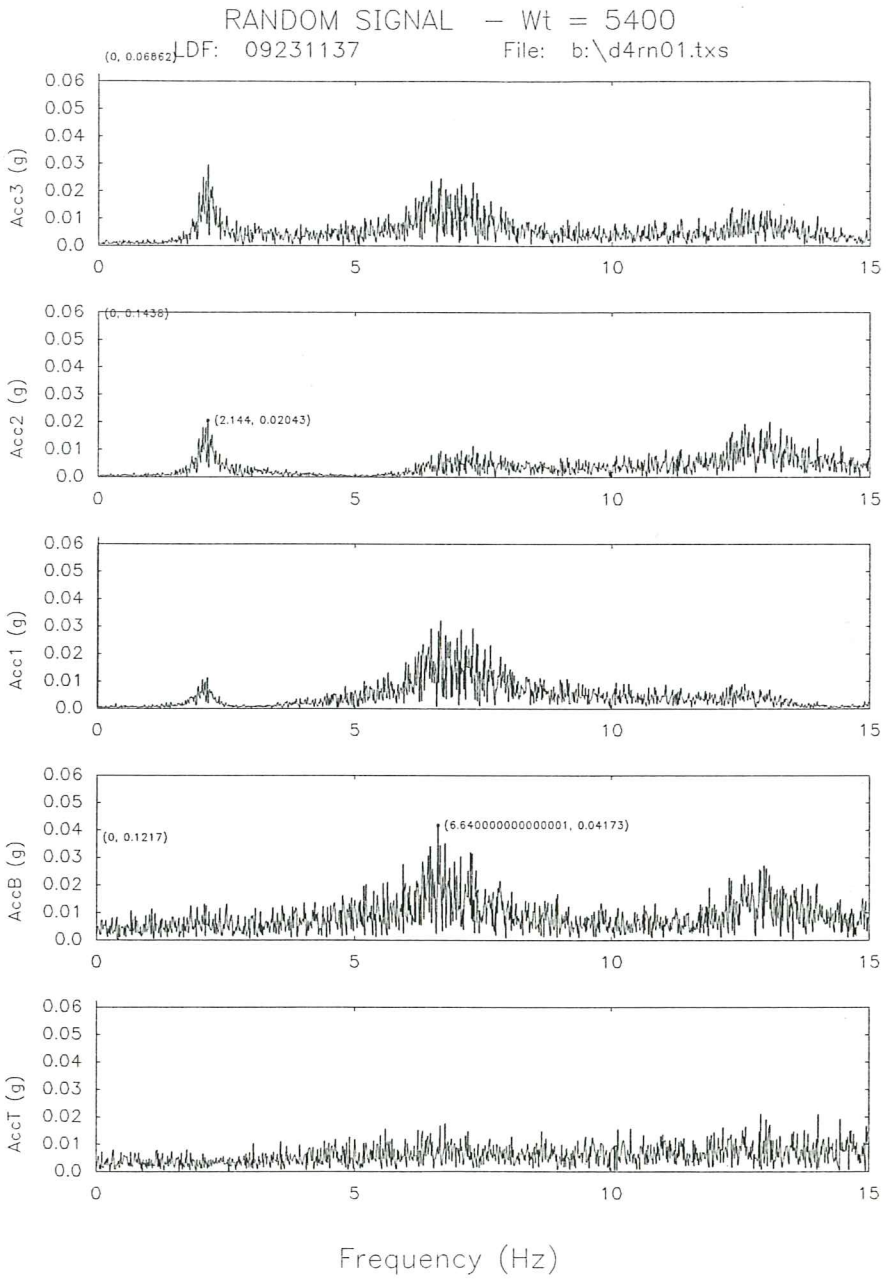

Fig. 16b. Fourier spectra of the accelerations for the base isolated model subjected to a random signal.

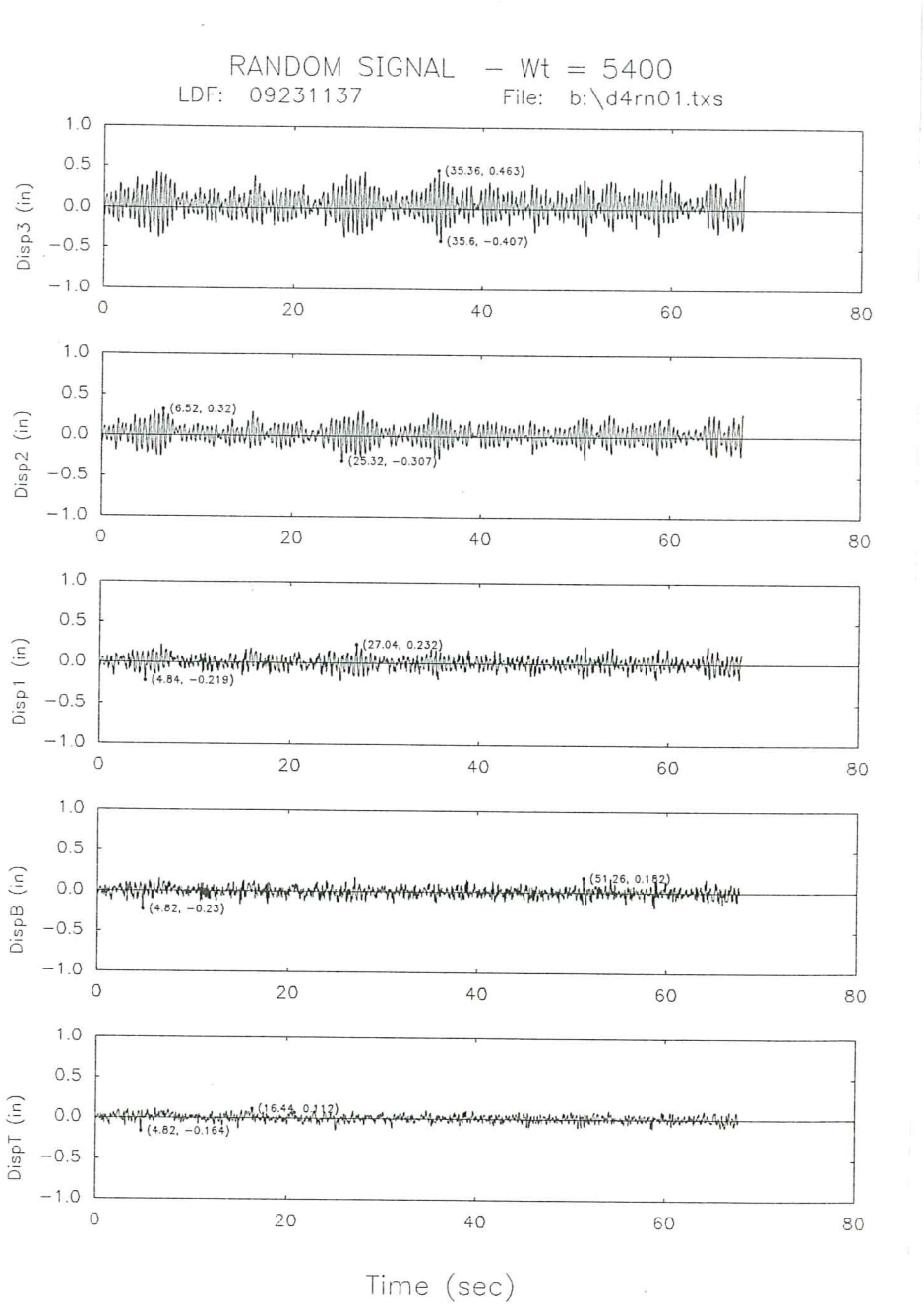

Fig. 16c. Displacement time responses for the base isolated model subjected to a random signal.

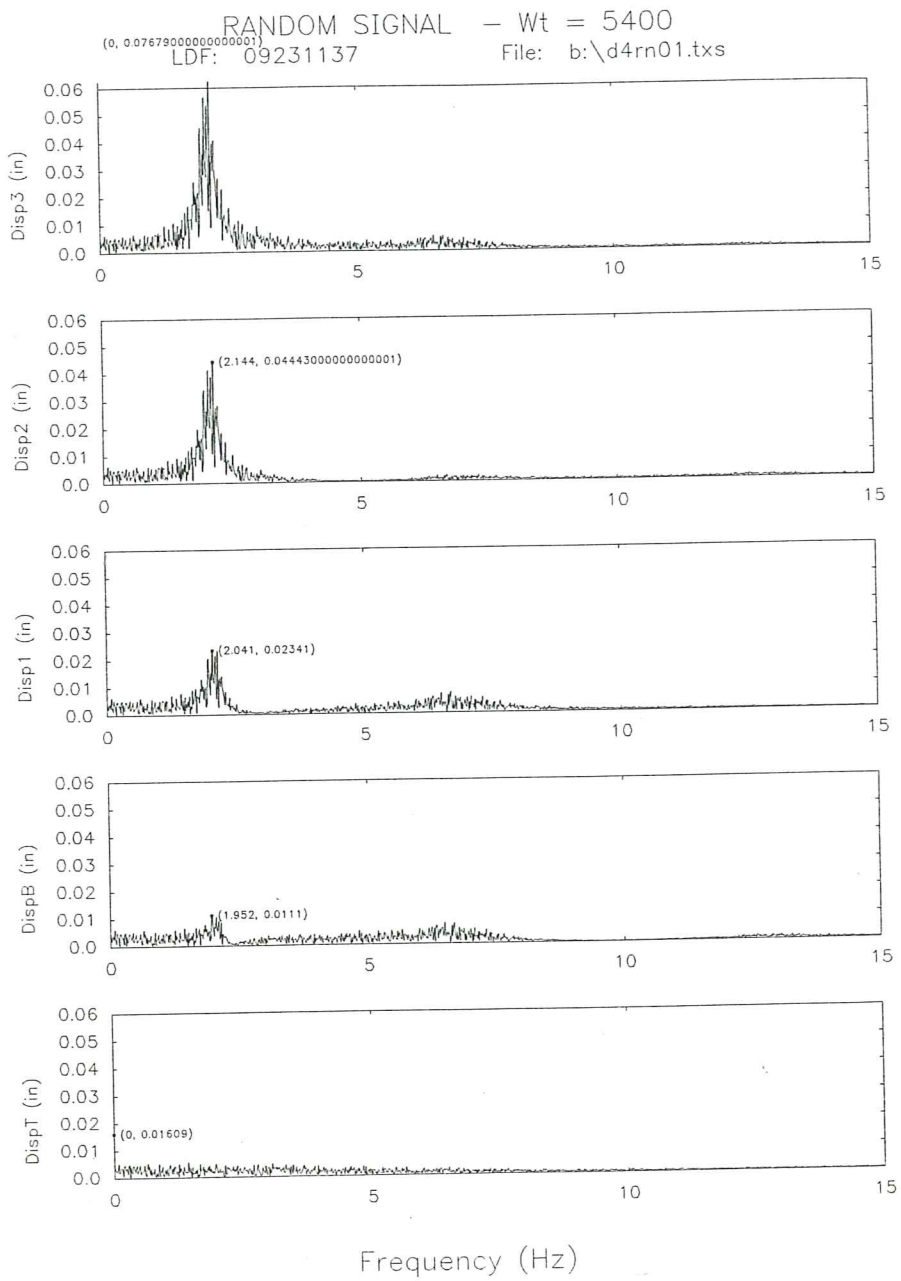

Fig. 16d. Fourier spectra of the displacements for the base isolated model subjected to a random signal.

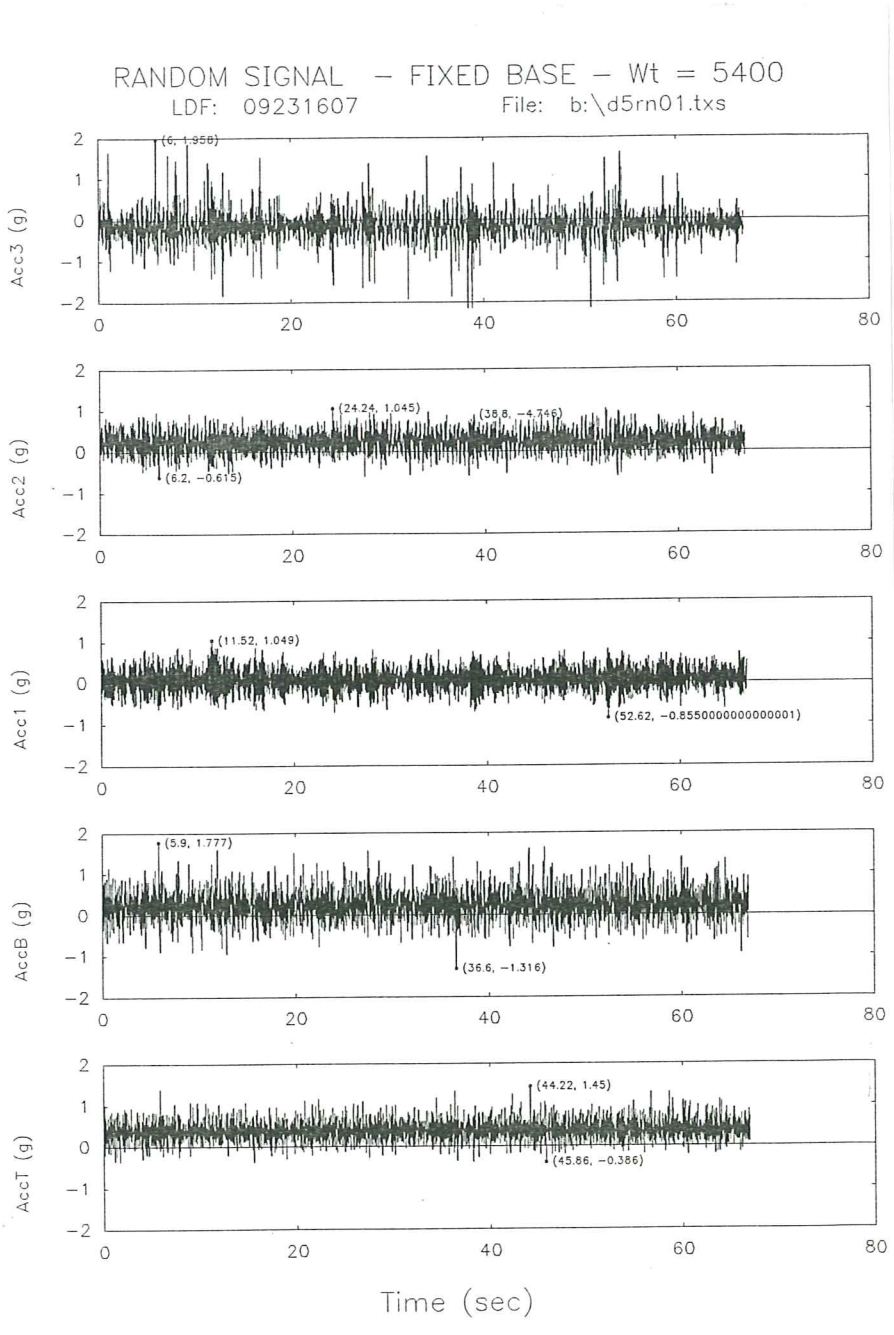

Fig. 17a. Acceleration time response for the fixed base model subected to a random signal.

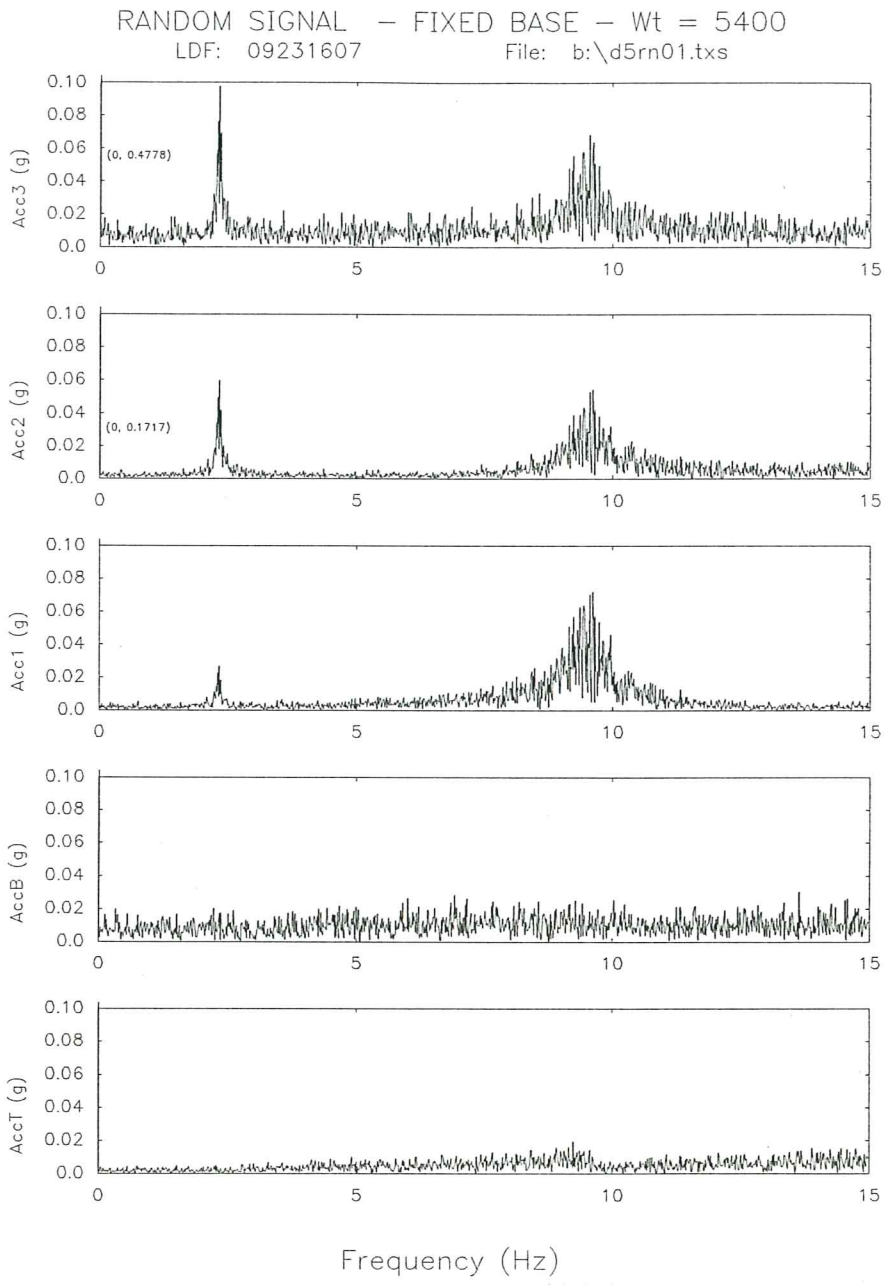

Fig. 17b. Fourier spectra of the accelerations for the fixed base model subjected to a random signal.

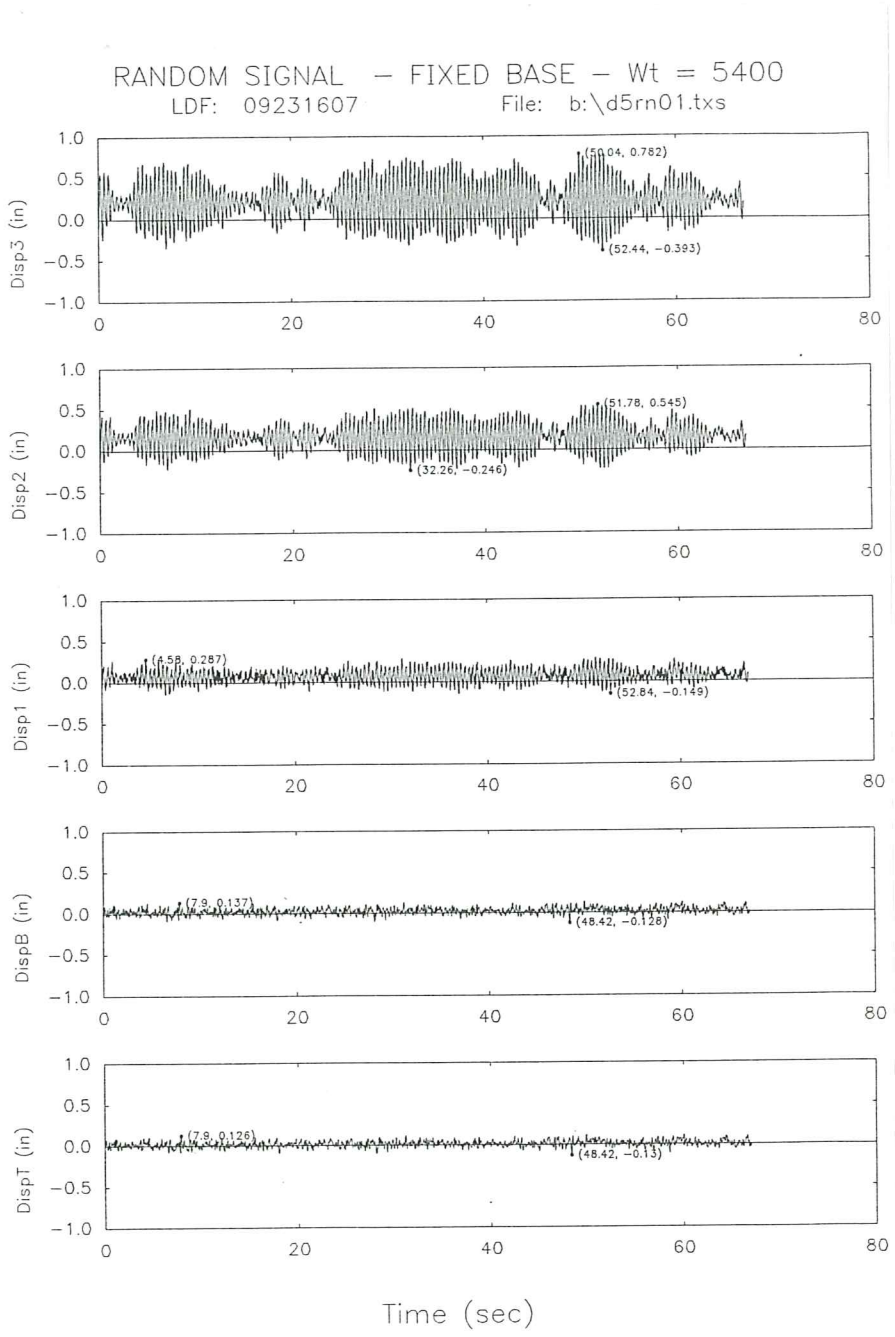

Fig. 17c. Displacement time responses for the fixed base model subjected to a random signal.

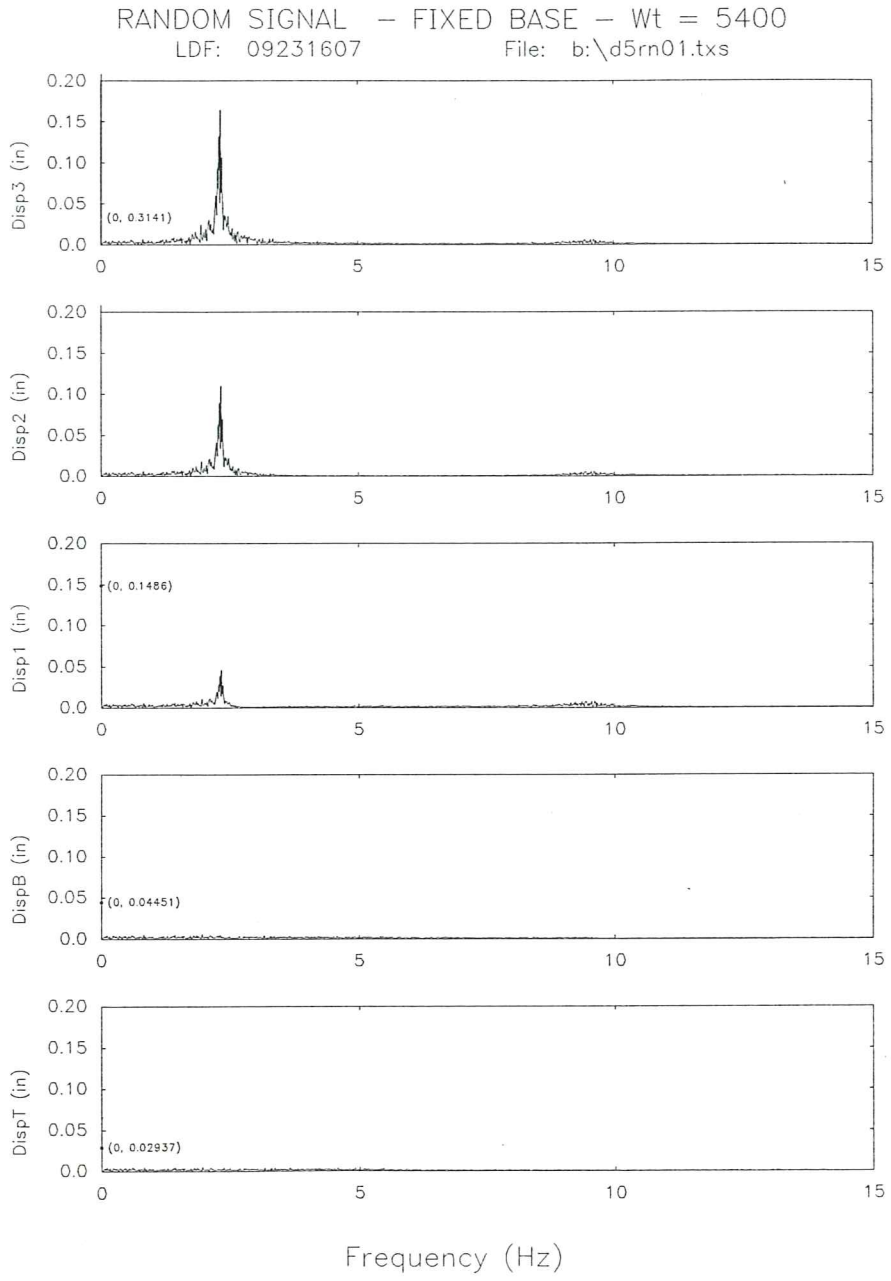

Fig. 17d. Fourier spectra of the displacements for the fixed base model subjected to a random signal.

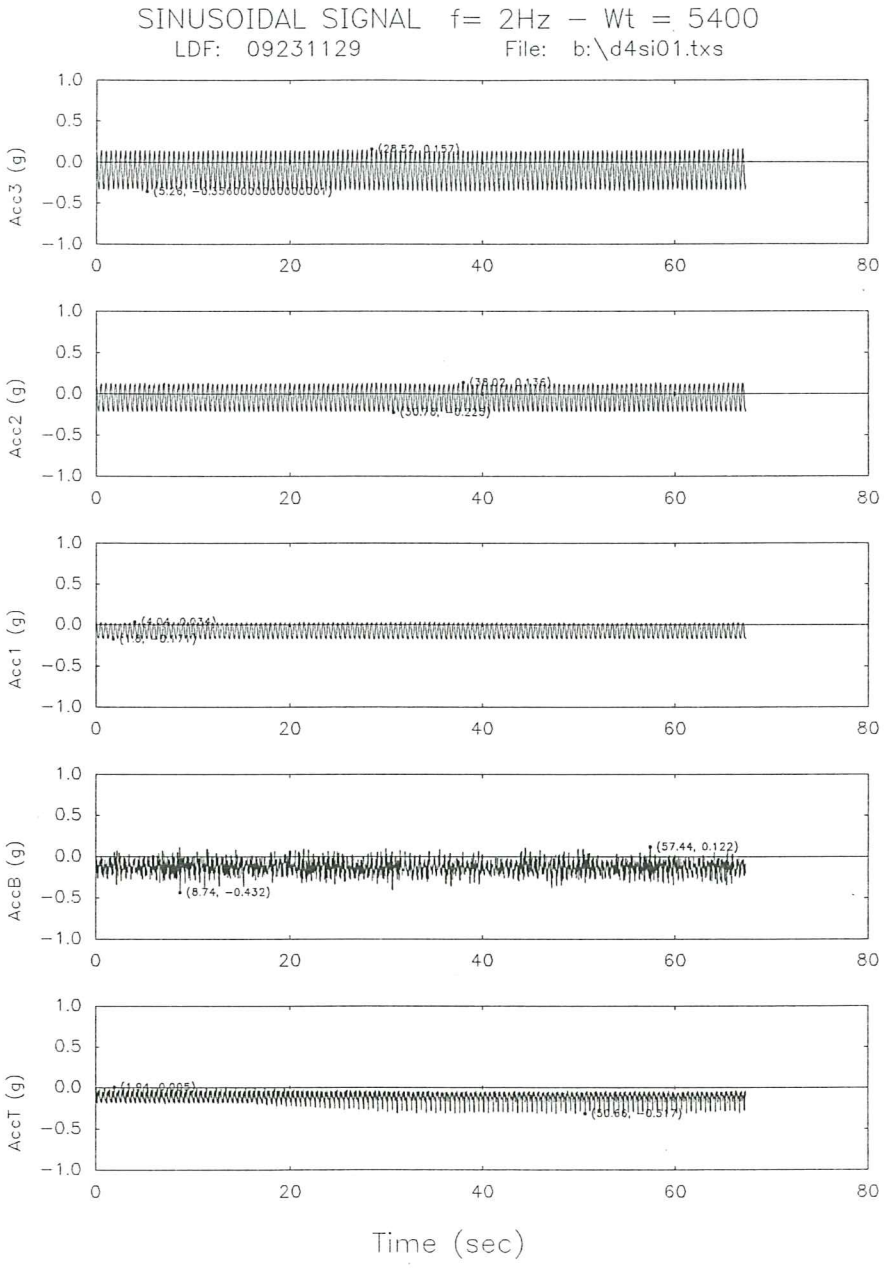

Fig. 18a. Acceleration time response for the base isolated model subjected to a sinusoidal signal (f=2Hz).

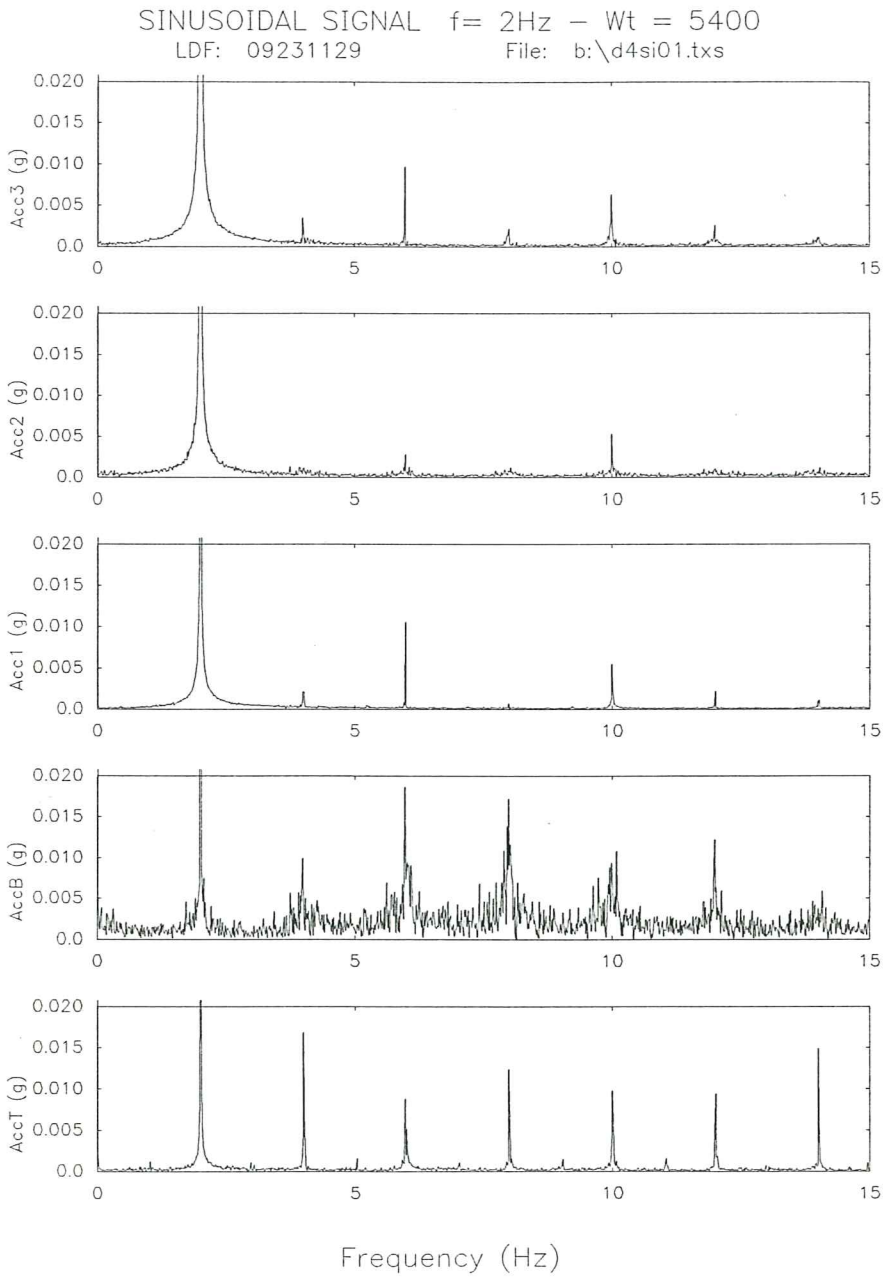

Fig. 18b. Fourier spectra of the accelerations for the base isolated model subjected to a sinusoidal signal (f=2Hz).

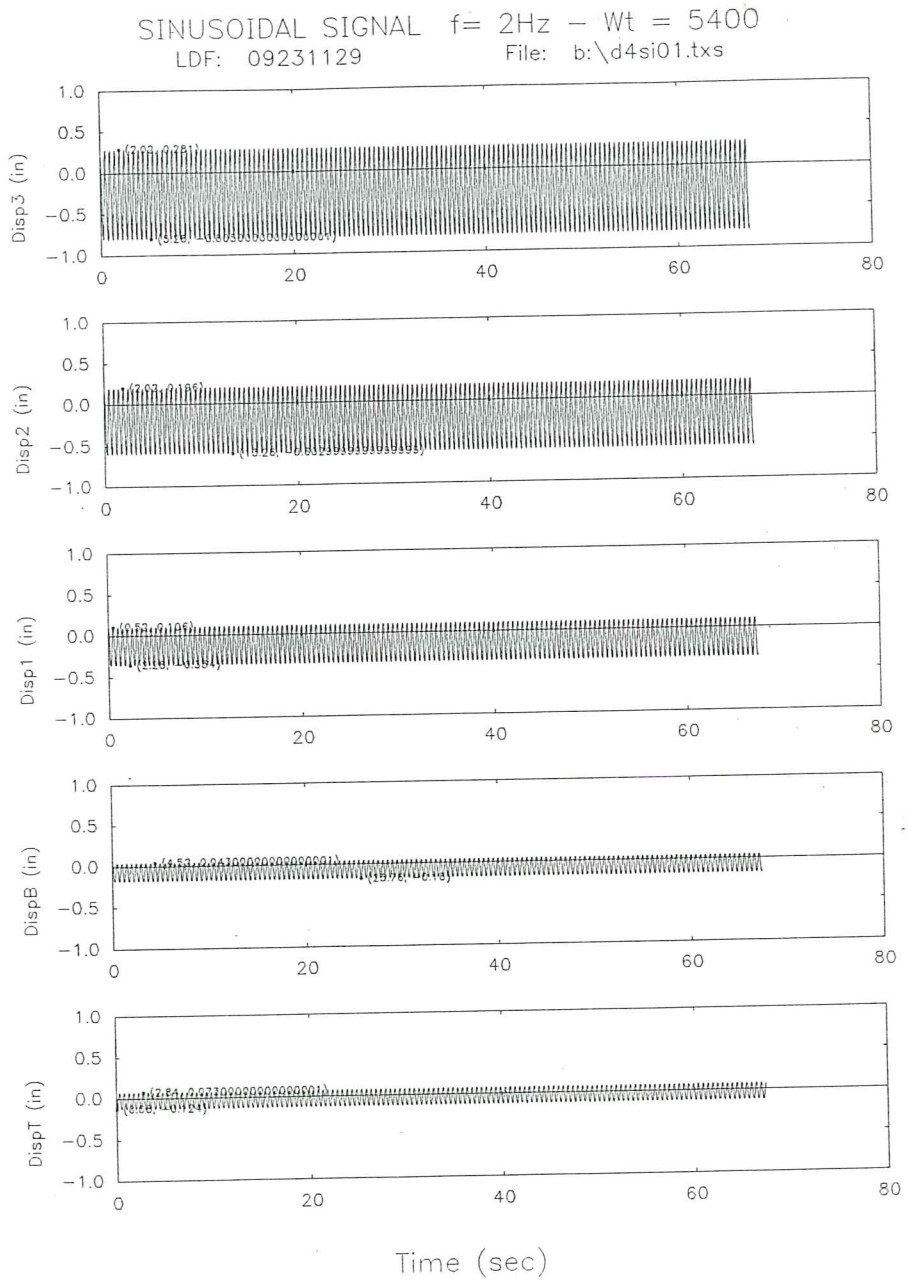

Fig. 18c. Displacement time response for the base isolated model subjected to a sinusoidal signal (f=2Hz).

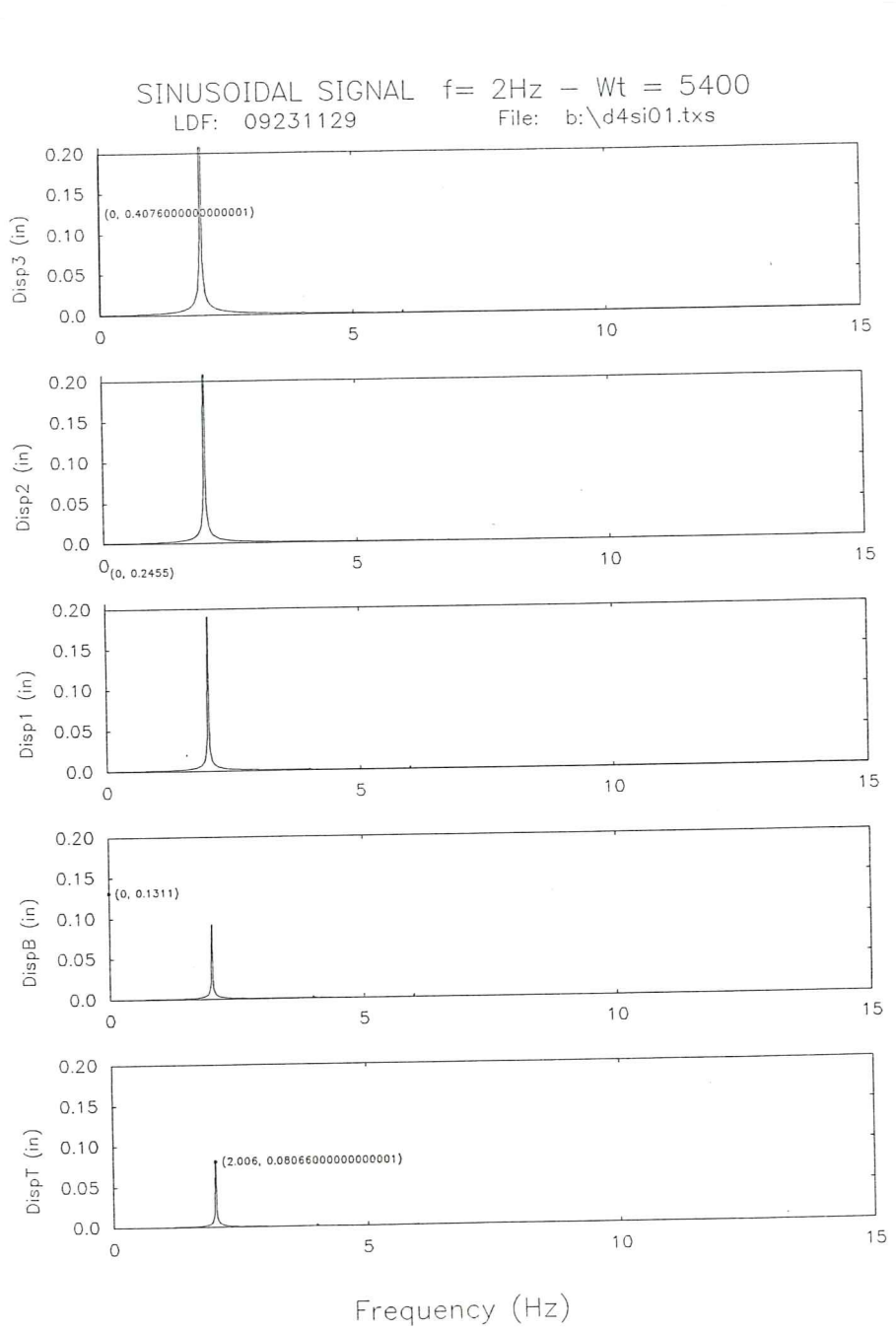

Fig. 18d. Fourier spectra of the displacements for the base isolated model subjected to a sinusoidal signal (f=2Hz).

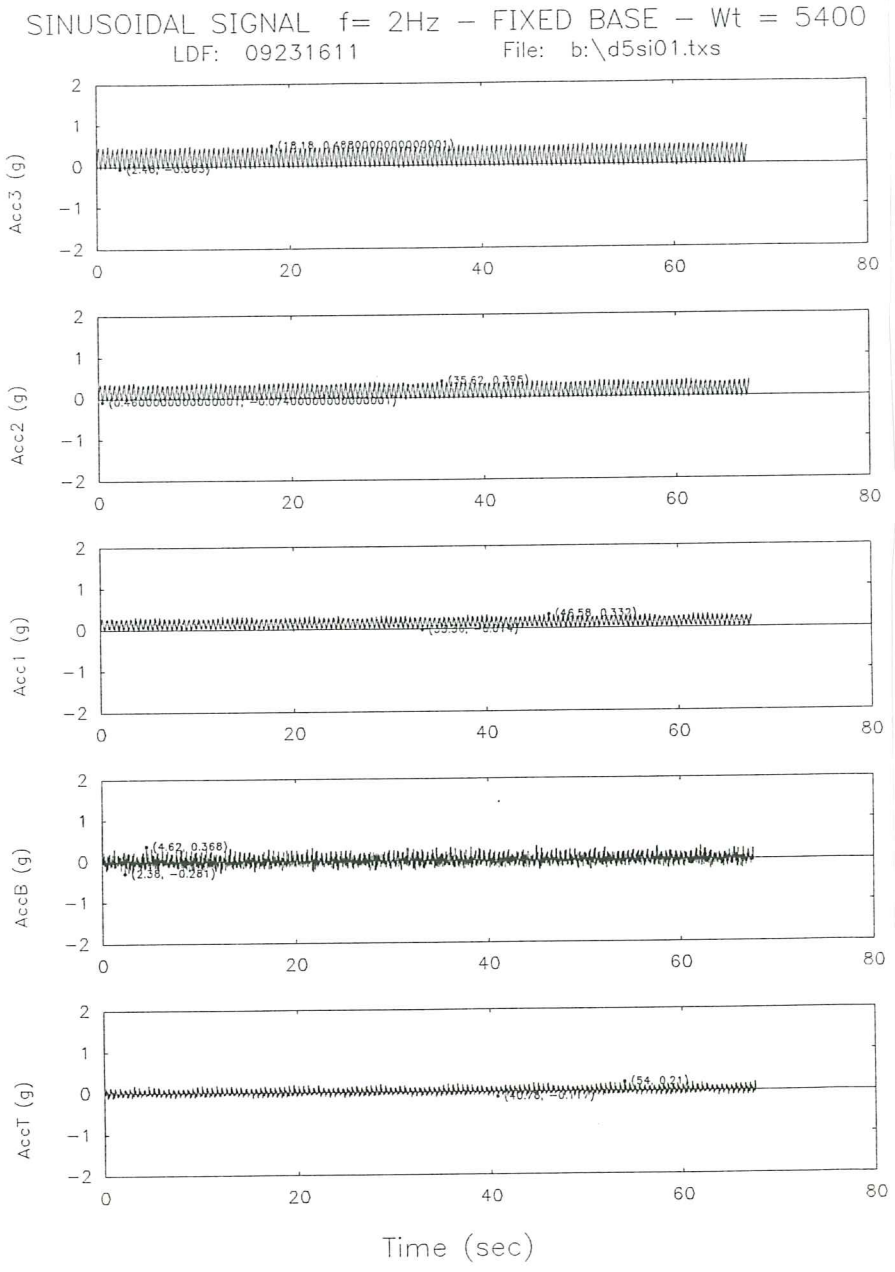

Fig. 19a. Acceleration time response for the fixed base model subected to a sinusoidal signal (f=2Hz).

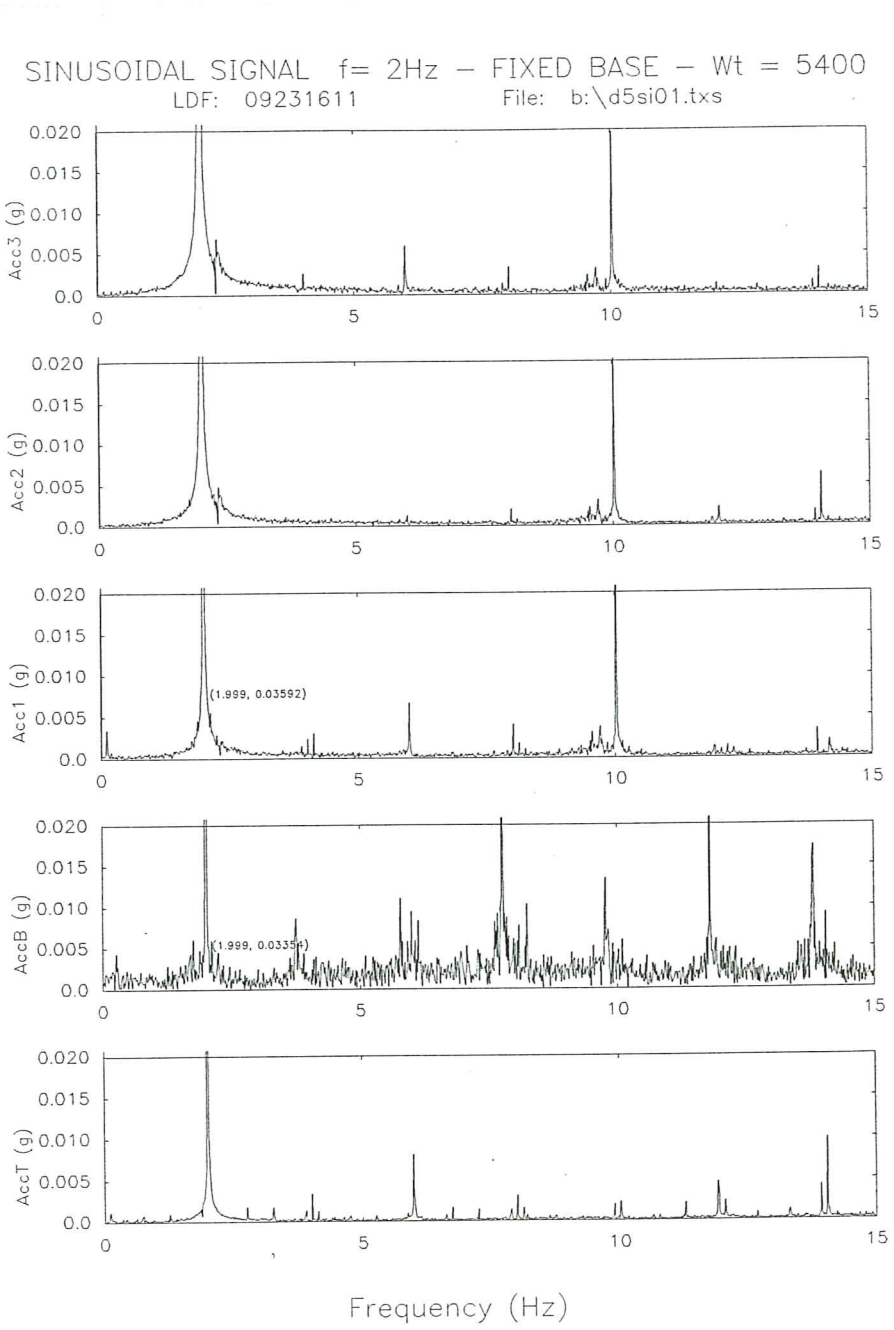

Fig. 19b. Fourier spectra of the accelerations for the fixed base model subjected to a sinusoidal signal (f=2Hz).

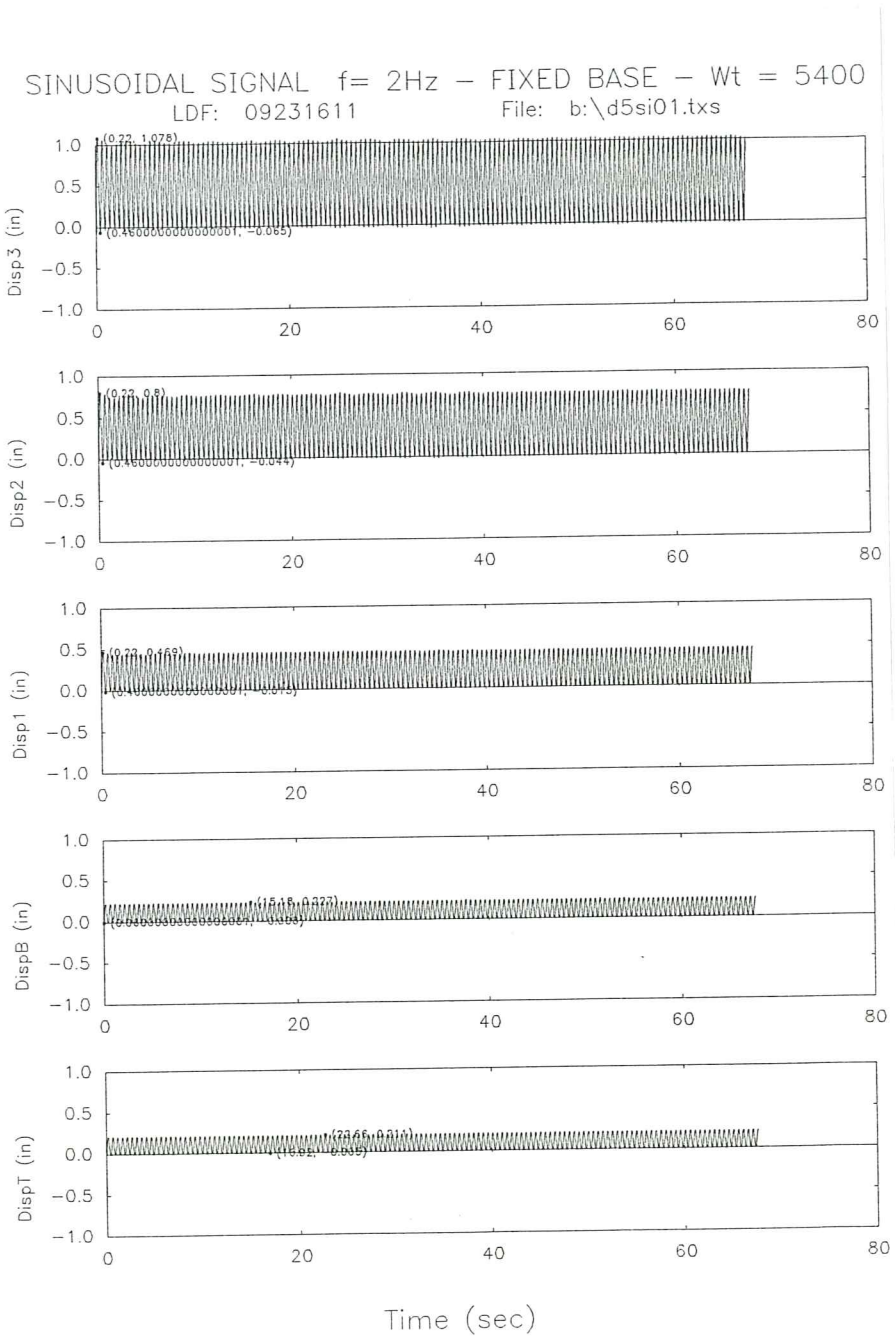

Fig. 19c. Displacement time responses for the fixed base model subjected to a sinusoidal signal (f=2Hz).

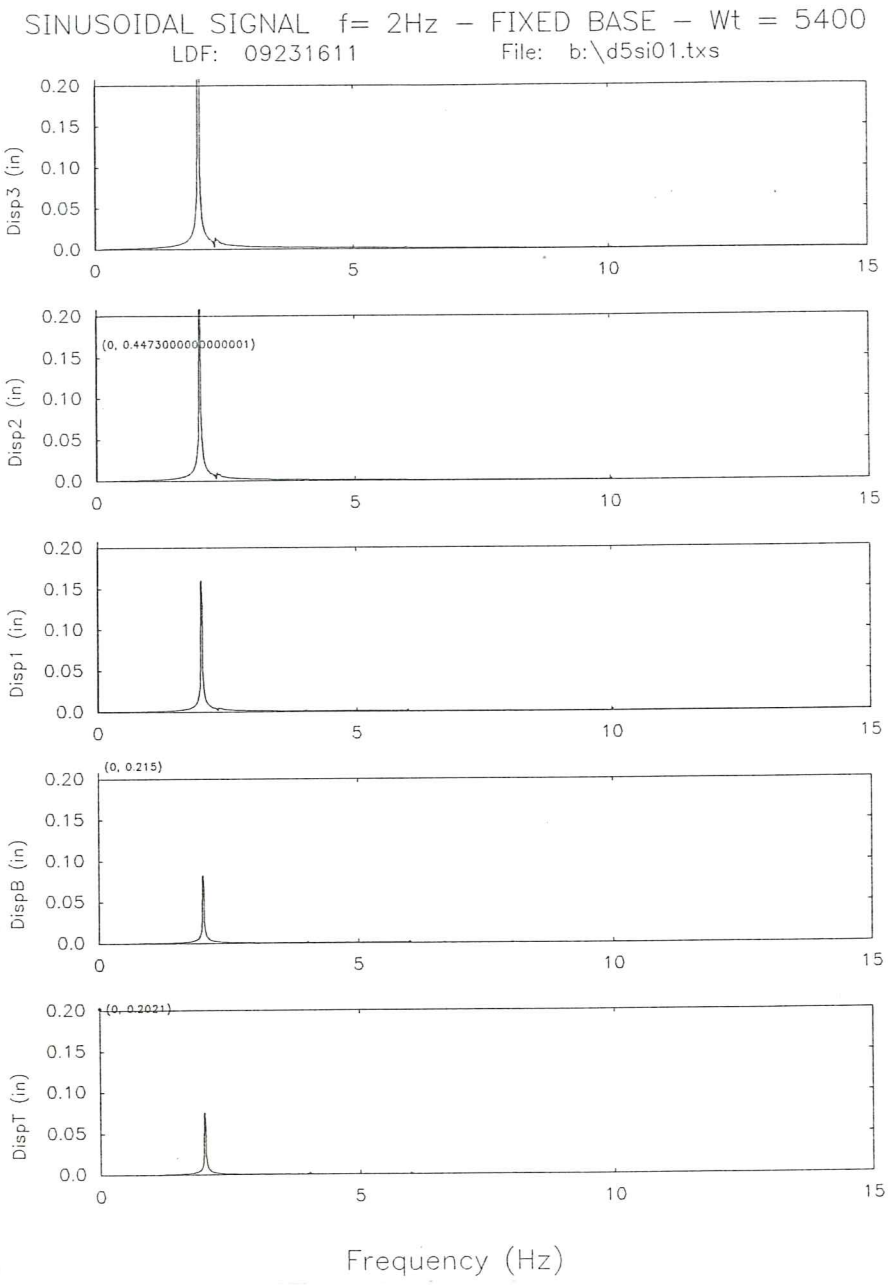

Fig. 19d. Fourier spectra of the displacements for the fixed base model subjected to a sinusidal signal (f=2Hz).

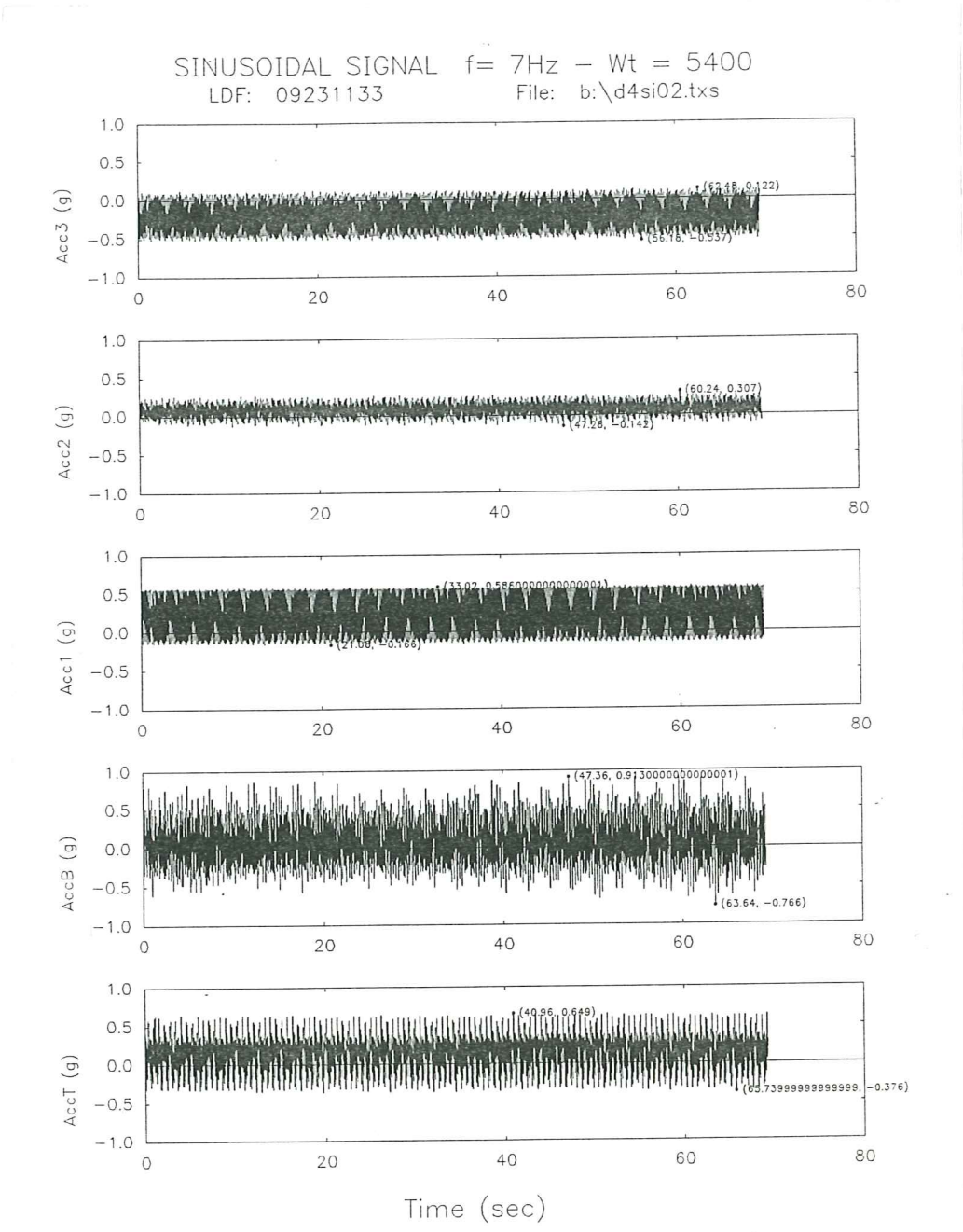

Fig. 20a. Acceleration time response for the base isolated model subjected to a sinusoidal signal (f=7Hz).

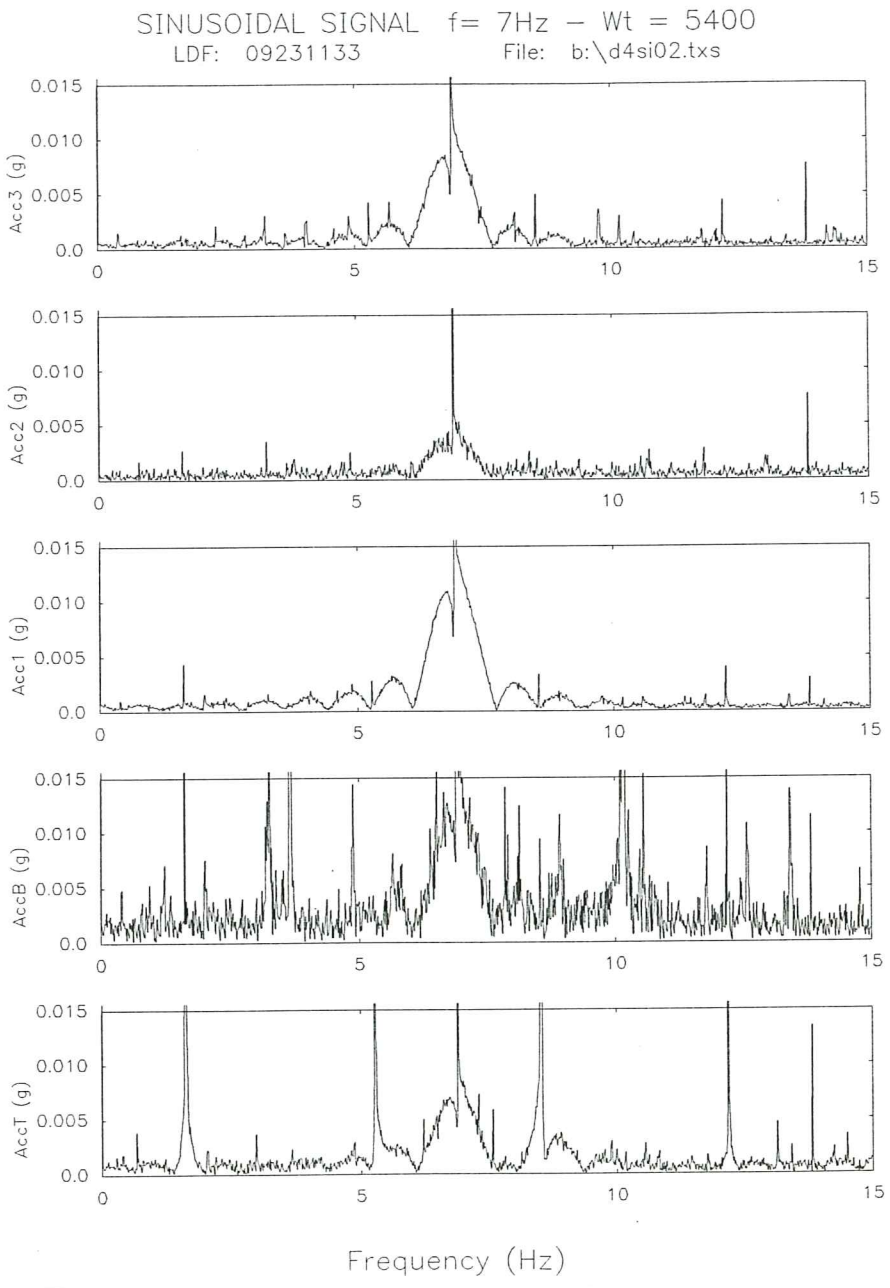

Fig. 20b. Fourier spectra of the accelerations for the base isolated model subjected to a sinusoidal signal (f=7Hz).

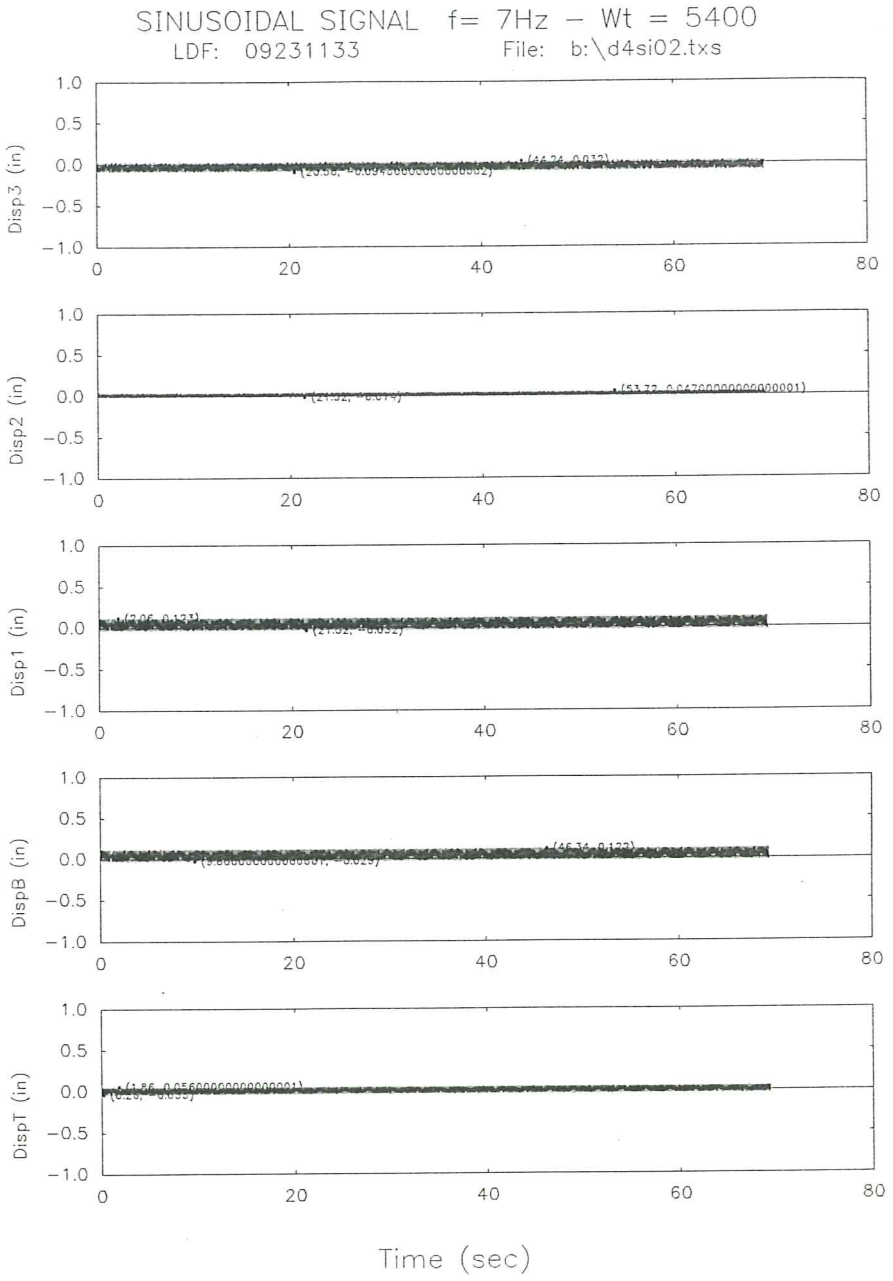

Fig. 20c. Displacement time responses for the base isolated model subjected to a sinusoidal signal (f=7Hz).

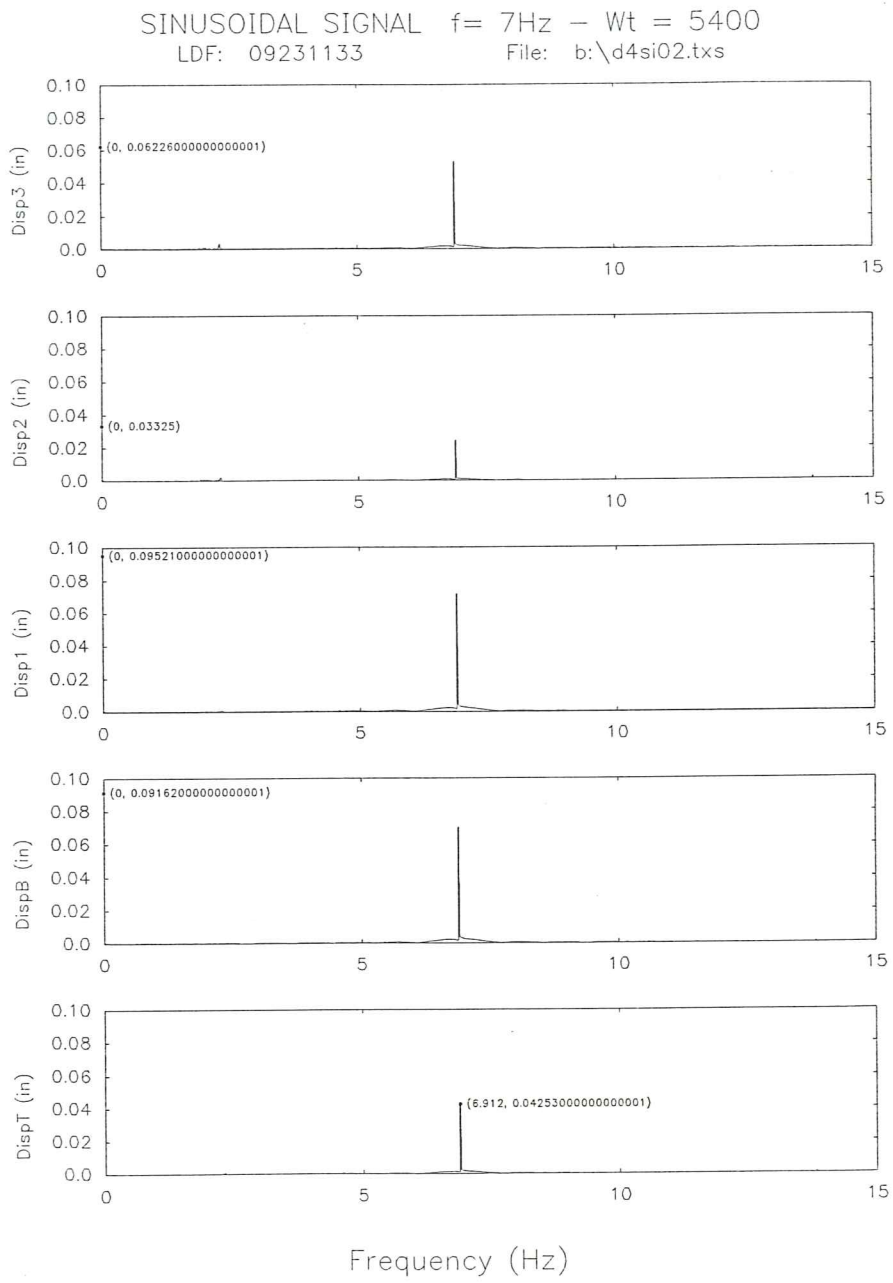

Fig. 20d. Fourier spectra of the displacements for the base isolated model subjected to a sinusoidal signal (f=7Hz).

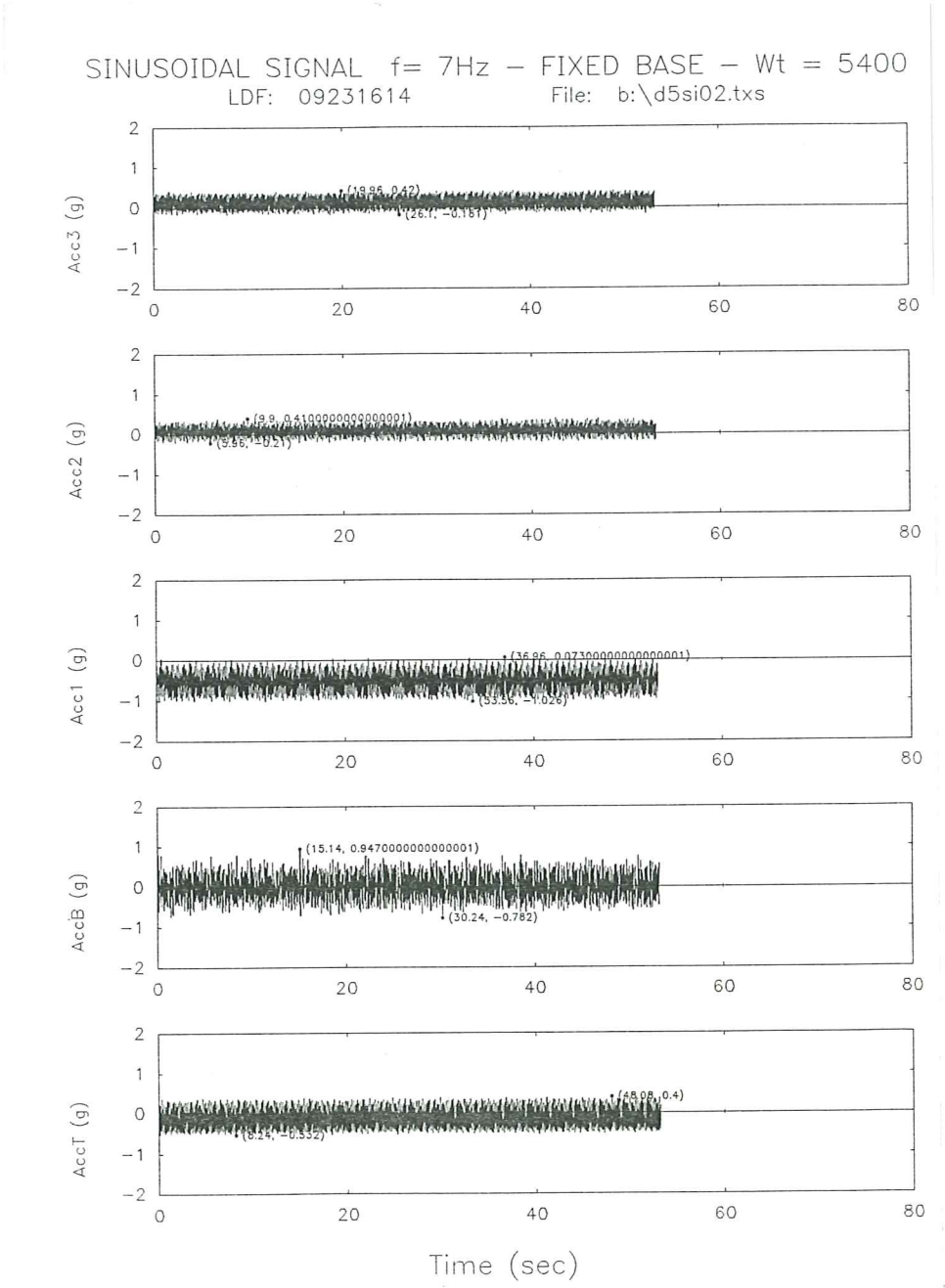

Fig. 21a. Acceleration time response for the fixed base model subected to a sinusoidal signal (f=7Hz).

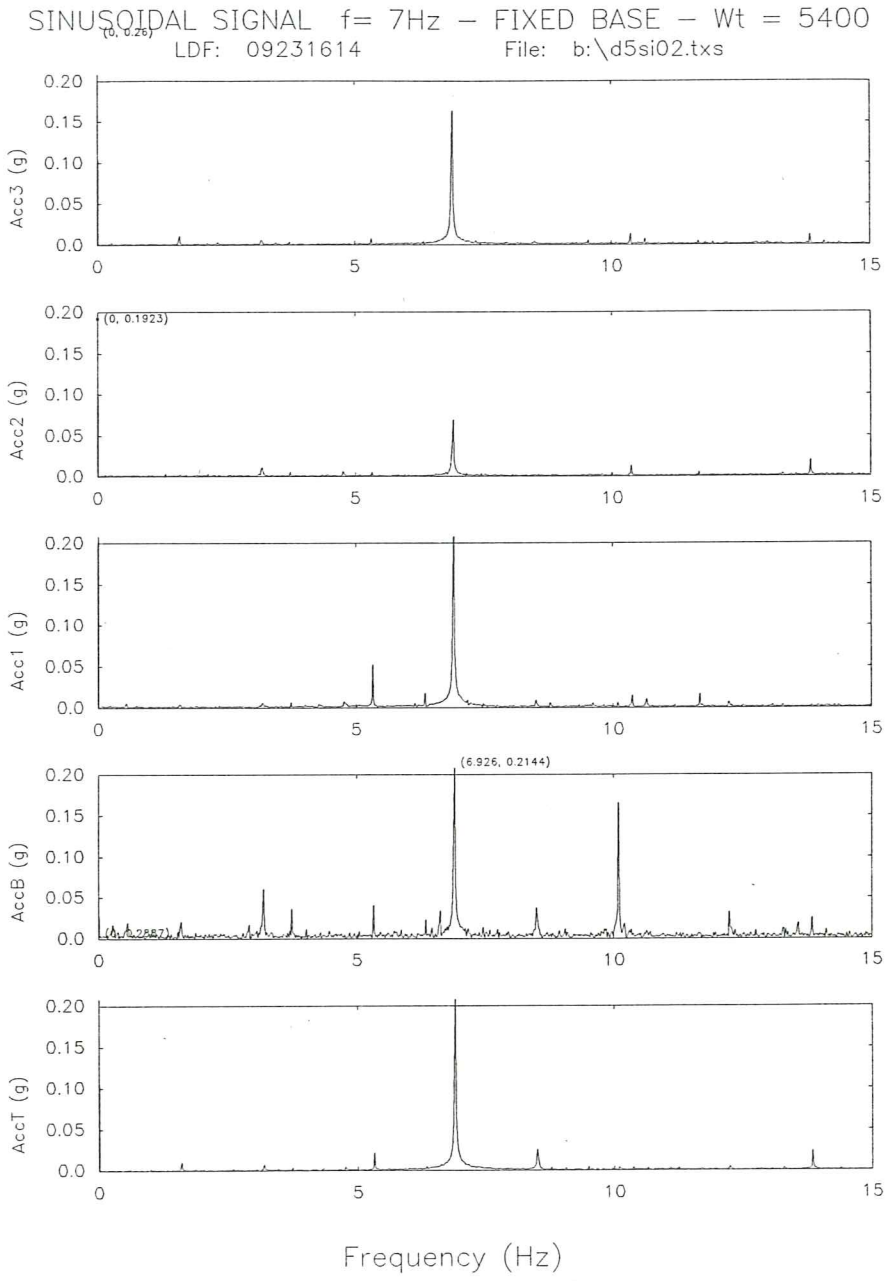

Fig. 21b. Fourier spectra of the accelerations for the fixed base model subjected to a sinusoidal signal (f=7Hz).

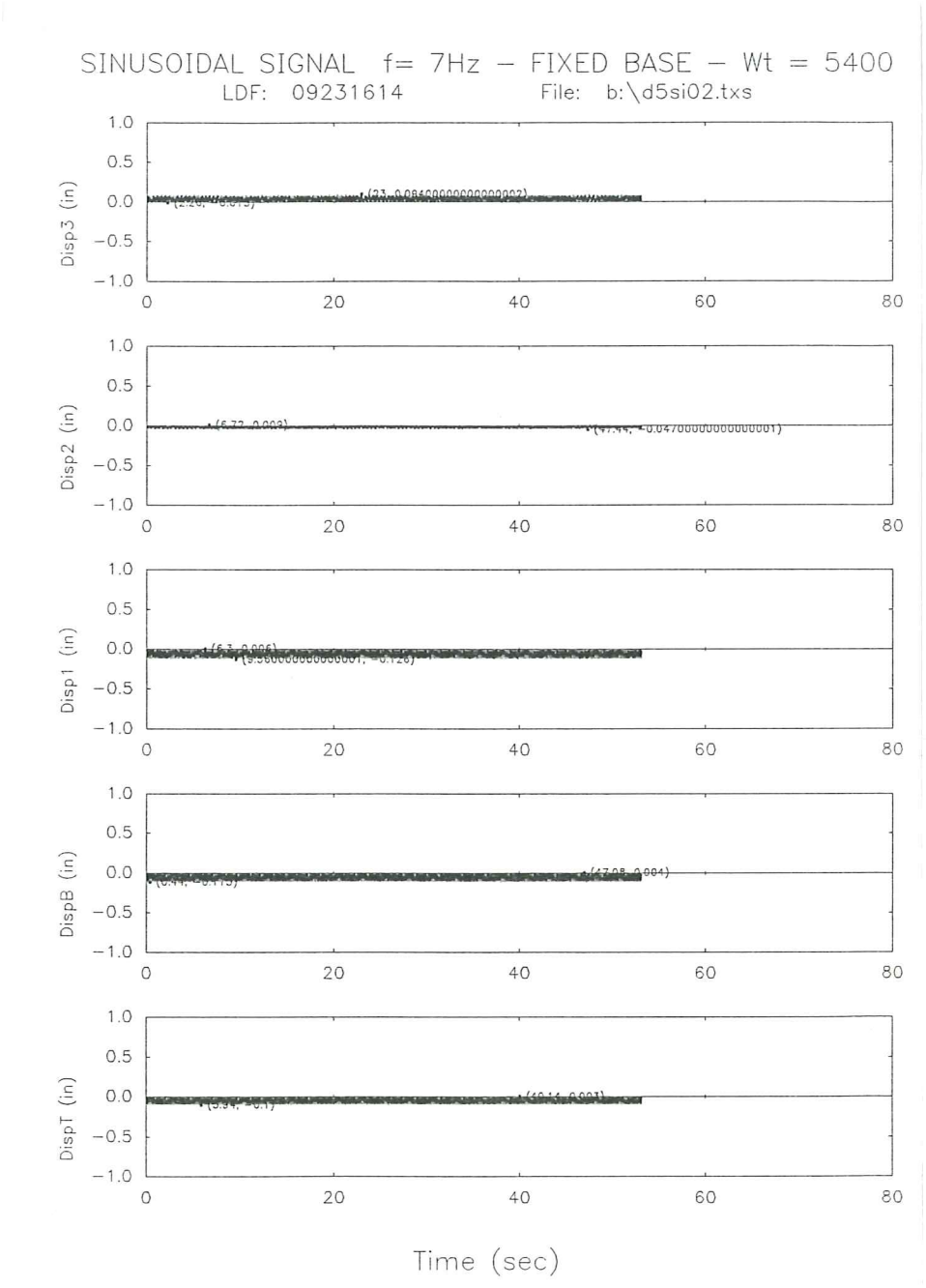

Fig. 21c. Displacement time responses for the fixed base model subjected to a sinusoidal signal (f=7Hz).

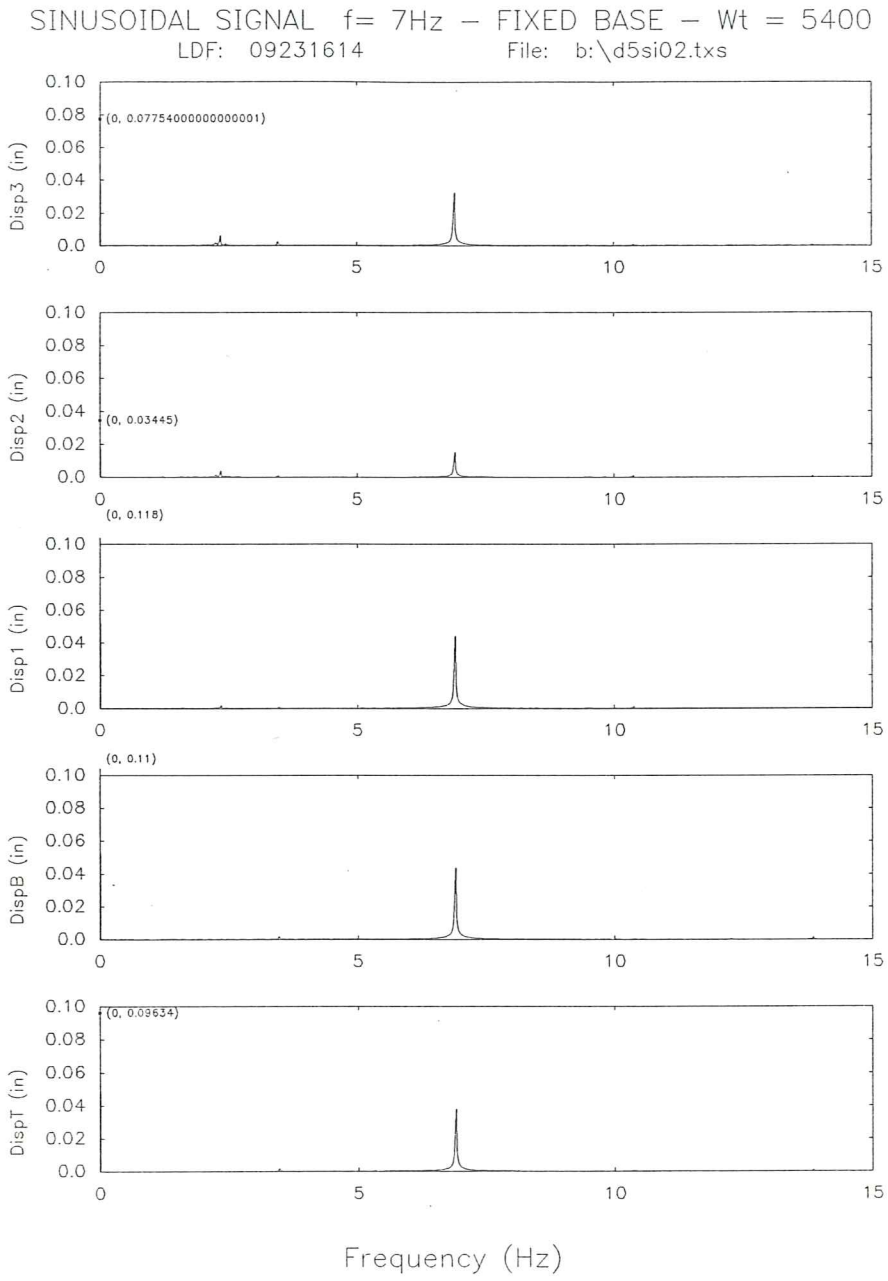

Fig. 21d. Fourier spectra of the displacements for the fixed base model subjected to a sinusidal signal (f=7Hz).

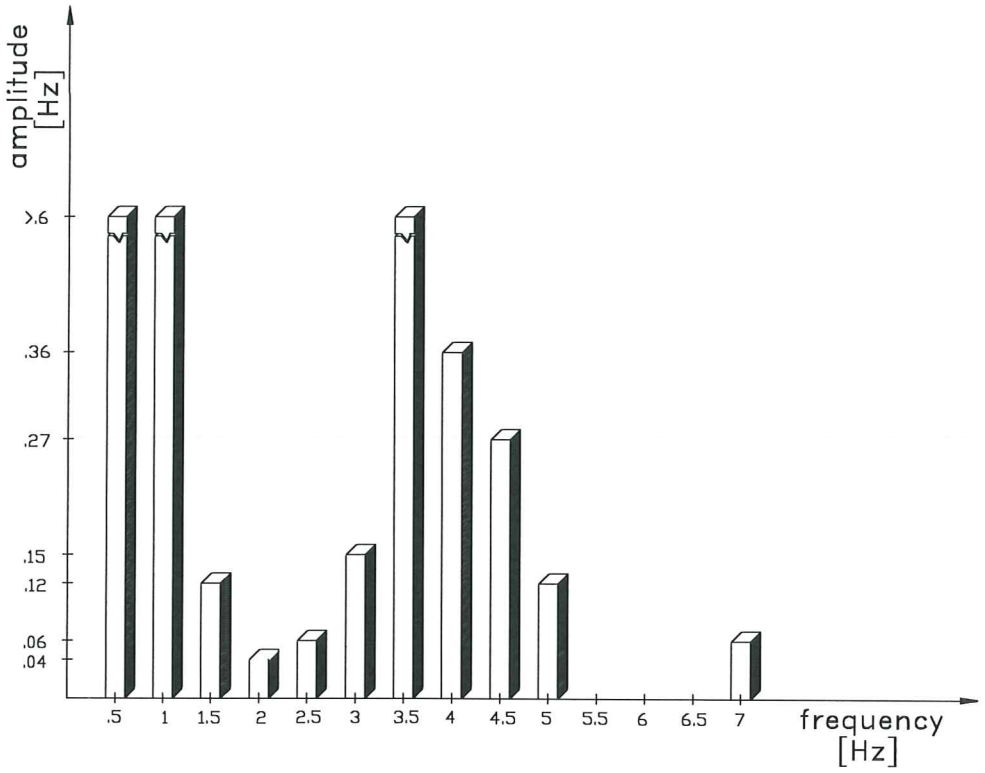

Fig. 22. Amplitude at rolling.

8.3 EARTHQUAKE MOTION TEST RESULTS

The behaviour of the base isolated model and the fixed base model under the same input earthquake was analysed and developed.

The isolated model response is compared to the fixed model one.

- El Centro

The Fourier spectra of the ground displacements of this signal present high peak values for frequencies between 0.5Hz and 1.5Hz (Figure 13a), that is far from the first natural frequency of the system. In this range of frequencies the isolation system does not work and also the base isolated system behaves as a fixed base one (Figures 23, 24). The absolute displacement peak values are even higher for the base isolated model as the input displacement is slightly higher. The efficacy of the isolation system is evident for frequencies around the first natural frequency (2.5Hz), that is for frequencies with lower input energy content.

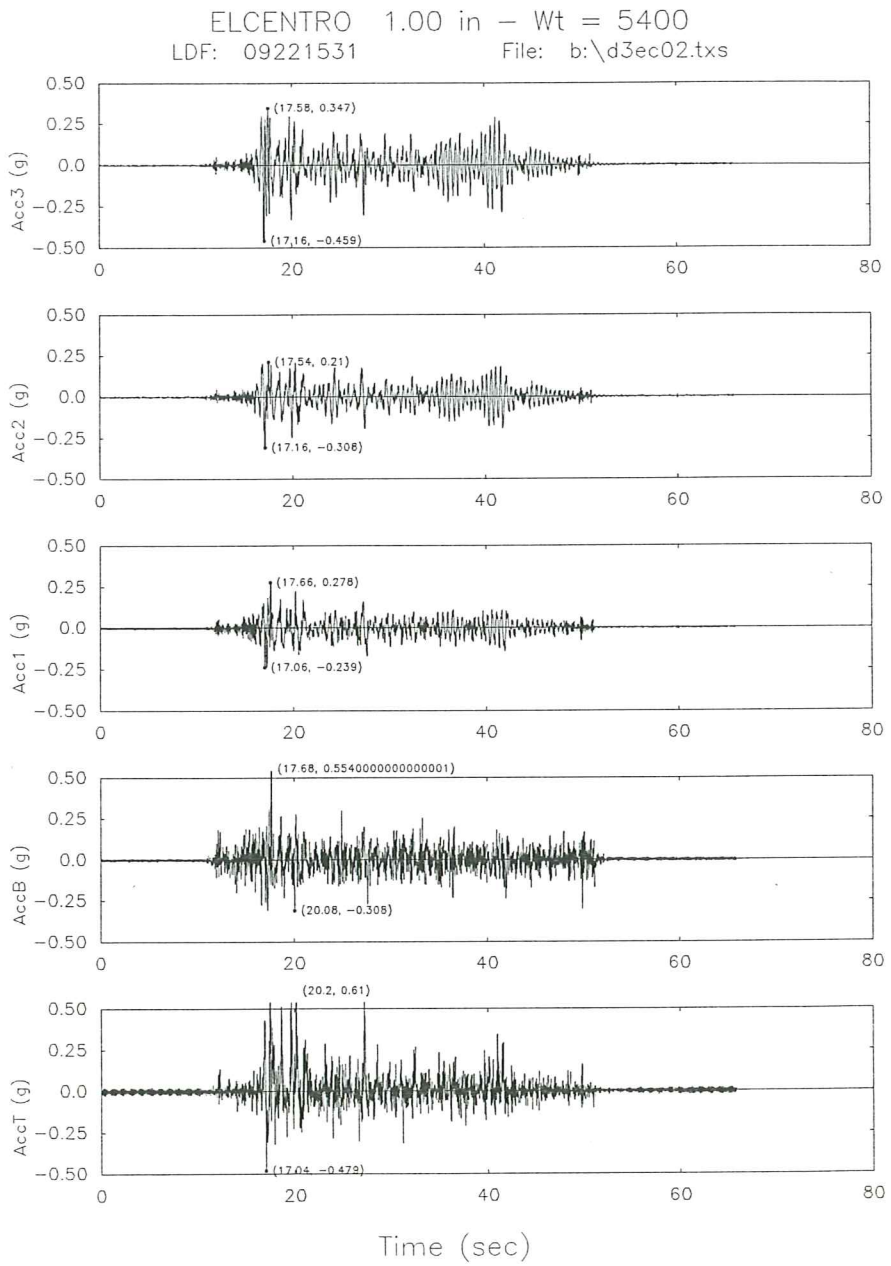

Fig. 23a. Acceleration time response for the base isolated model subjected to El Centro signal.

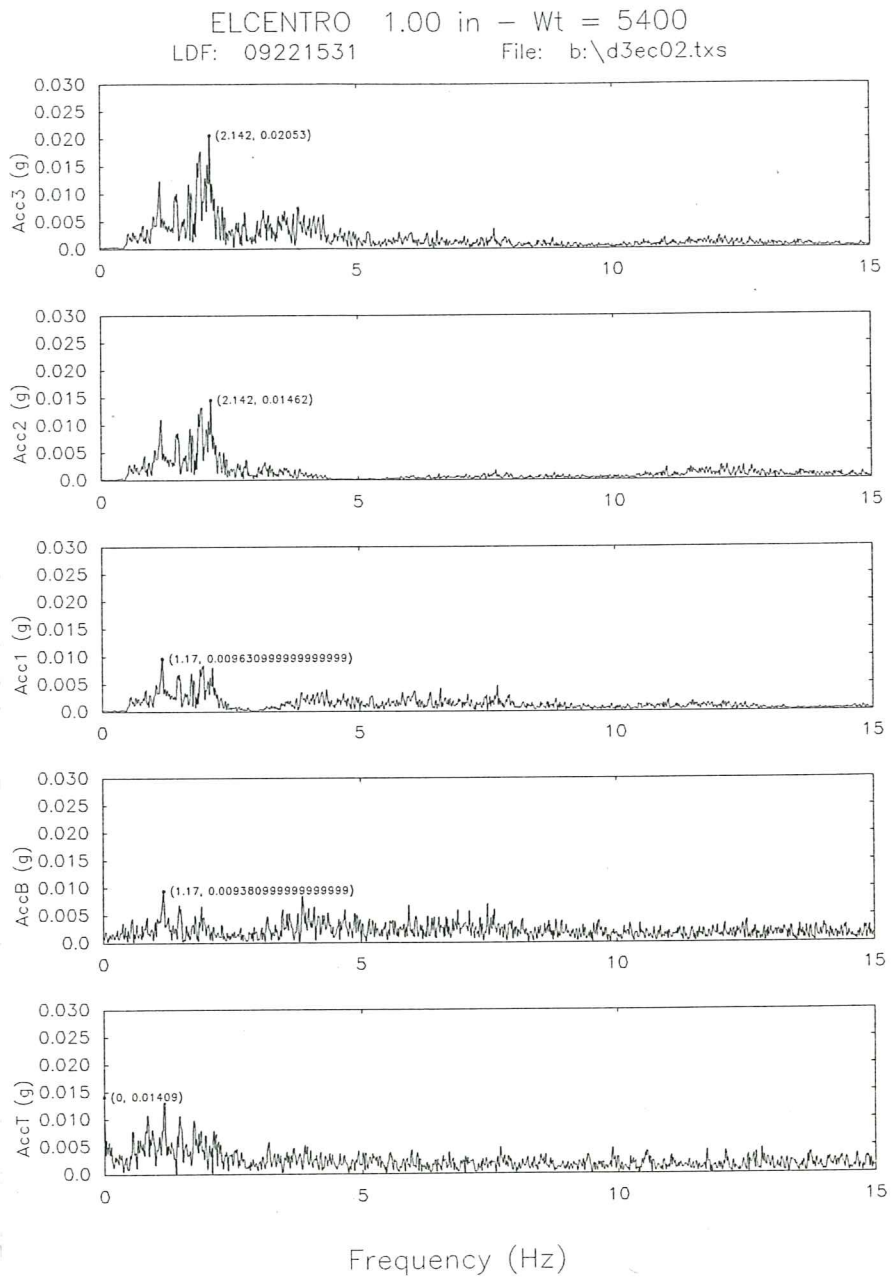

Fig. 23b. Fourier spectra of the accelerations for the base isolated model subjected to El Centro signal.

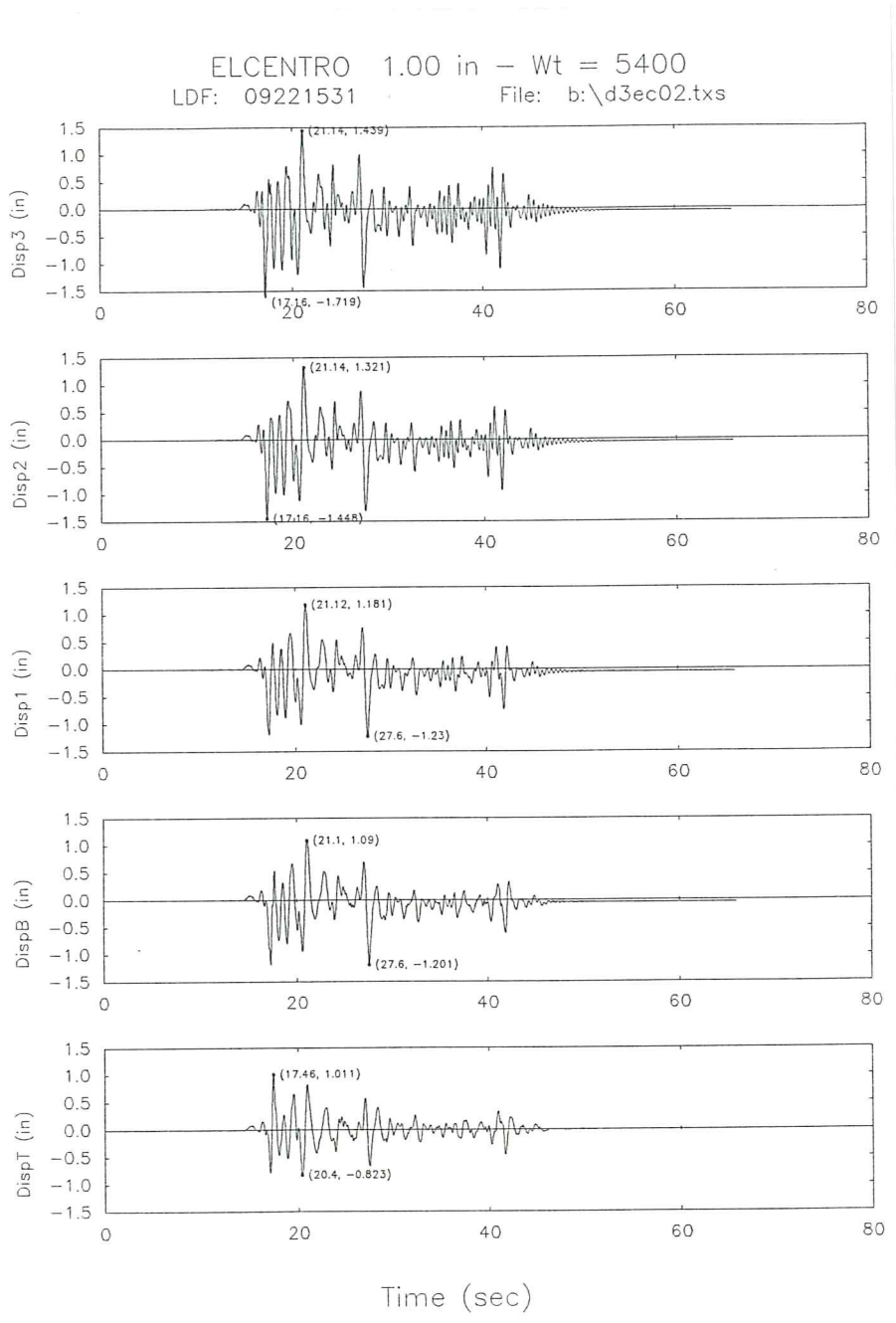

Fig. 23c. Displacement time responses for the base isolated model subjected to El Centro signal.

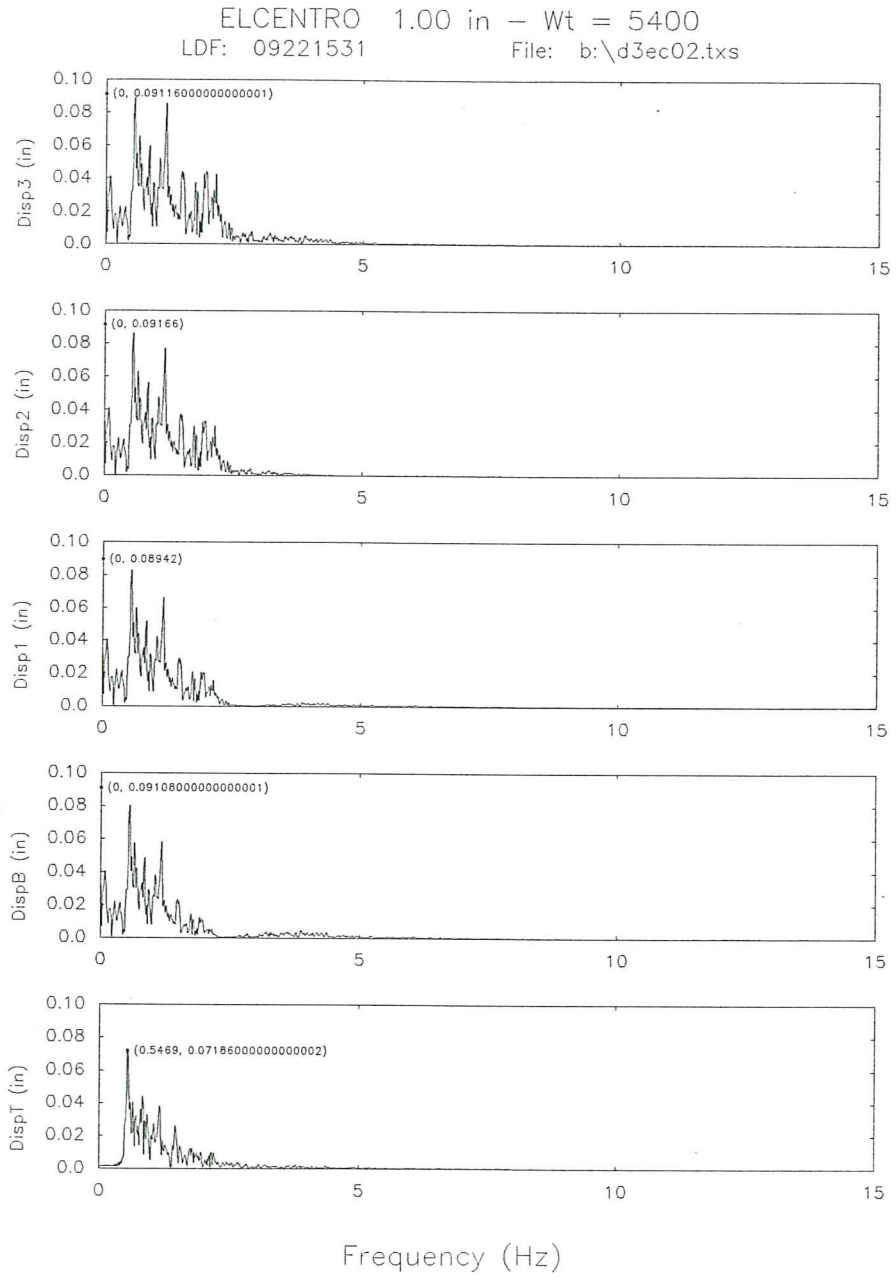

Fig. 23d. Fourier spectra of the displacements for the base isolated model subjected to El Centro signal.

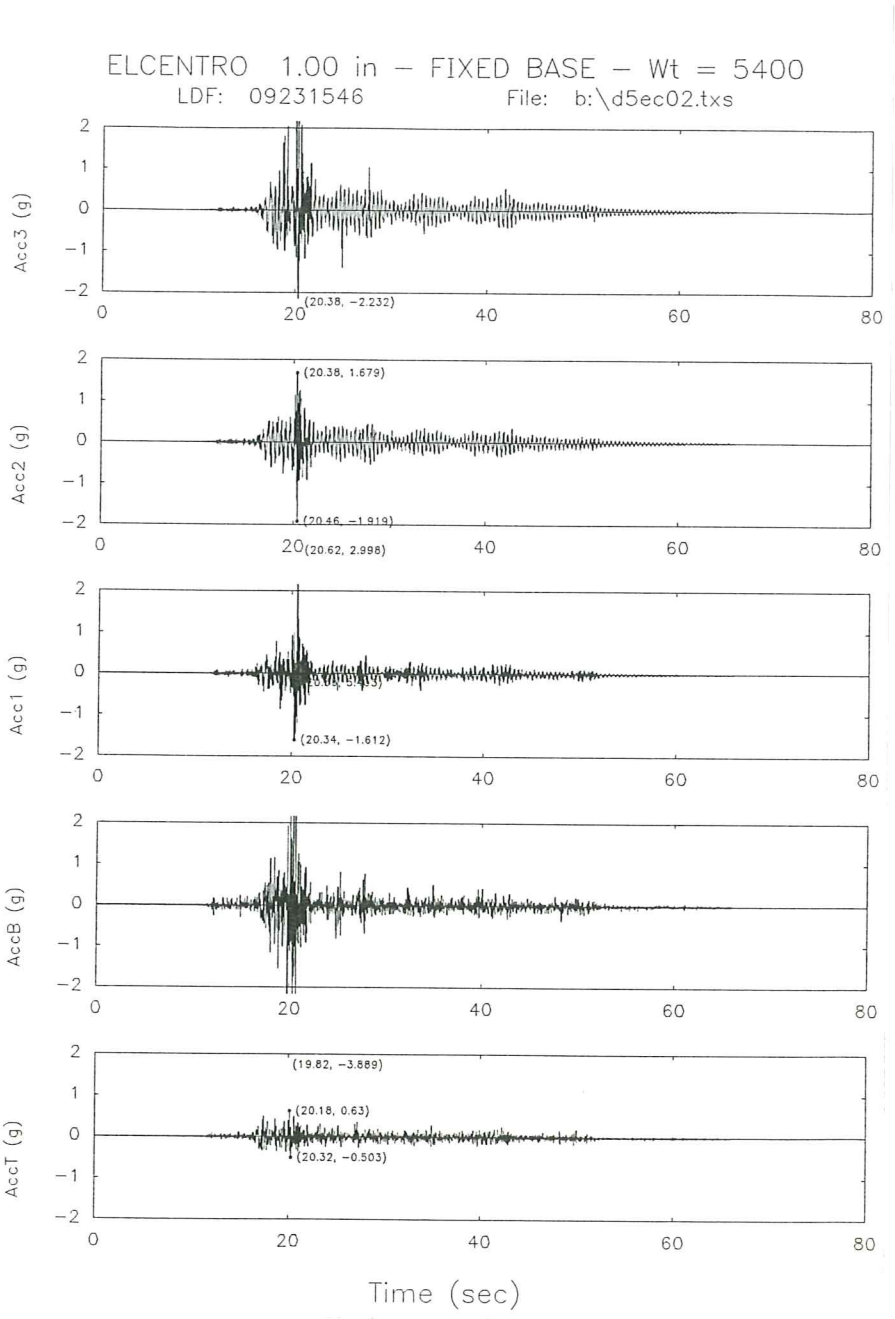

Fig. 24a. Acceleration time response for the fixed base model subected to El Centro signal.

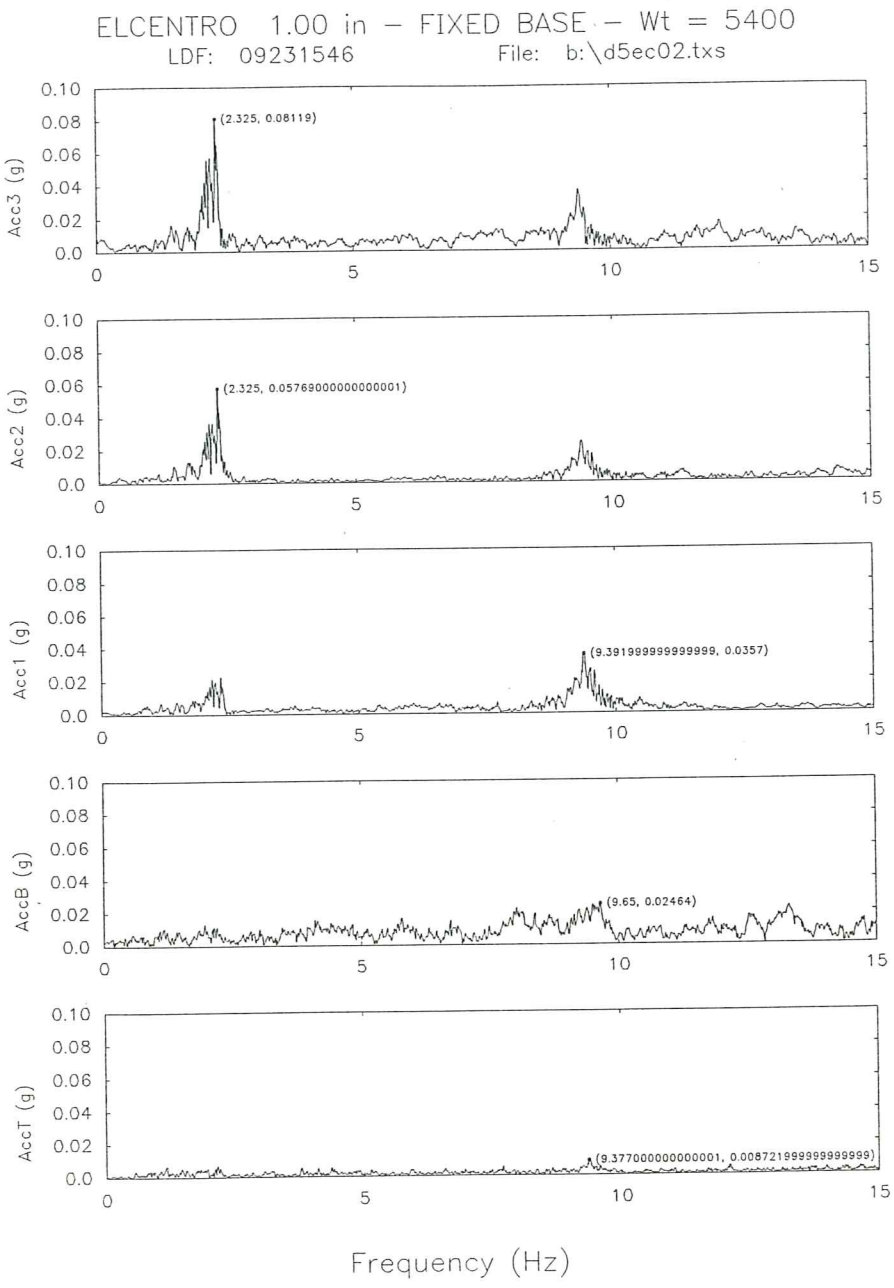

Fig. 24b. Fourier spectra of the accelerations for the fixed base model subjected to El Centro signal.

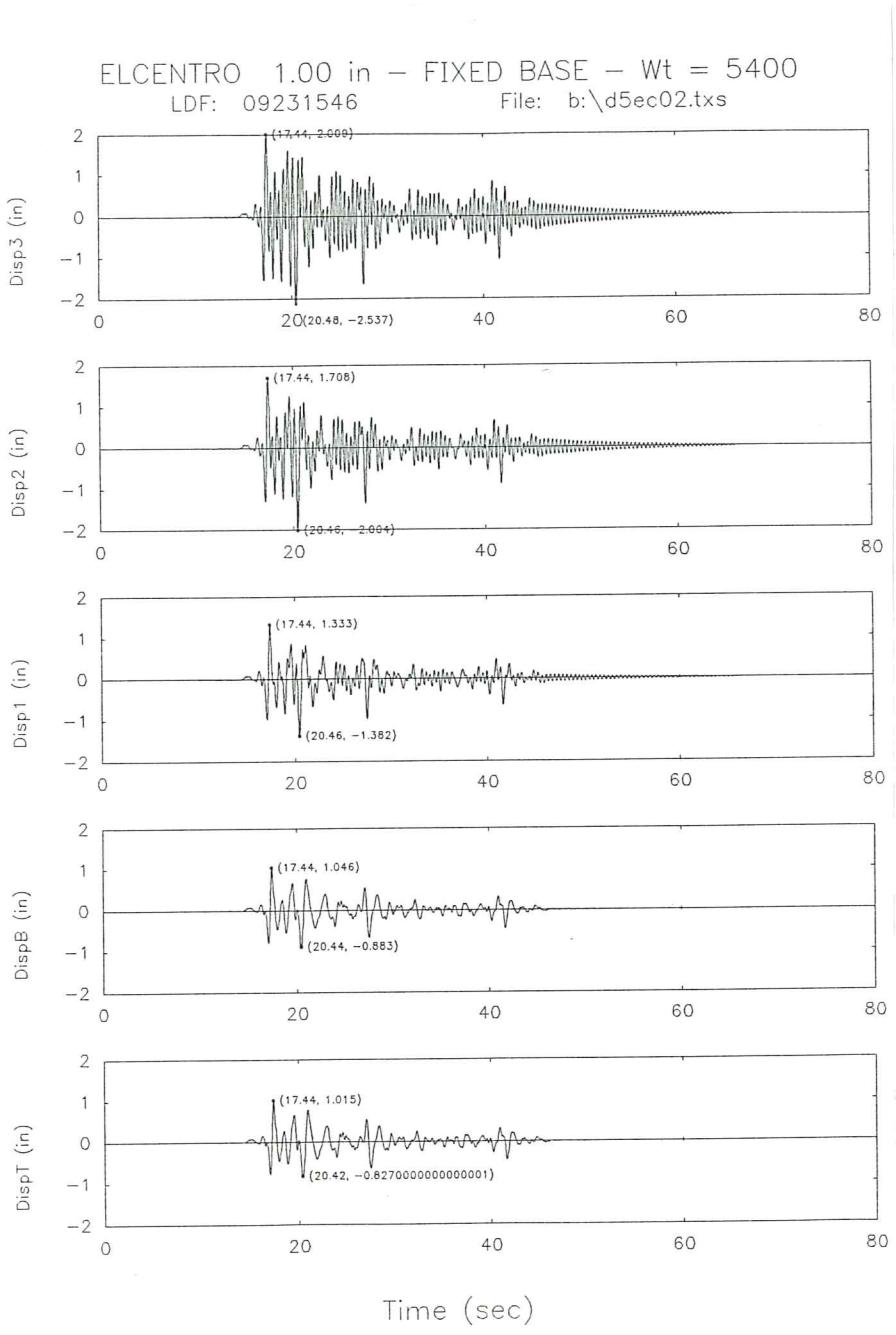

Fig. 24c. Displacement time responses for the fixed base model subjected to El Centro signal.

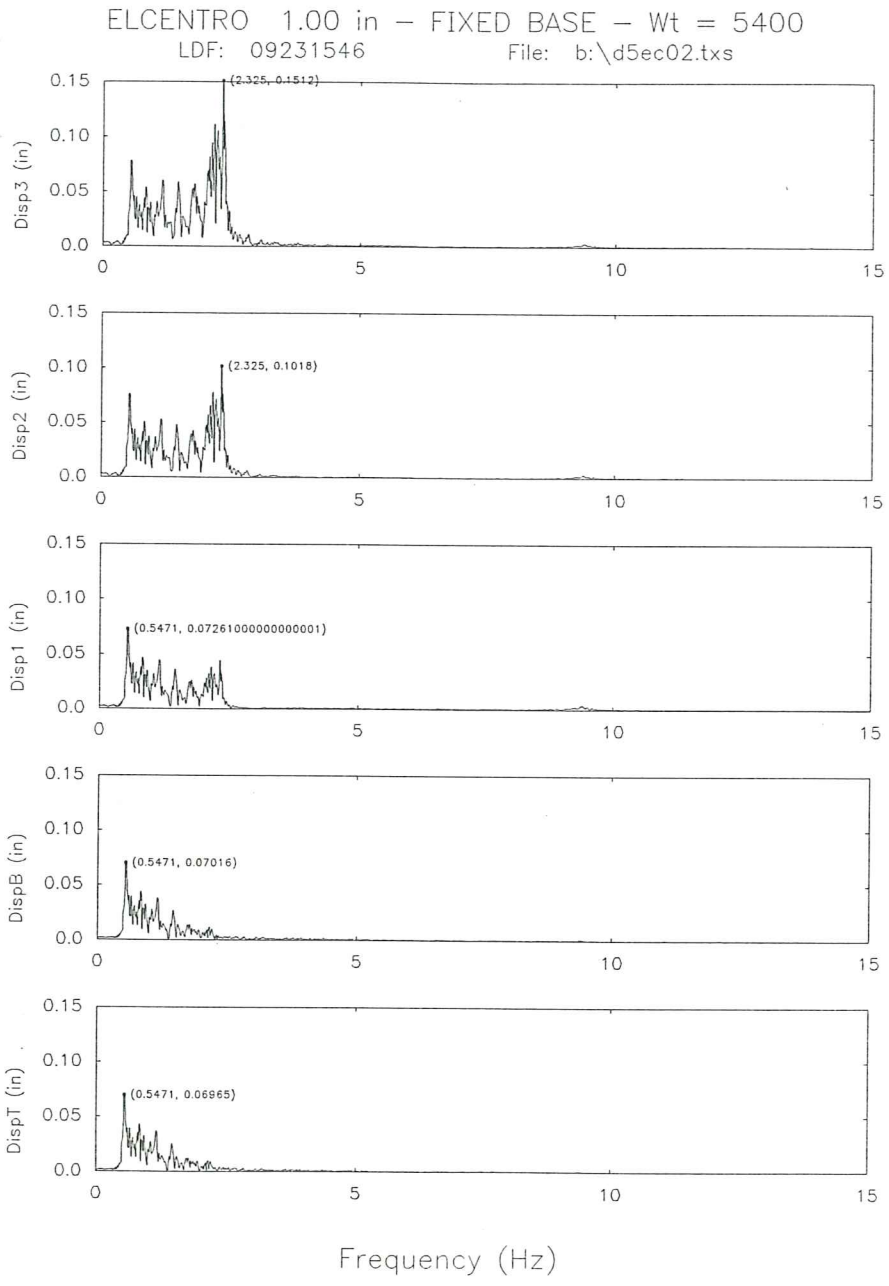

Fig. 24d. Fourier spectra of the displacements for the fixed base model subjected to El Centro signal.

- Parkfield

Comparing the base isolated system with the fixed base one it is possible to notice that the absolute displacements tend to zero more rapidly. The displacement peaks are lower in the important range of frequencies around 2.5Hz. Moreover there is a peak close to 0 Hz frequency which is not present in the fixed frame (Figures 25, 26).

- Dumbarton

The Fourier spectra of the displacements of this signal shows resonance effects for very low frequencies, less than 0.9Hz (Figure 13b), far from the first natural frequency of the system (2.5Hz). The isolation system has no efficacy because it does not start to work for the low frequencies excited by this signal (Figure 27, 28). Both systems work as fixed base systems, with large displacements at low frequencies, which rapidly tend to zero for frequencies higher than the first natural frequency.

On the contrary the Fourier spectra of the accelerations presents lower peaks and wider distributions around 2.5 Hz and 8 Hz for the base isolated model. The reduction of the peaks is relevant for the acceleration responses at each floor.

The deflected shapes at maximum story displacements have been plotted for each signal and for the two different cases of base isolated model and fixed base model (Figures 29a, 29b, 29c, 29d).

Table T-4 shows the maximum shear values for the base isolated model and the fixed base one. In the last case it is possible to notice that the shear value is higher for the fixed base frame. This confirms the effectiveness of this new device in base isolating a structure.

Figures 30 show the F-δ diagrams for some interesting signals. F is the force at the base, while δ is the relative base displacement. It is especially evident the wide area of the hysteresis loops for the isolated model in response to El Centro earthquake with a maximum amplitude of 1.50 inch (Figures 30a). Therefore the base isolated system is able to dissipate a large amount of energy.

The same result can be achieved from the hysteresis cycles in Figures 30b, 30c, 30d for a sinusoidal signal (f=2Hz) and a sweep frequency signal for a base isolated model and a fixed base model where the base isolated system shows a wider hysteresis cycle.

In Figures 31 the base shear and displacement for the base isolated and the fixed base models subjected to a sweep frequency input are plotted in the time domain. It is possible to notice that in the fixed base system the base displacement is lower than in the isolated model while the base shear is higher, especially around 10÷12 seconds.

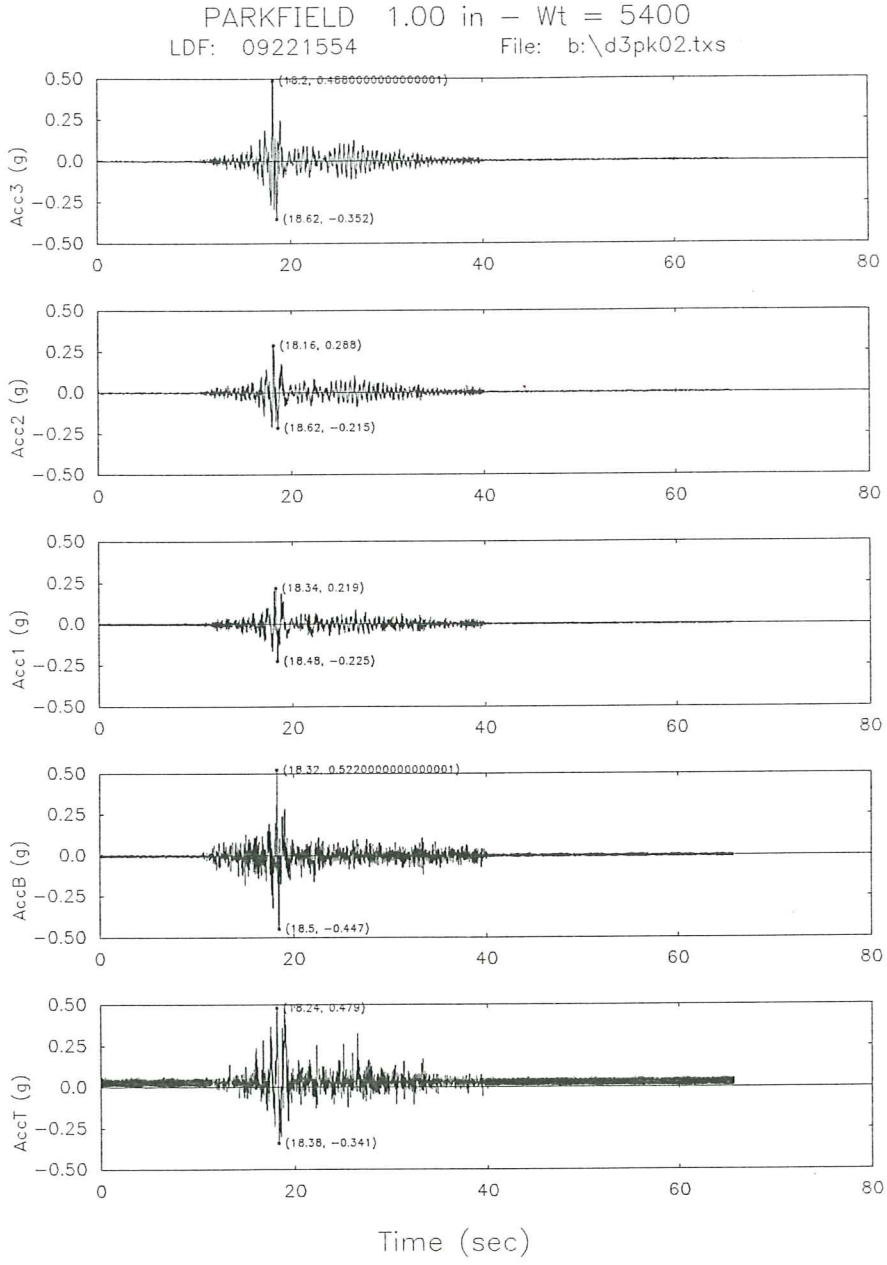

Fig. 25a. Acceleration time response for the base isolated model subjected to Parkfield signal.

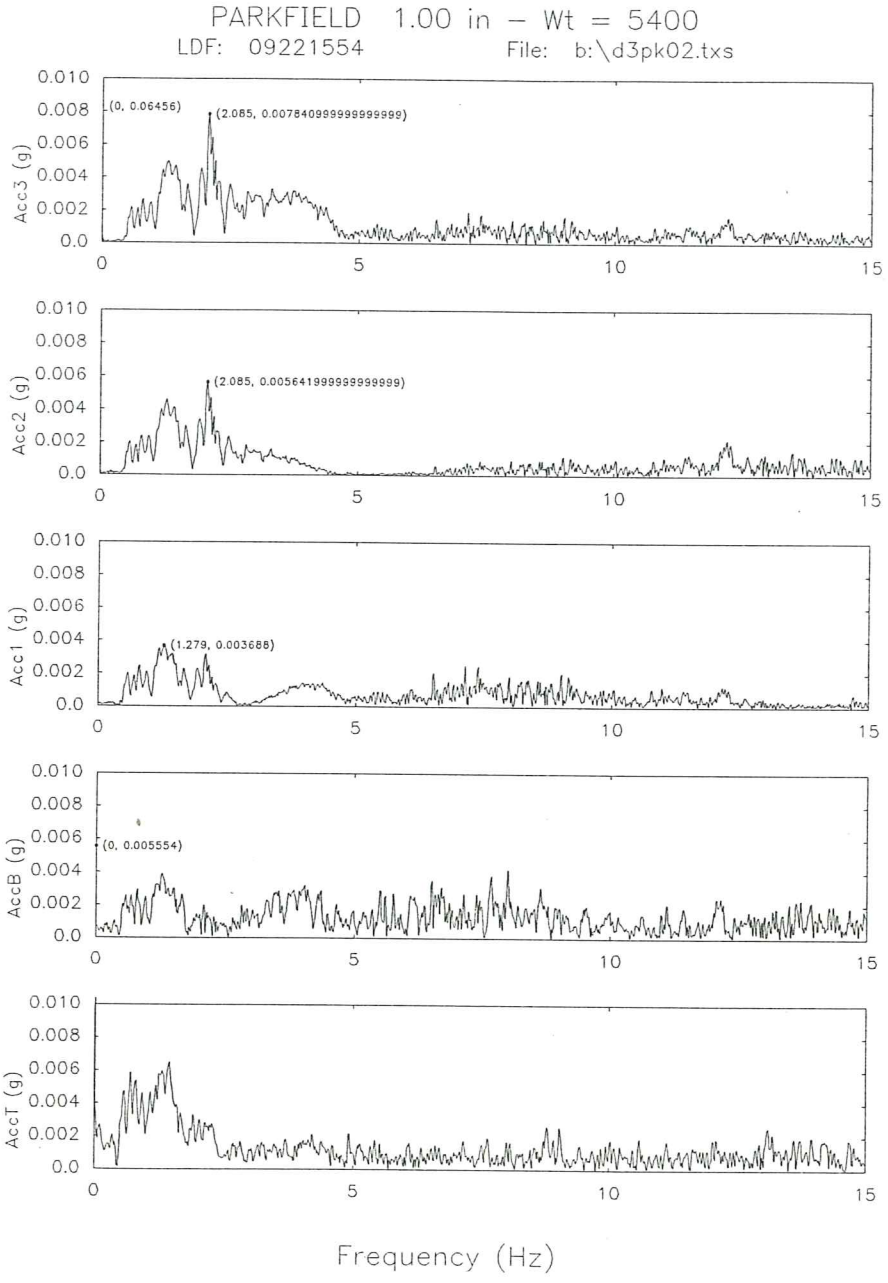

Fig. 25b. Fourier spectra of the accelerations for the base isolated model subjected to Parkfield signal.

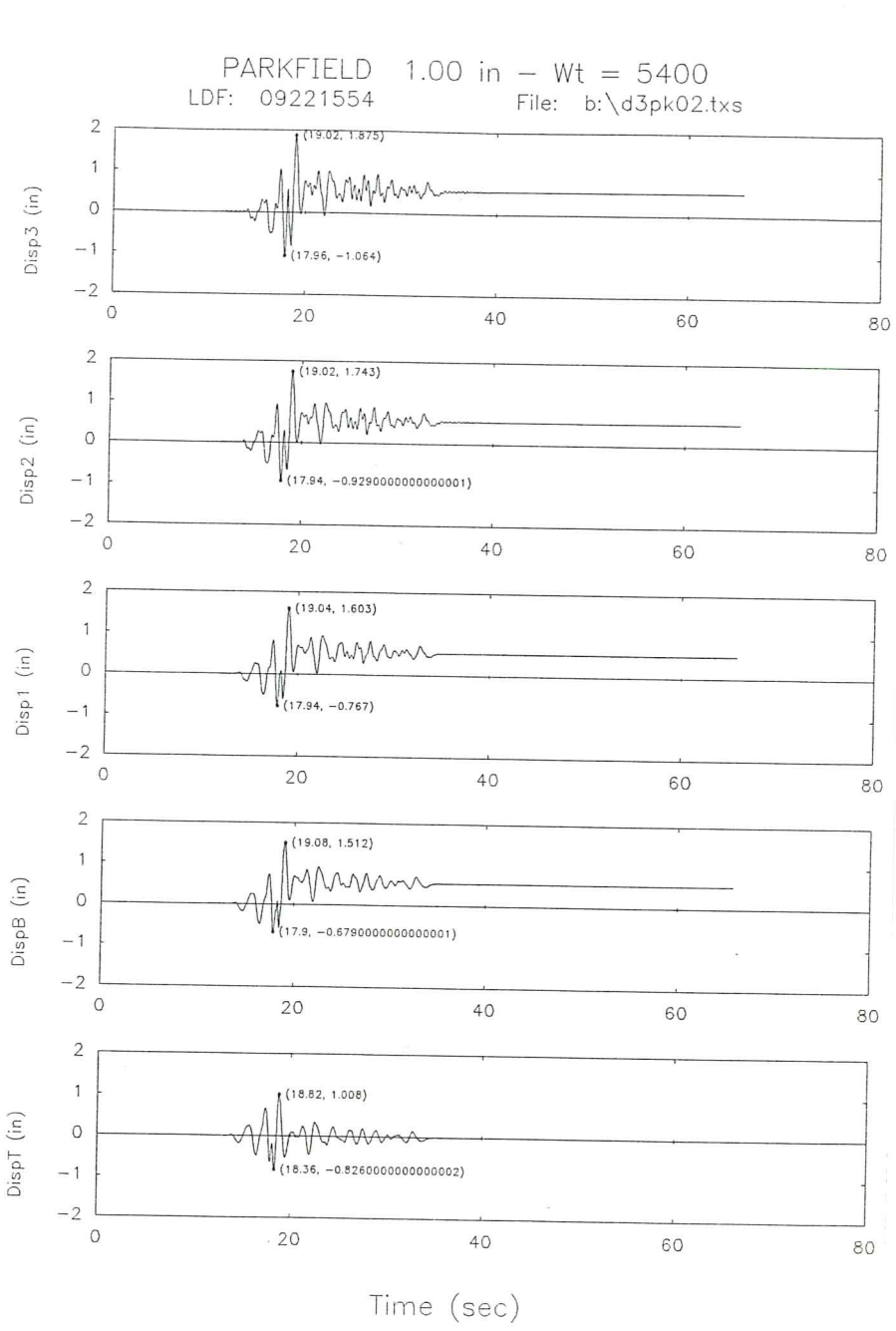

Fig. 25c. Displacement time responses for the base isolated model subjected to Parkfield signal.

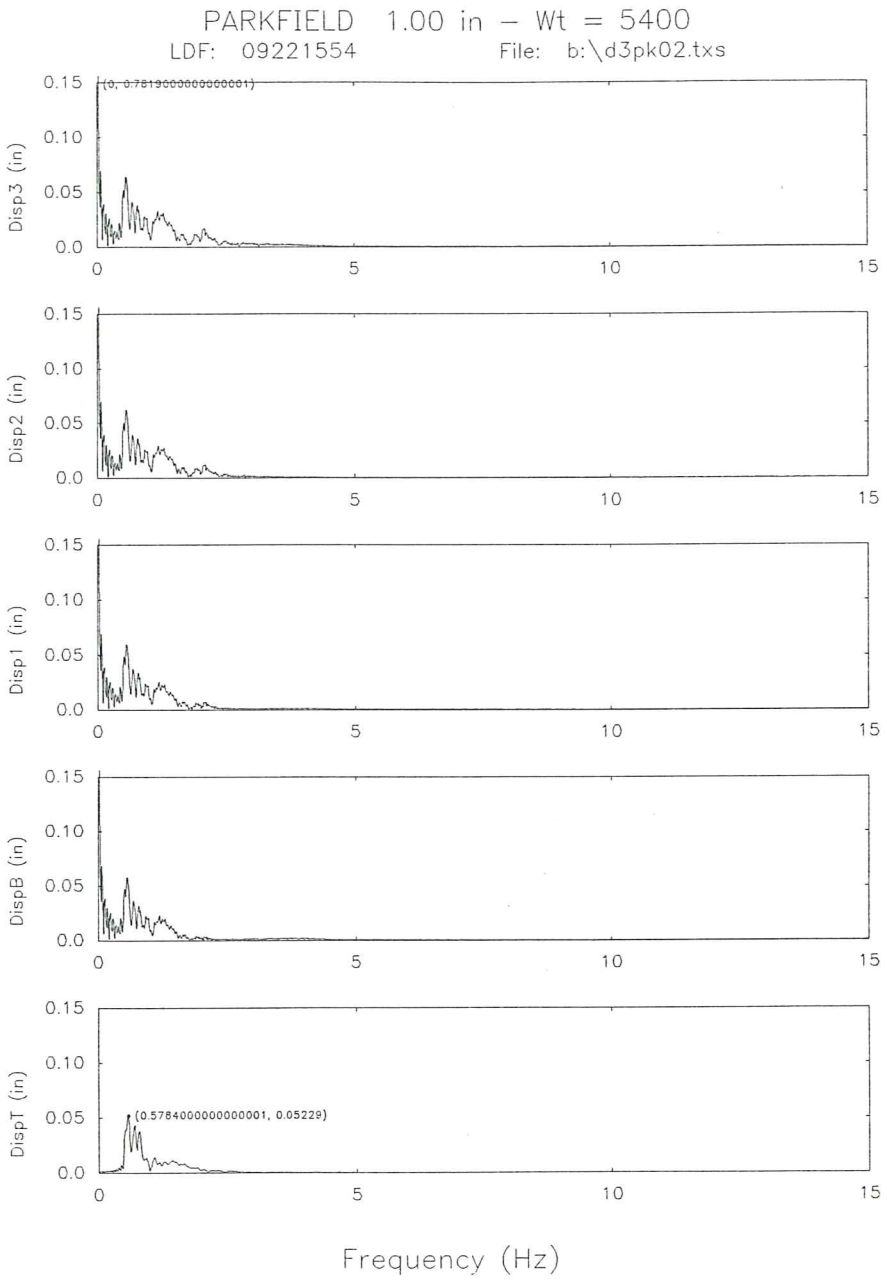

Fig. 25d. Fourier spectra of the displacements for the base isolated model subjected to Parkfield signal.

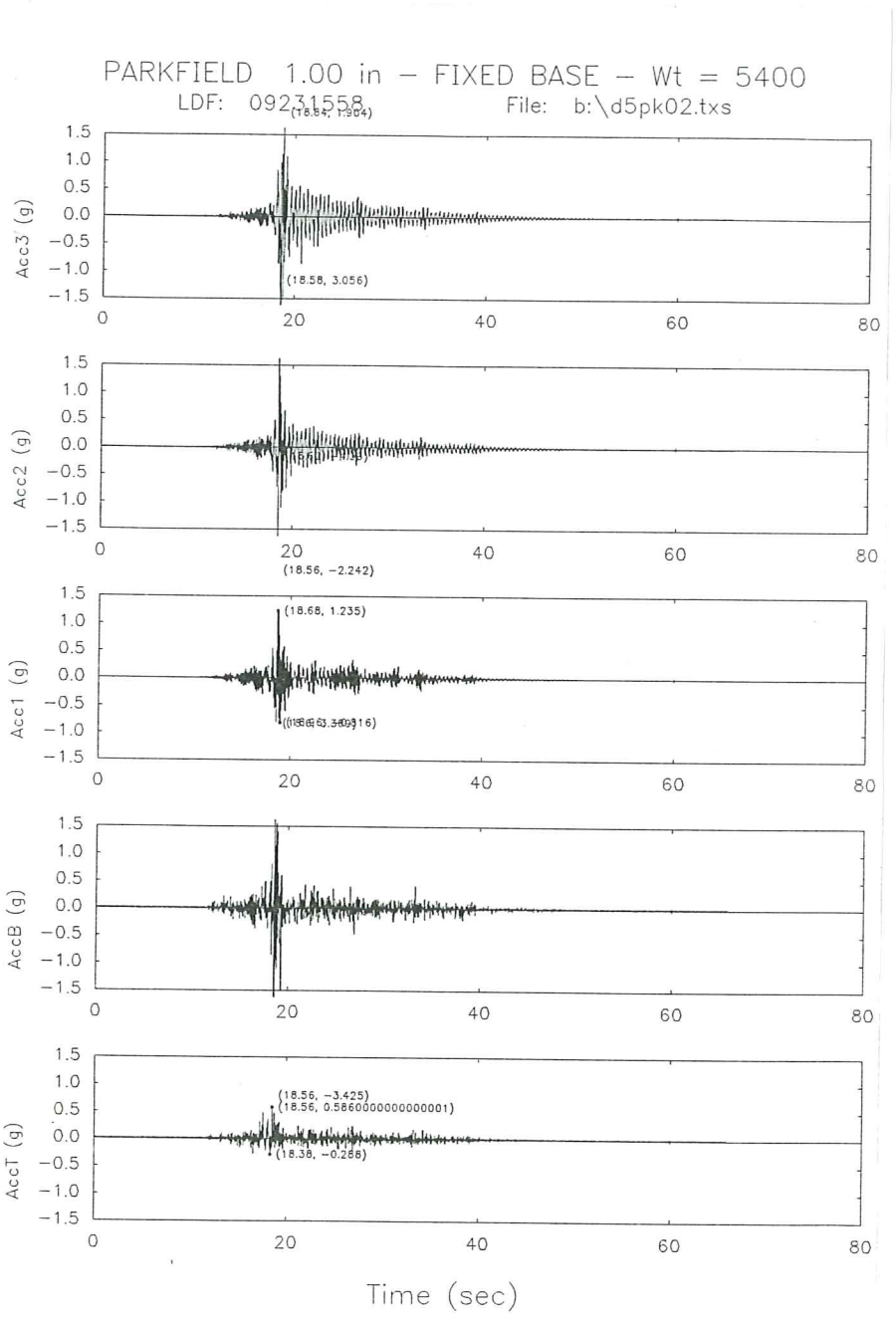

Fig. 26a. Acceleration time response for the fixed base model subected to Parkfield signal.

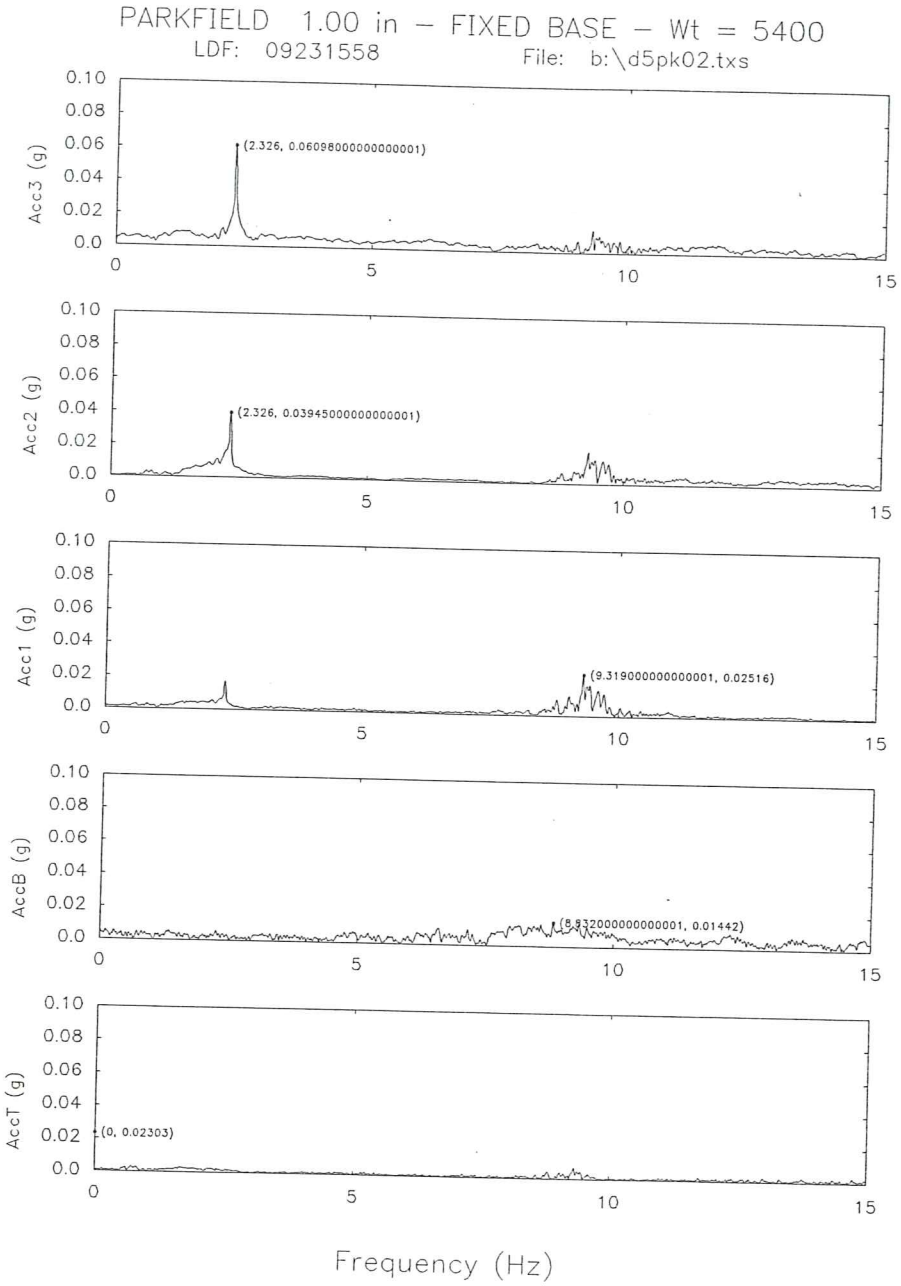

Fig. 26b. Fourier spectra of the accelerations for the fixed base model subjected to Parkfield signal.

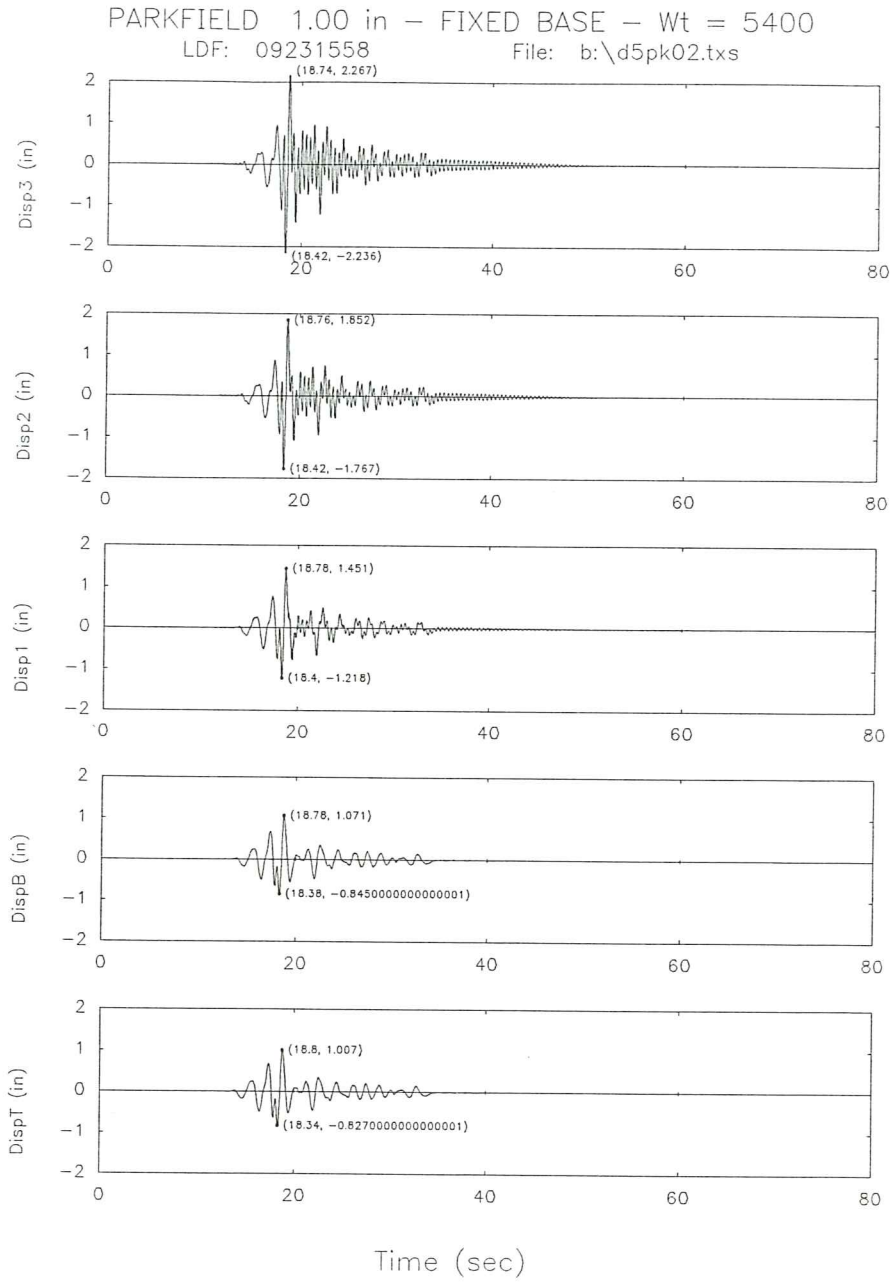

Fig. 26c. Displacement time responses for the fixed base model subjected to Parkfield signal.

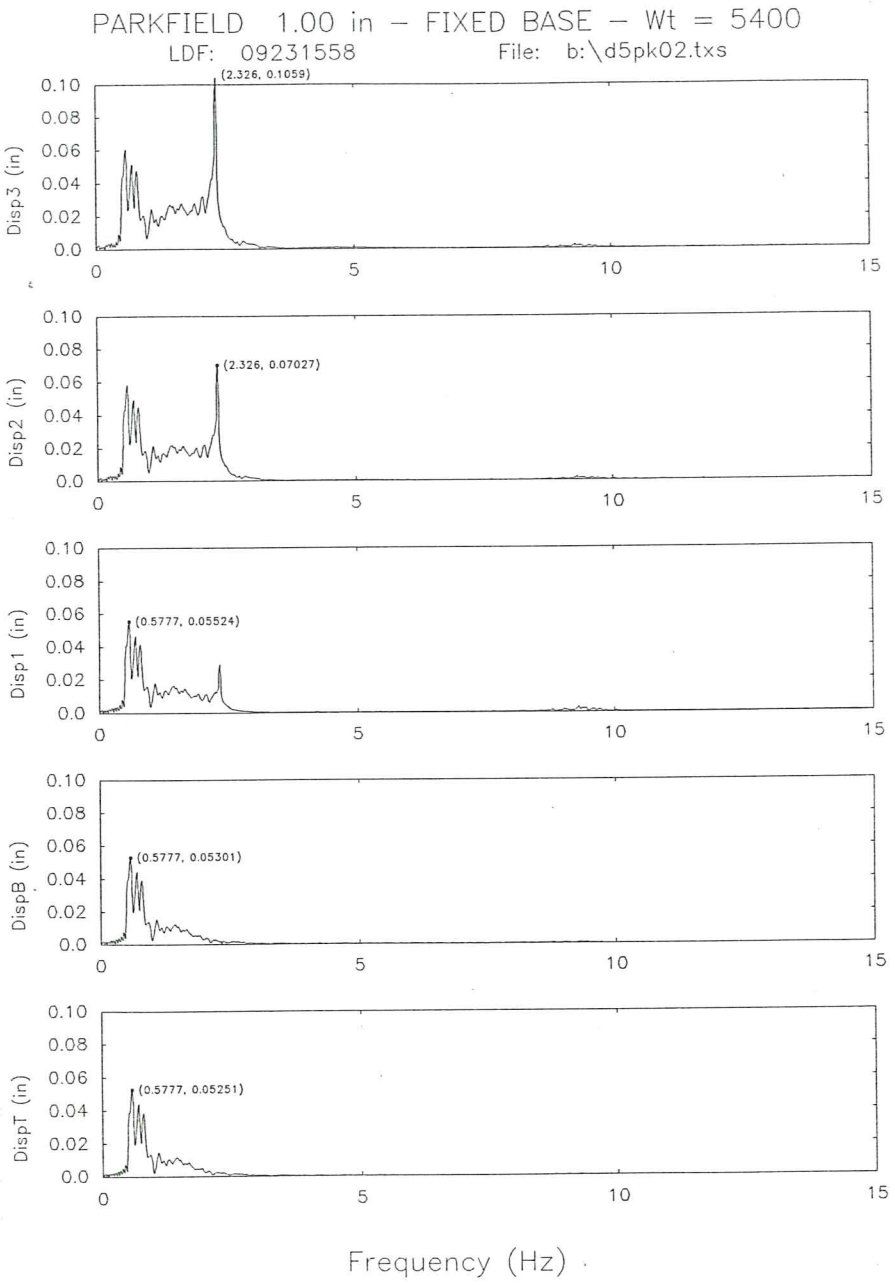

Fig. 26d. Fourier spectra of the displacements for the fixed base model subjected to Parkfield signal.

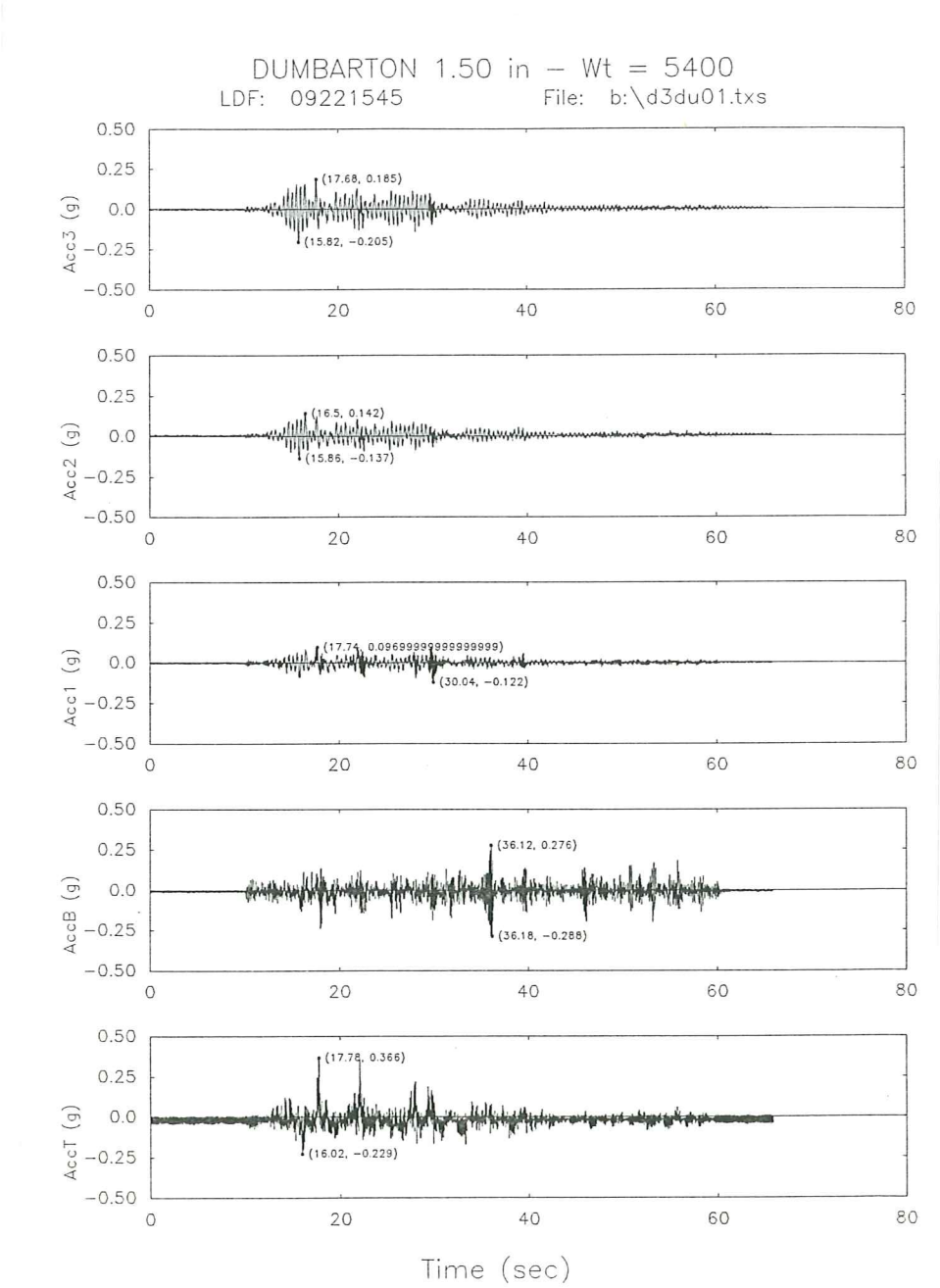

Fig. 27a. Acceleration time response for the base isolated model subjected to Dumbarton signal.

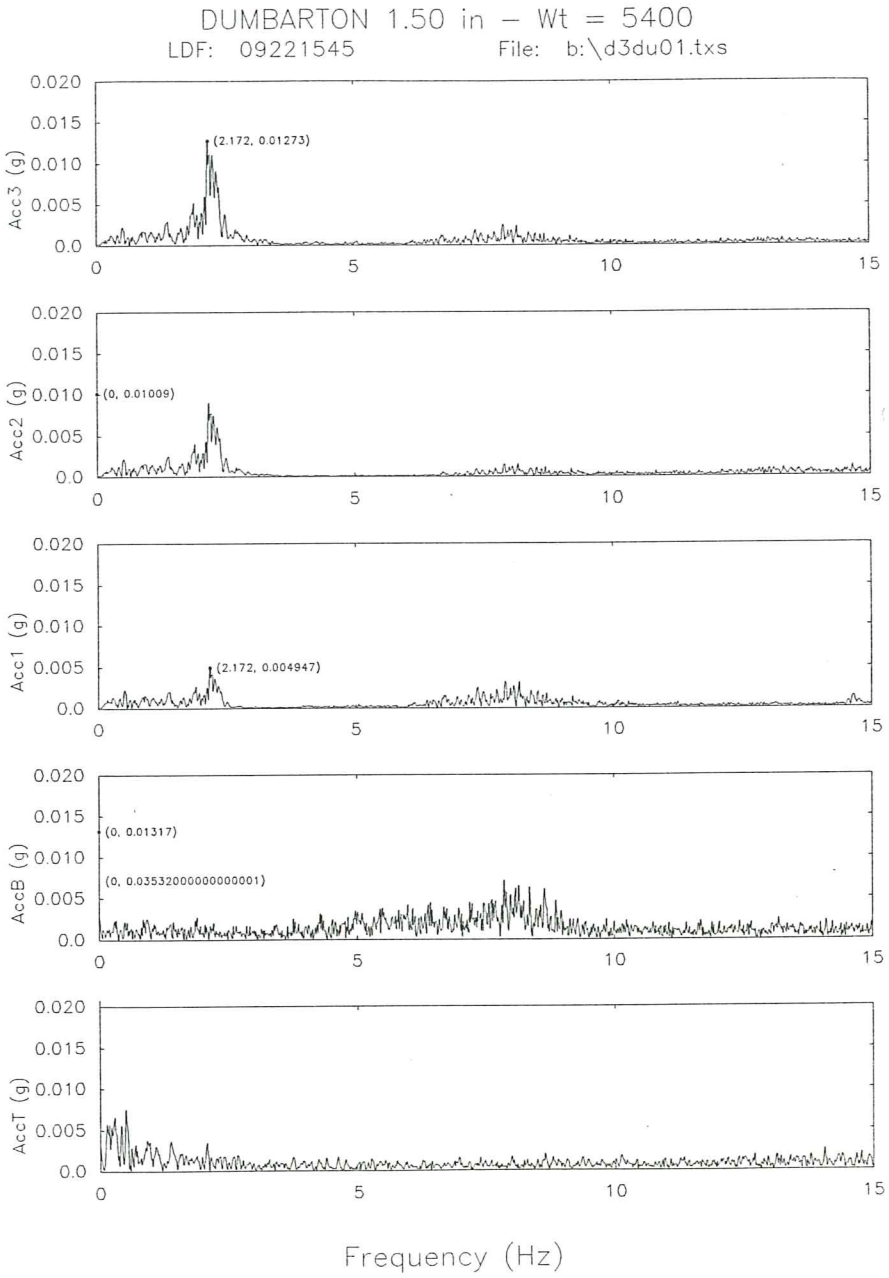

Fig. 27b. Fourier spectra of the accelerations for the base isolated model subjected to Dumbarton signal.

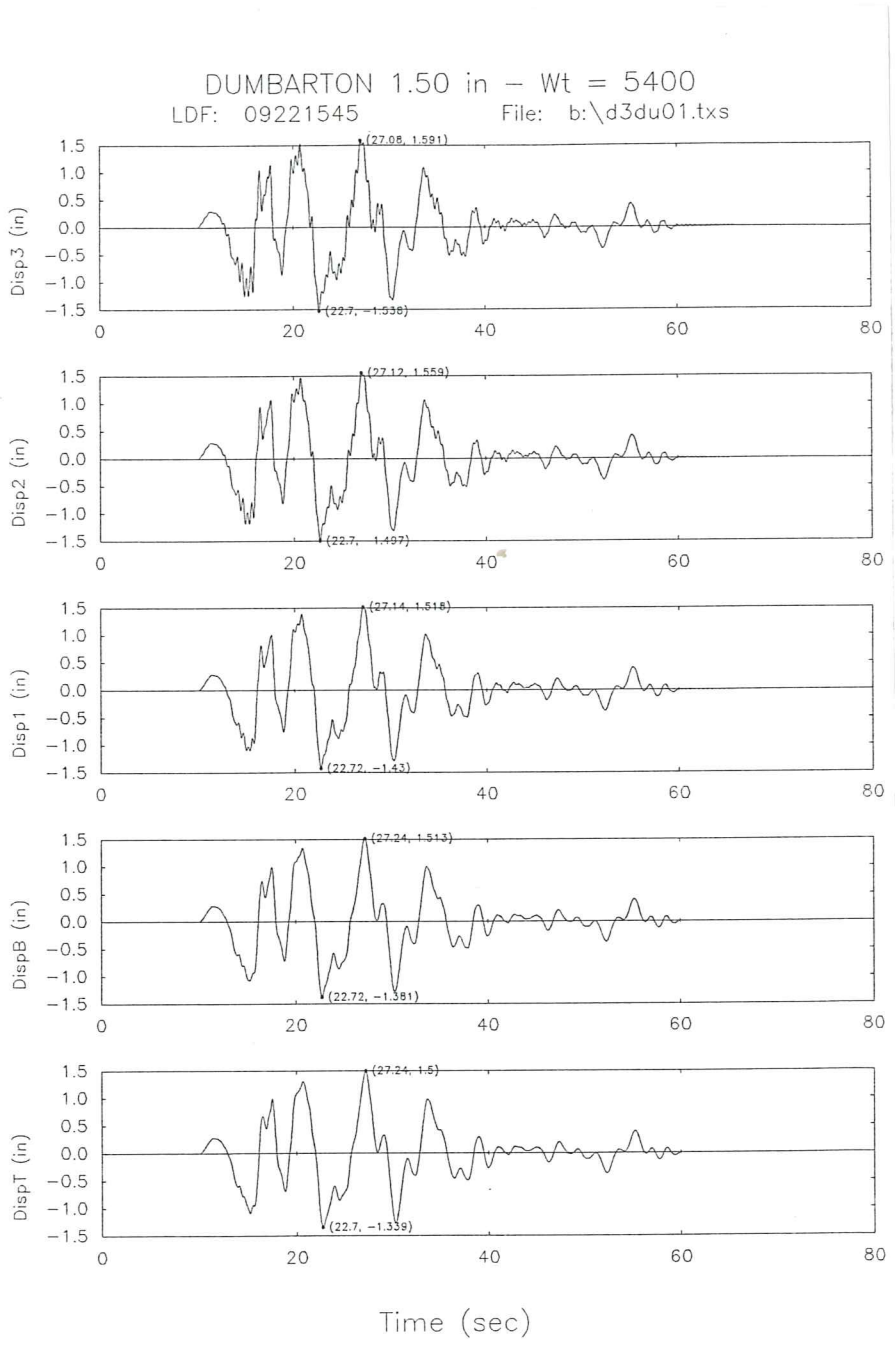

Fig. 27c. Displacement time responses for the base isolated model subjected to Dumbarton signal.

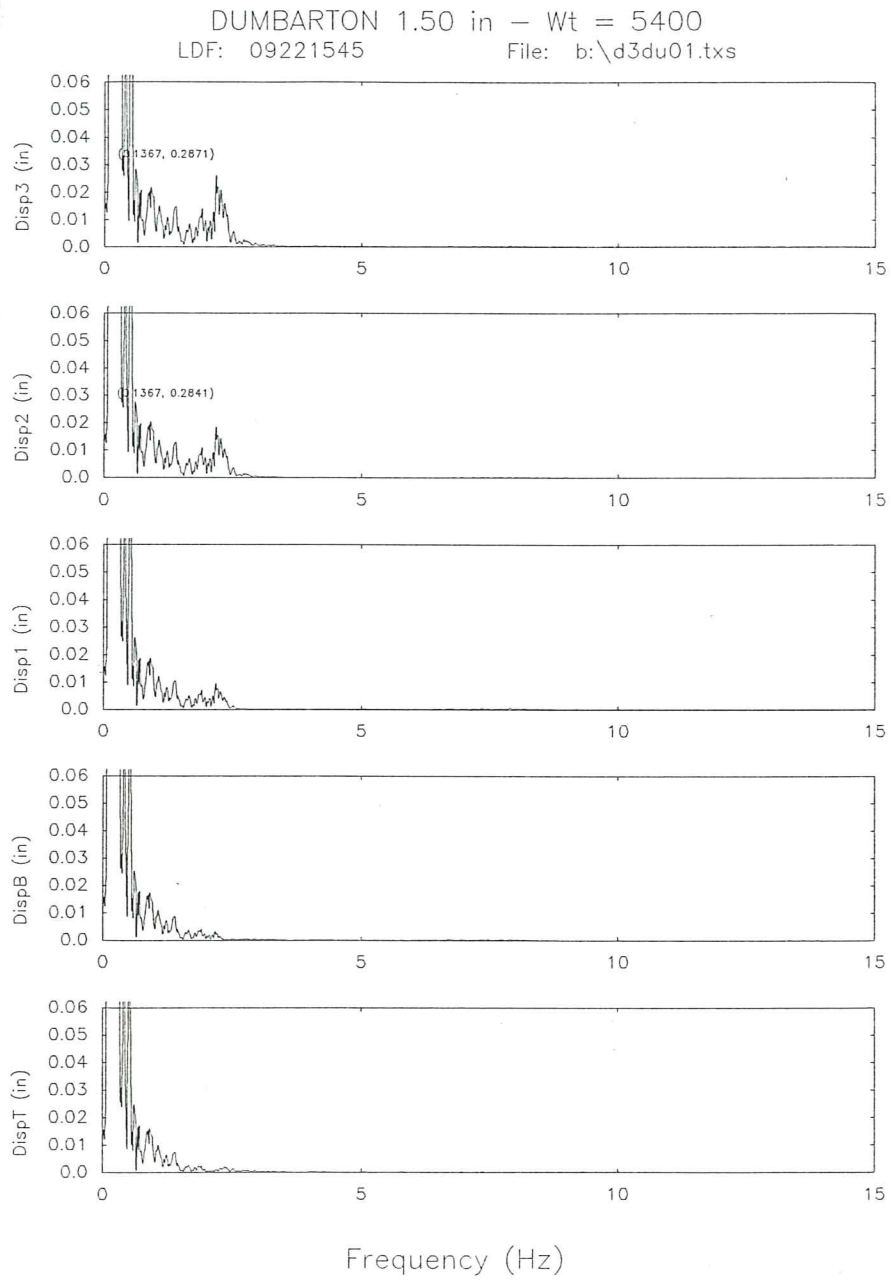

Fig. 27d. Fourier spectra of the displacements for the base isolated model subjected to Dumbarton signal.

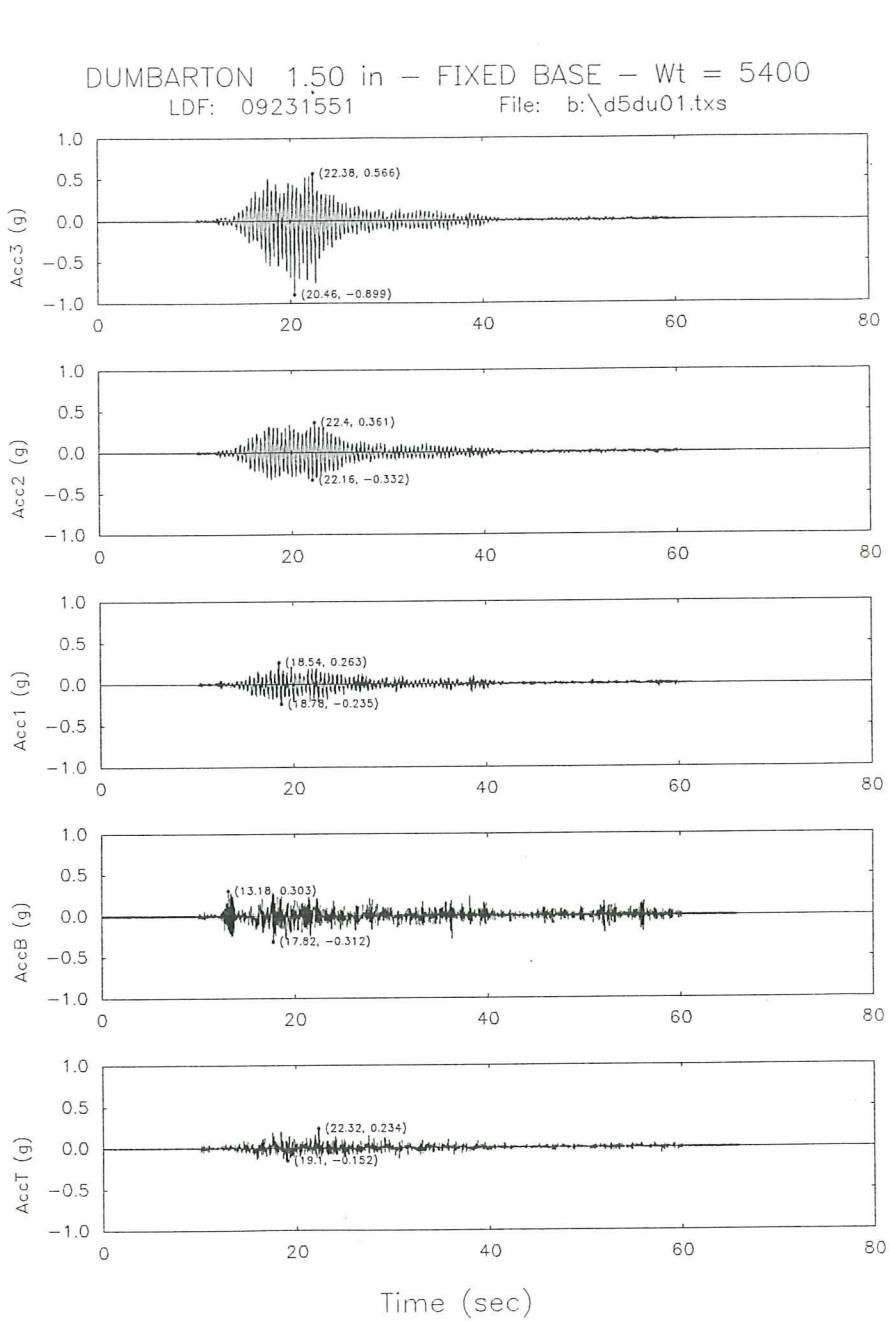

Fig. 28a. Acceleration time response for the fixed base model subected to Dumbarton signal.

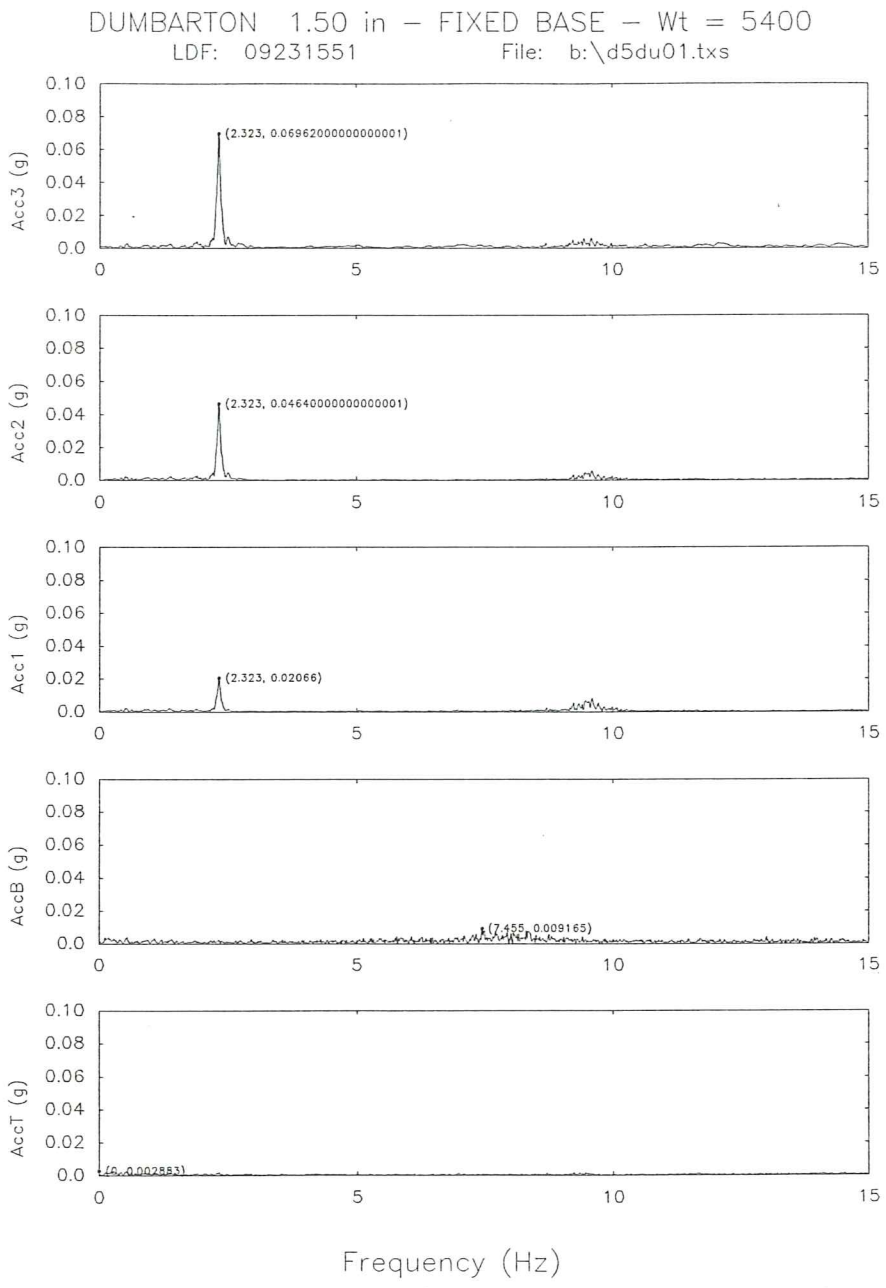

Fig. 28b. Fourier spectra of the accelerations for the fixed base model subjected to Dumbarton signal.

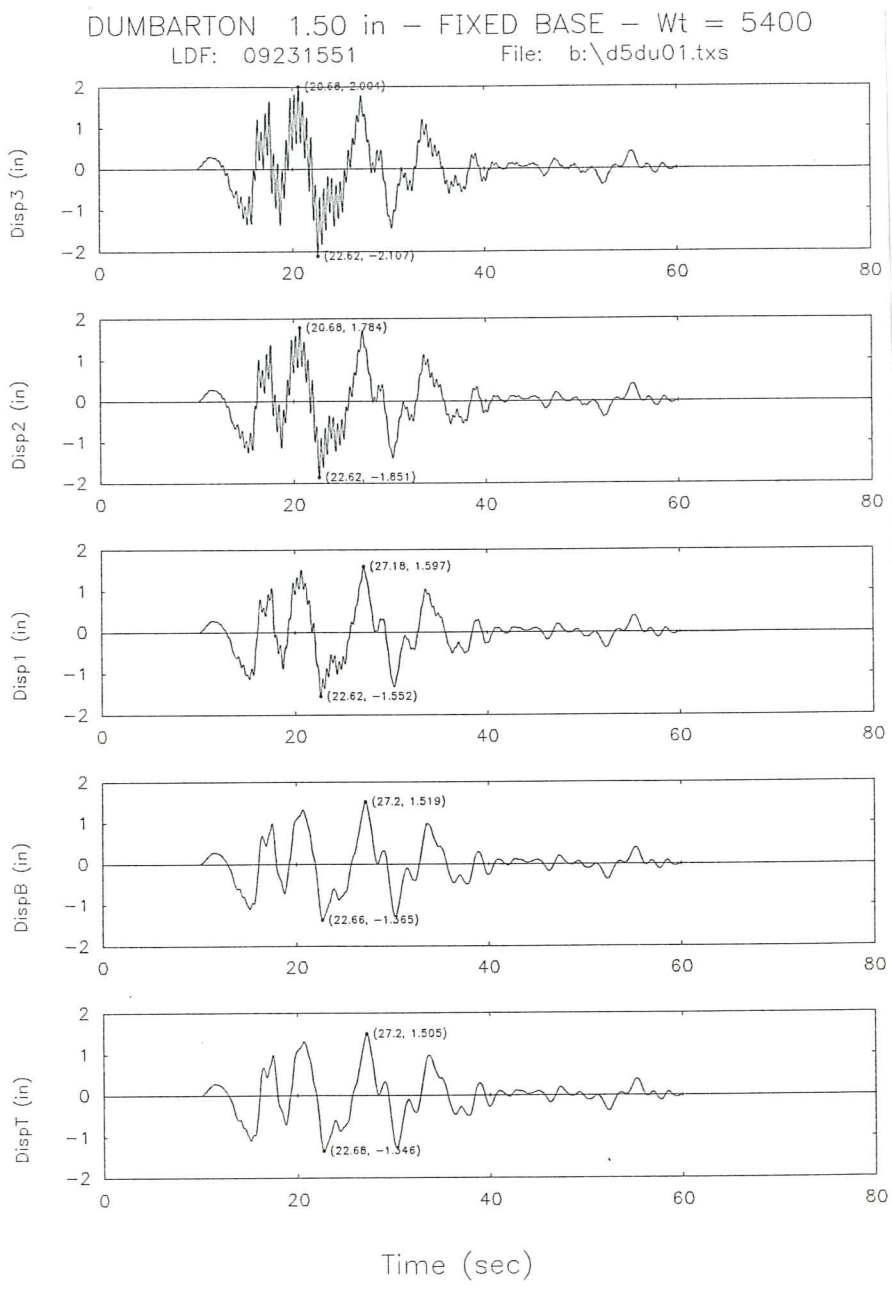

Fig. 28c. Displacement time responses for the fixed base model subjected to Dumbarton signal.

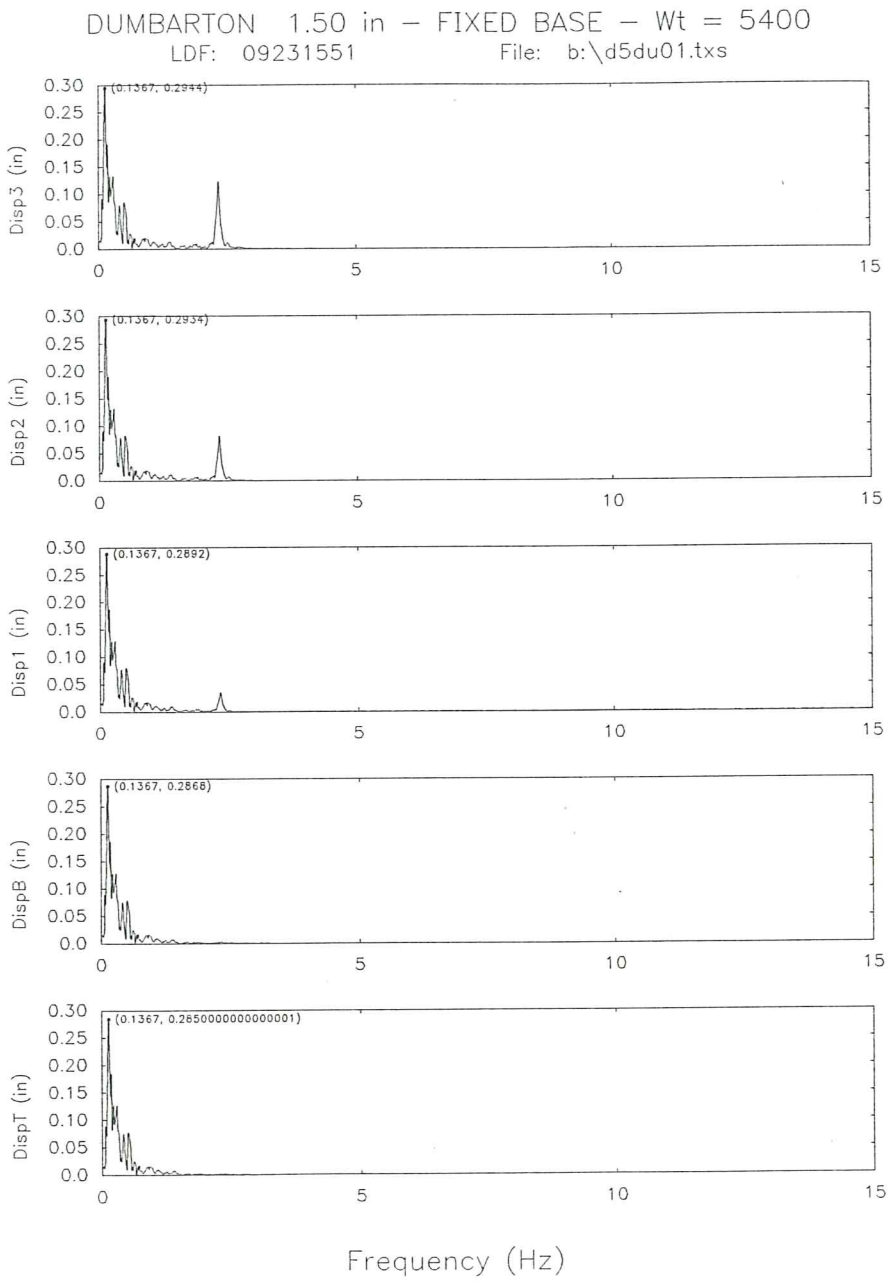

Fig. 28d. Fourier spectra of the displacements for the fixed base model subjected to Dumbarton signal.

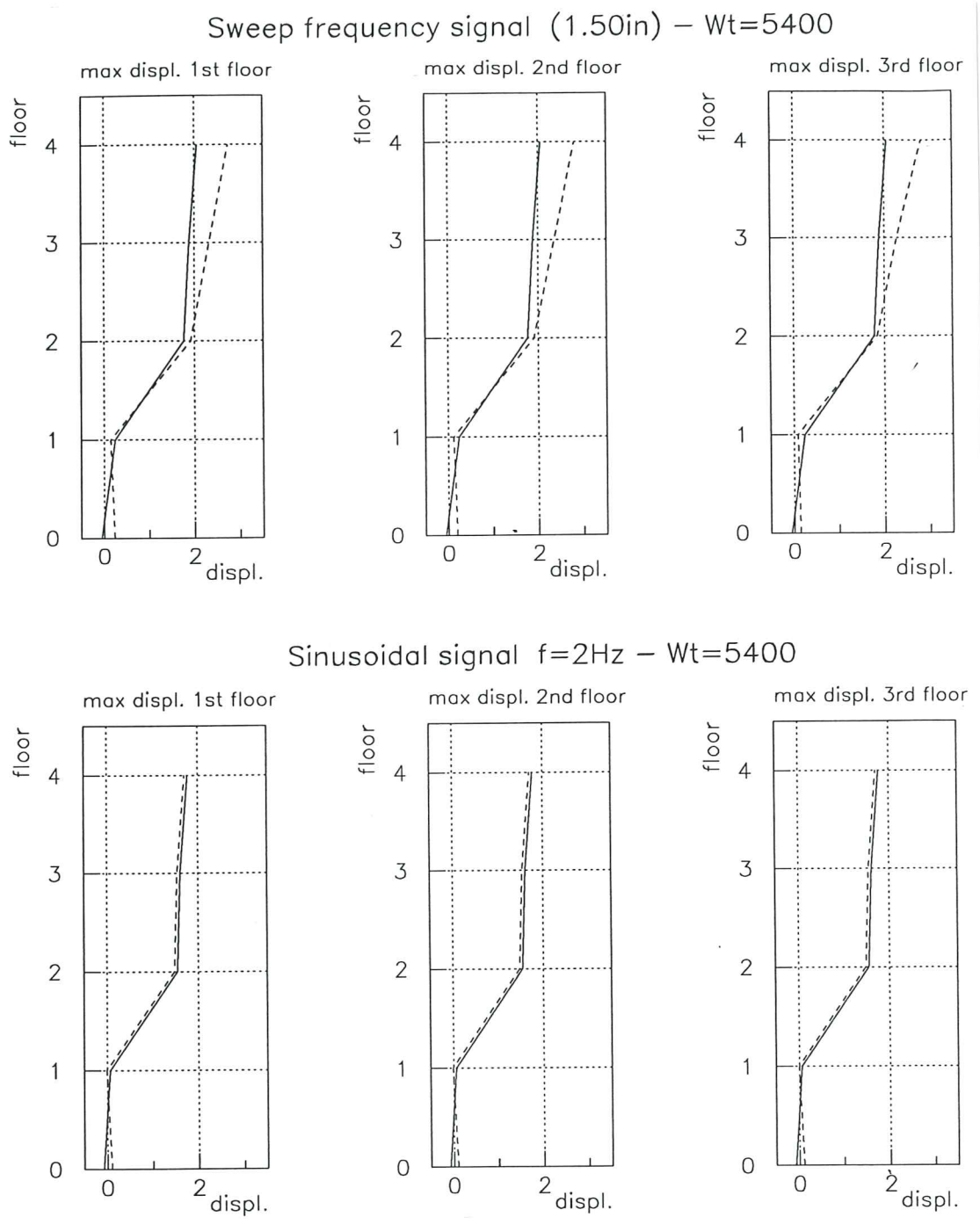

Fig. 29a. Deflected shape at maximum story displacements for a sweep frequency signal and a sinusoidal signal.

—— base isolated model.

---- fixed base model.

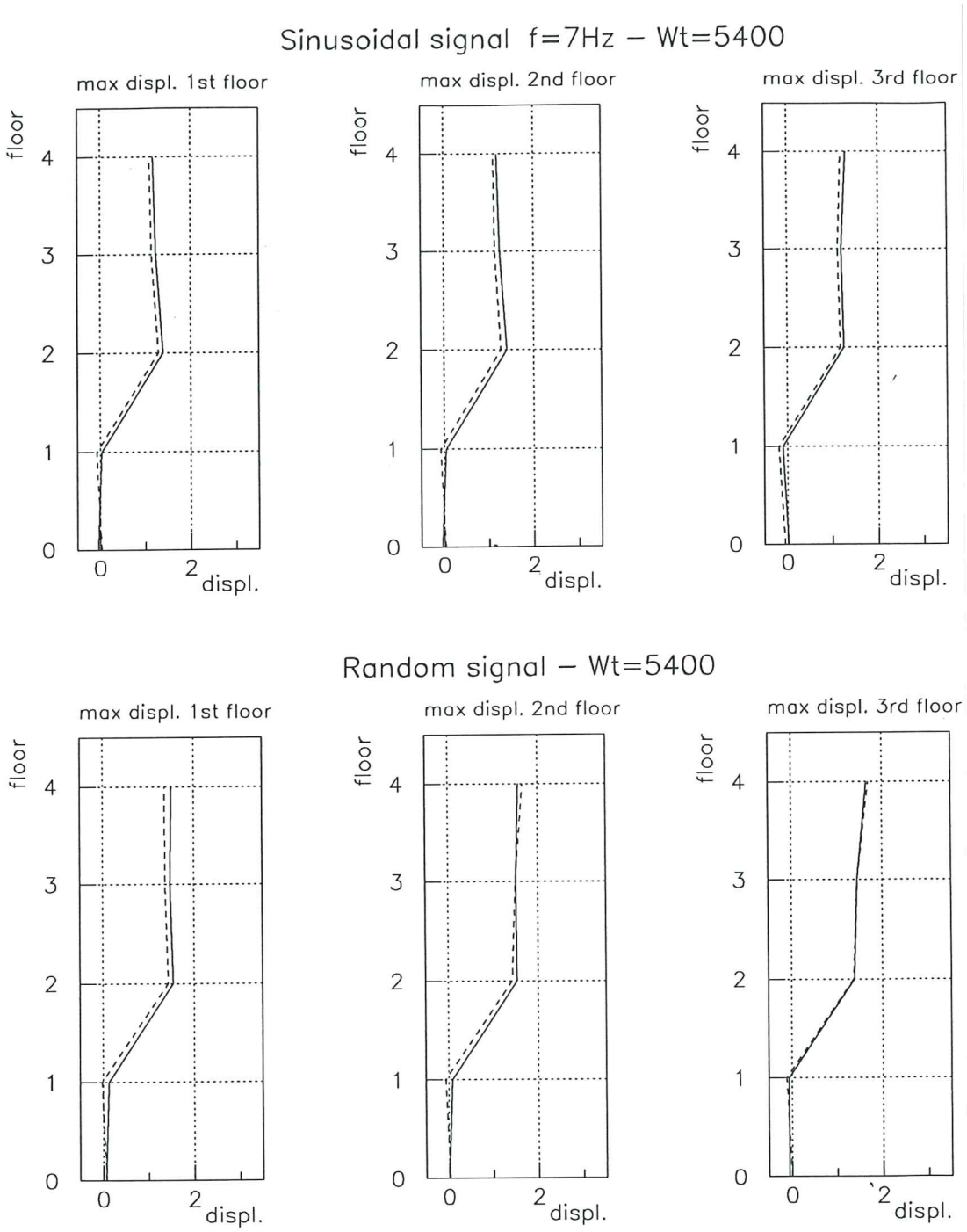

Fig. 29b. Deflected shape at maximum story displacements for a sinusoidal signal (f=7Hz) and a random signal.

—— base isolated model.

---- fixed base model.

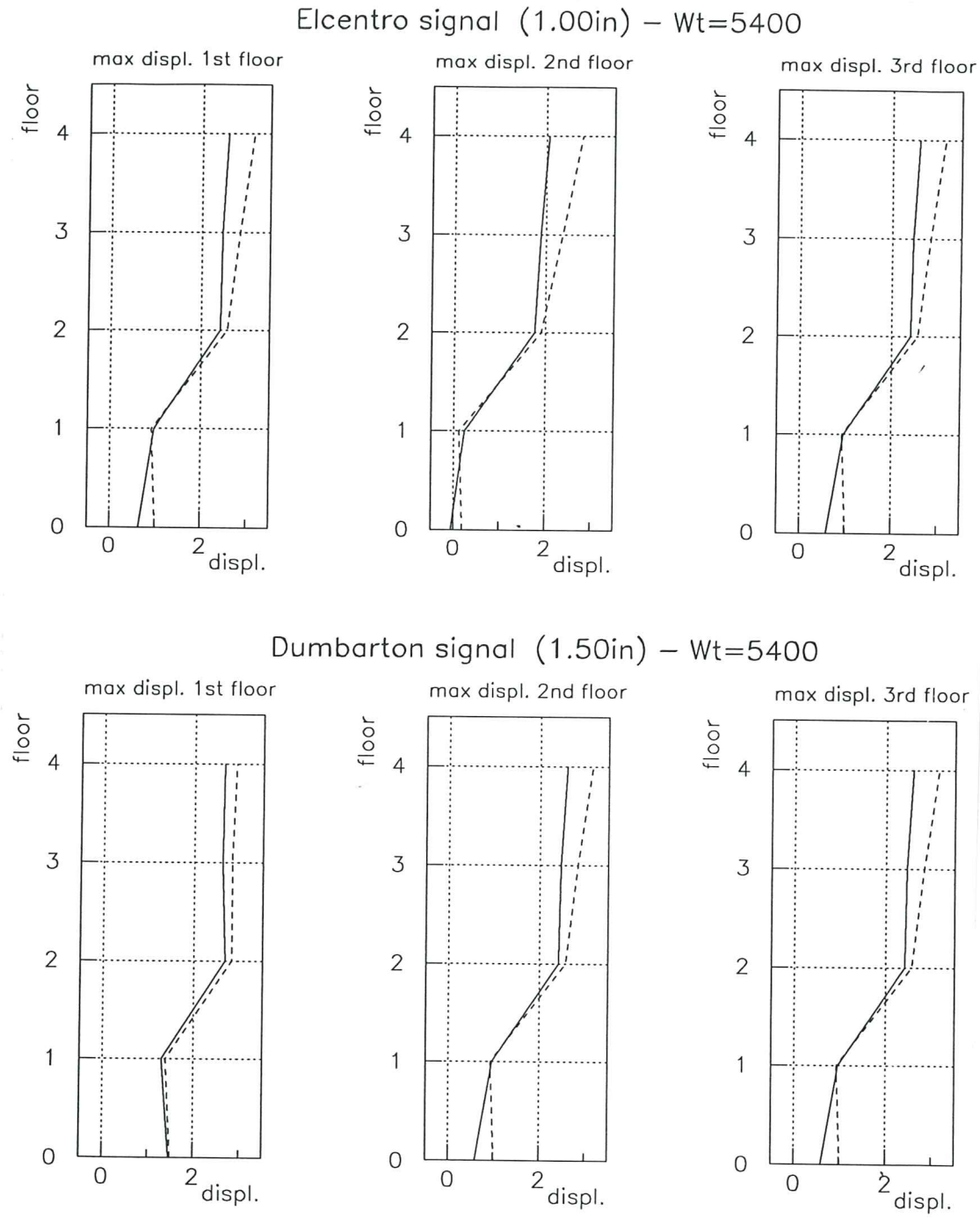

Fig. 29c. Deflected shape at maximum story displacements for El Centro signal and Dumbarton signal.

—— base isolated model.

---- fixed base model.

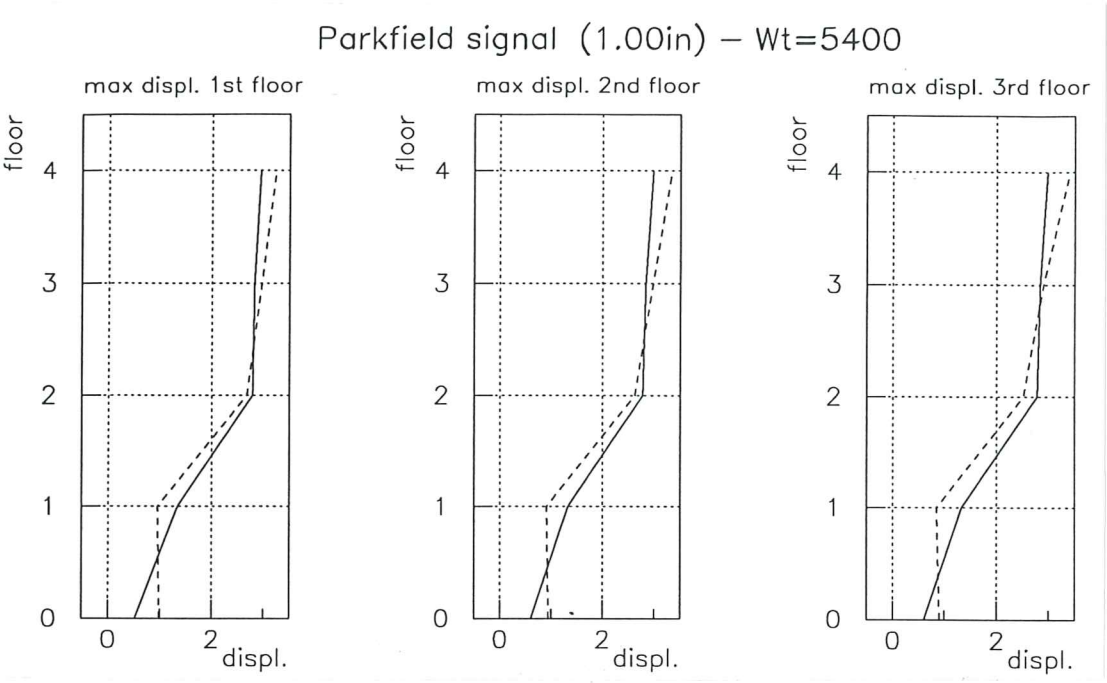

Fig. 29d. Deflected shape at maximum story displacements for Parkfield signal.
—— base isolated model.
---- fixed base model.

MAXIMUM BASE SHEAR [Kips]			
FILENAME	BASE ISOL.	FILENAME	FIXED BASE
d3sf01	1899.9	d5sf01	5418.4
d4si01	958.5	d5si01	1128.1
d4si02	1467.7	d5si02	1647.2
d4rn01	1715.4	d5rn01	3031.0
d3ec02	869.5	d5ec02	1203.5
d3du01	566.7	d5du01	1390.6
d3pk02	845.3	d5pk02	3828.5

Table T-4. Maximum base shear for the base isolated and fixed base frames.

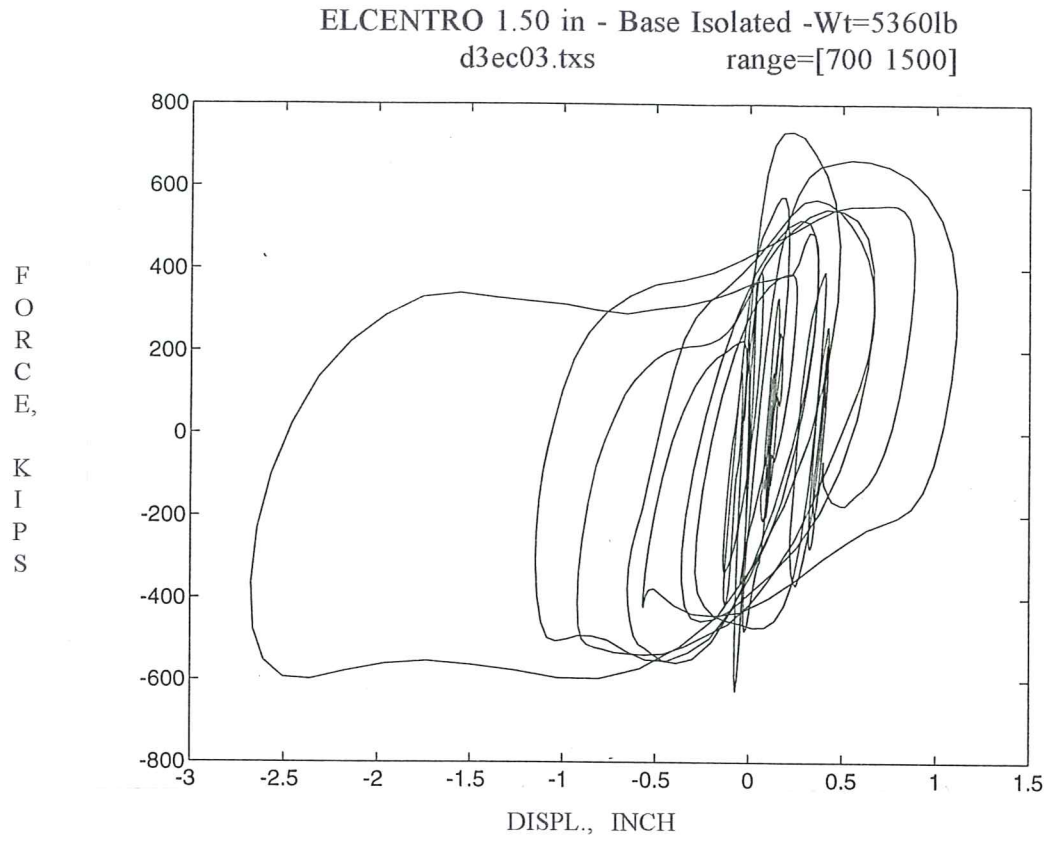

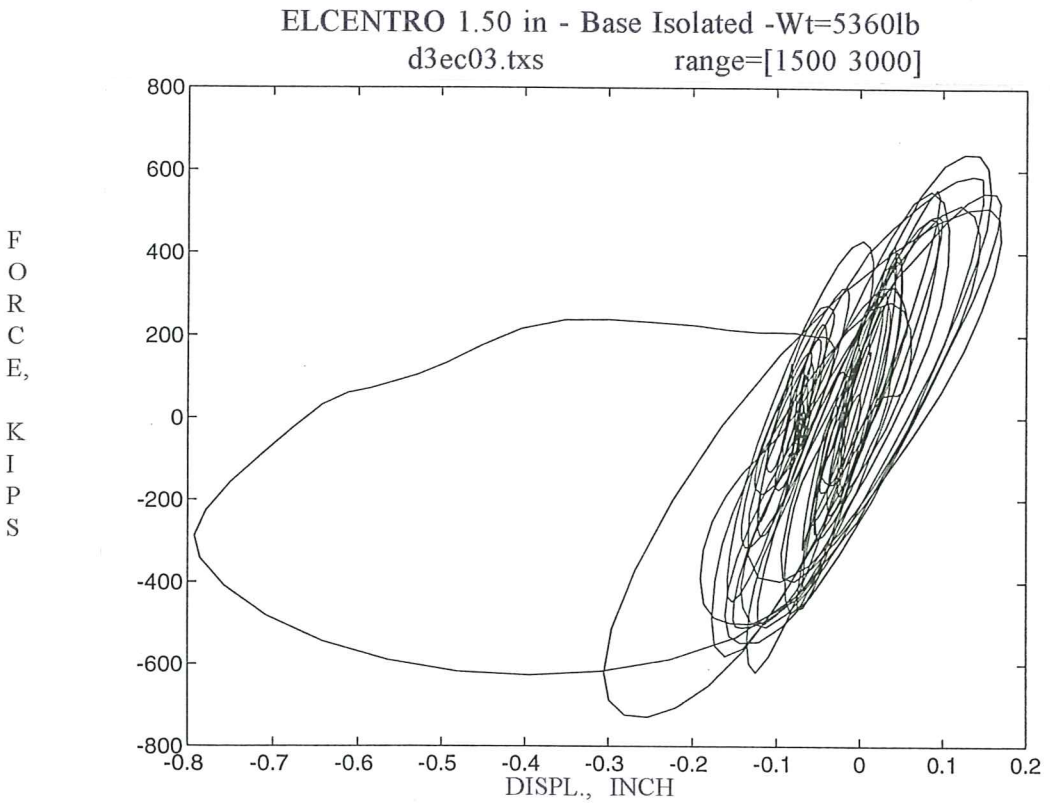

Fig. 30a. Base shear hysteresis loops for the base isolated model subjected to El Centro signal.

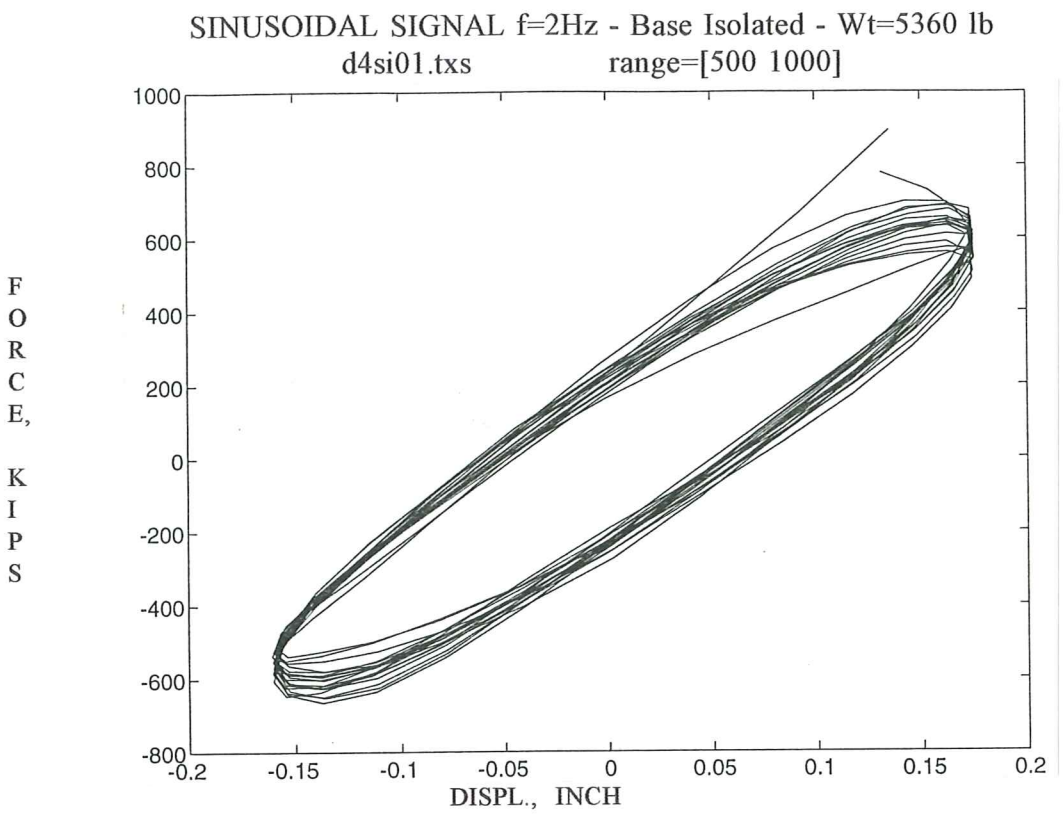

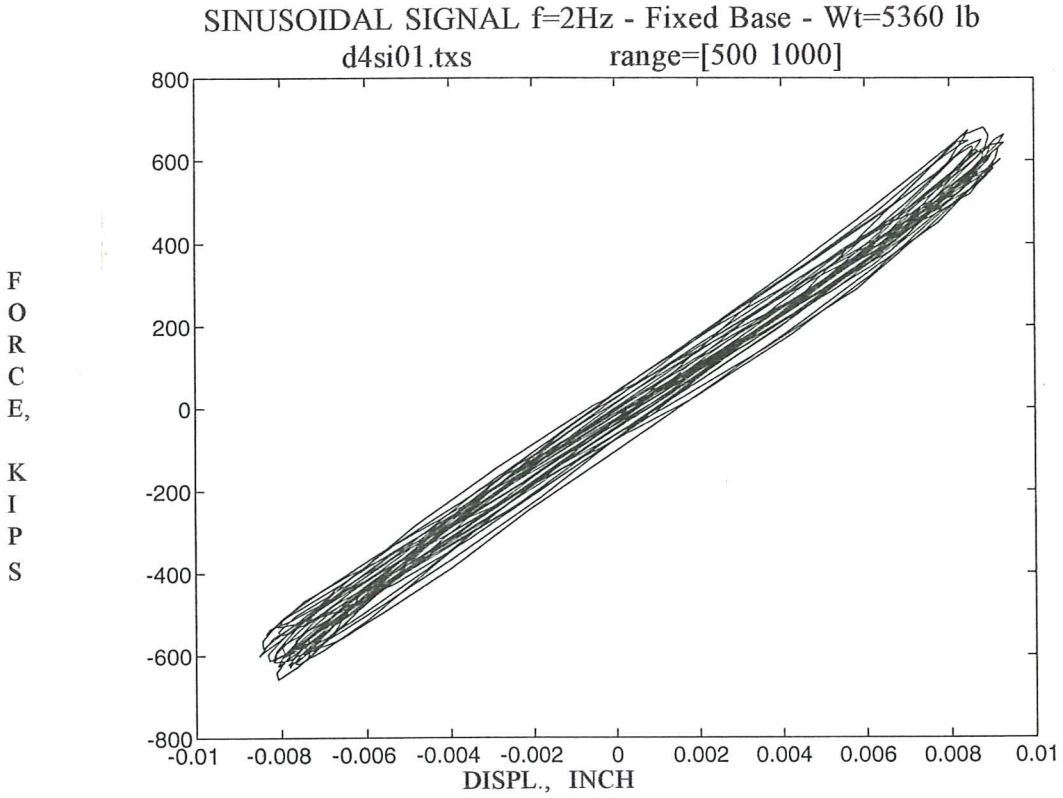

Fig. 30b. Base shear hysteresis loops for the base isolated and fixed base model subjected to a sinusoidal signal.

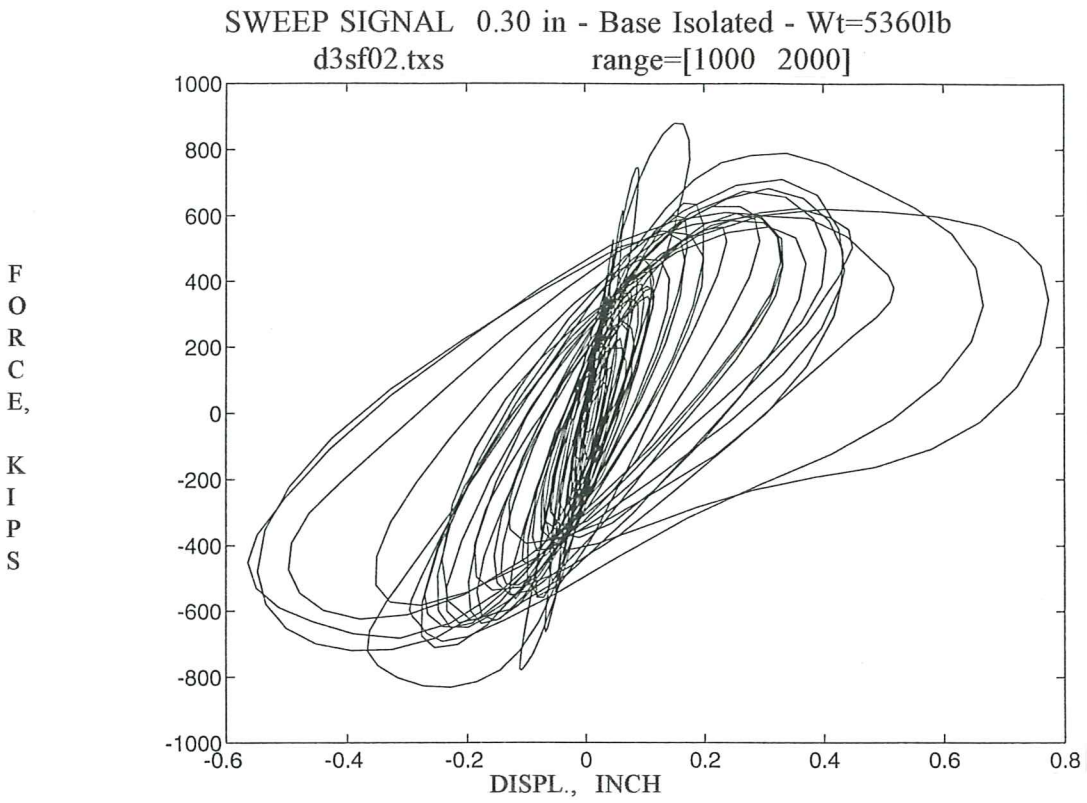

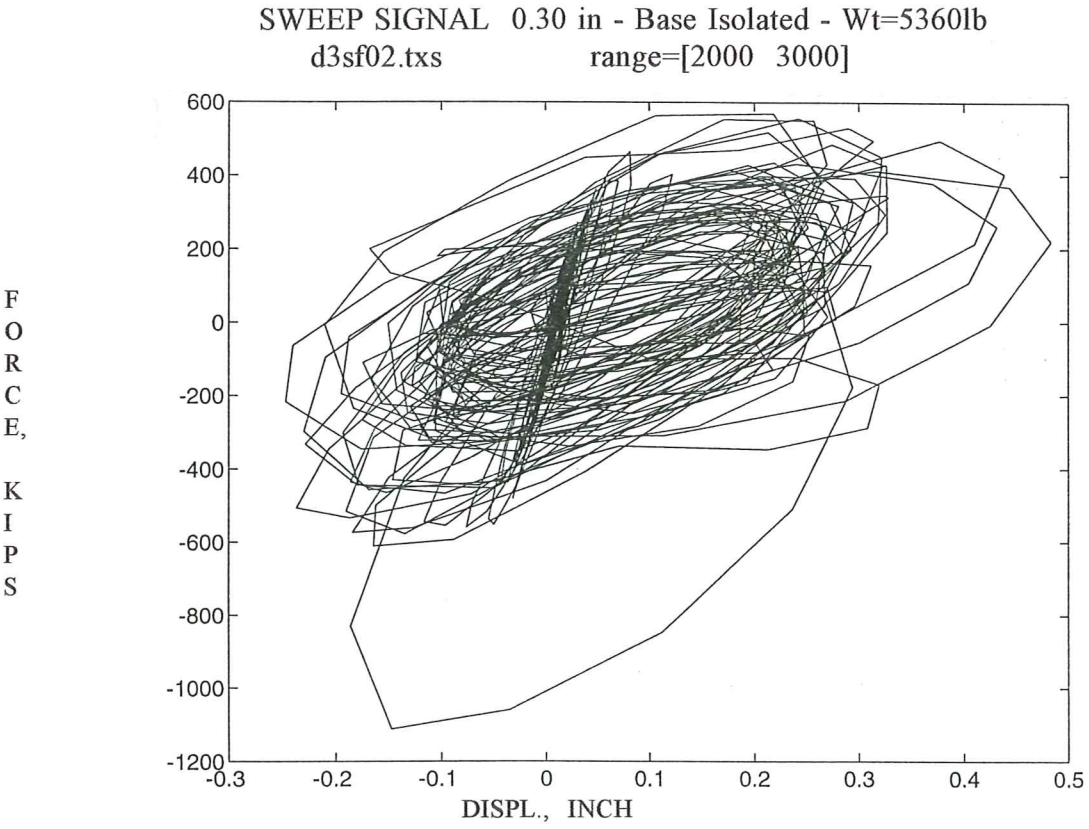

Fig. 30c. Base shear hysteresis loops for the base isolated model subjected to a sweep frequency signal.

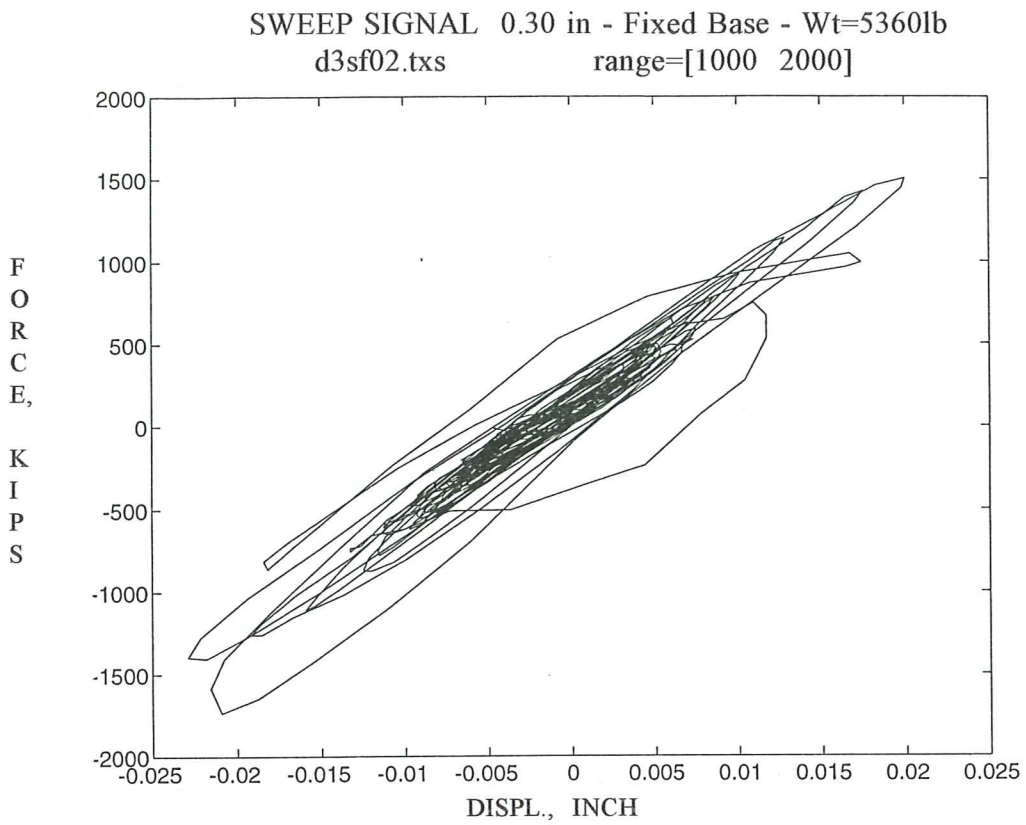

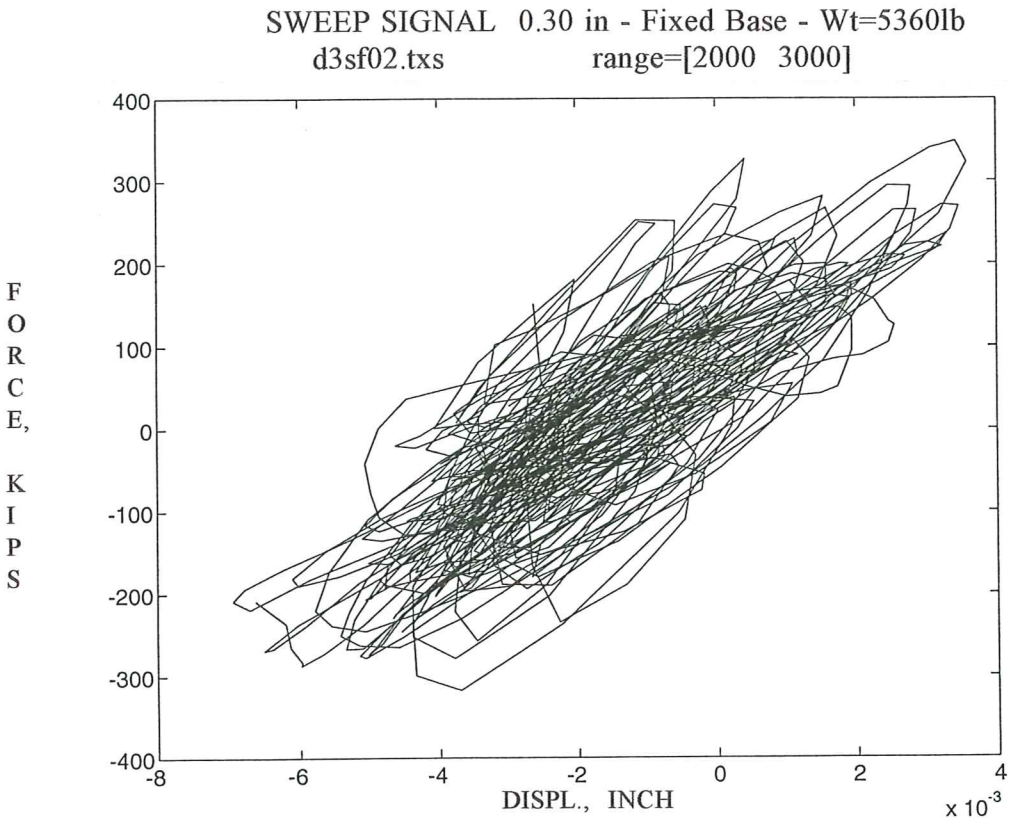

Fig. 30d. Base shear hysteresis loops for the fixed base model subjected to a sweep frequency signal.

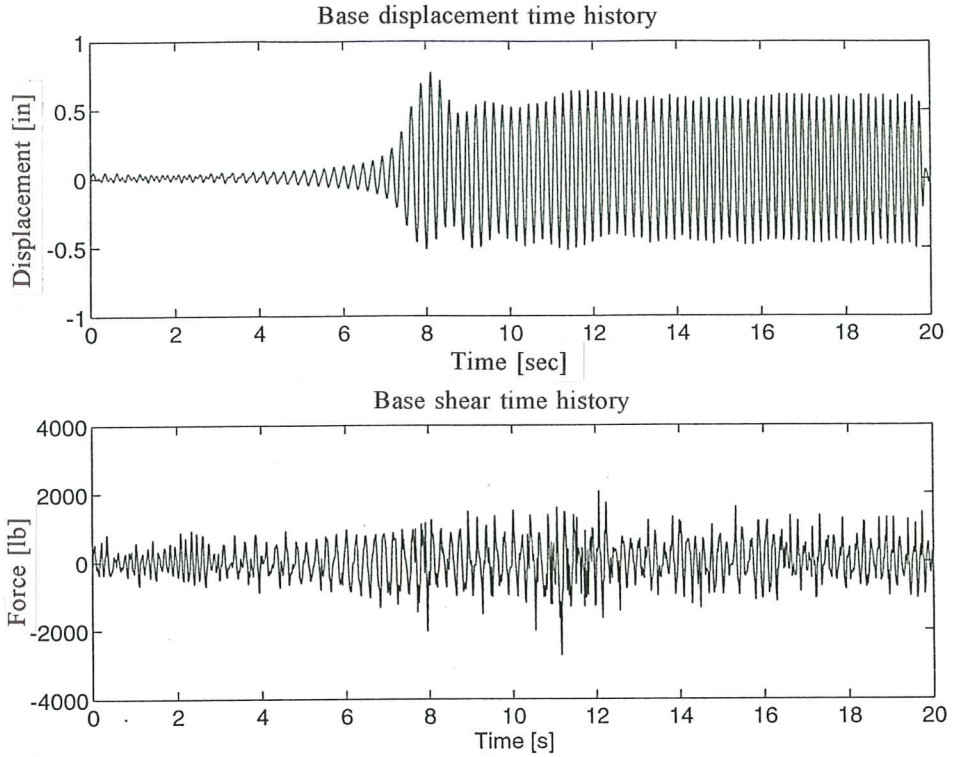

Fig. 31a. Base displacement time history and base shear time history for the base isolated model subjected to a sweep frequency signal. Range [1000 2000].

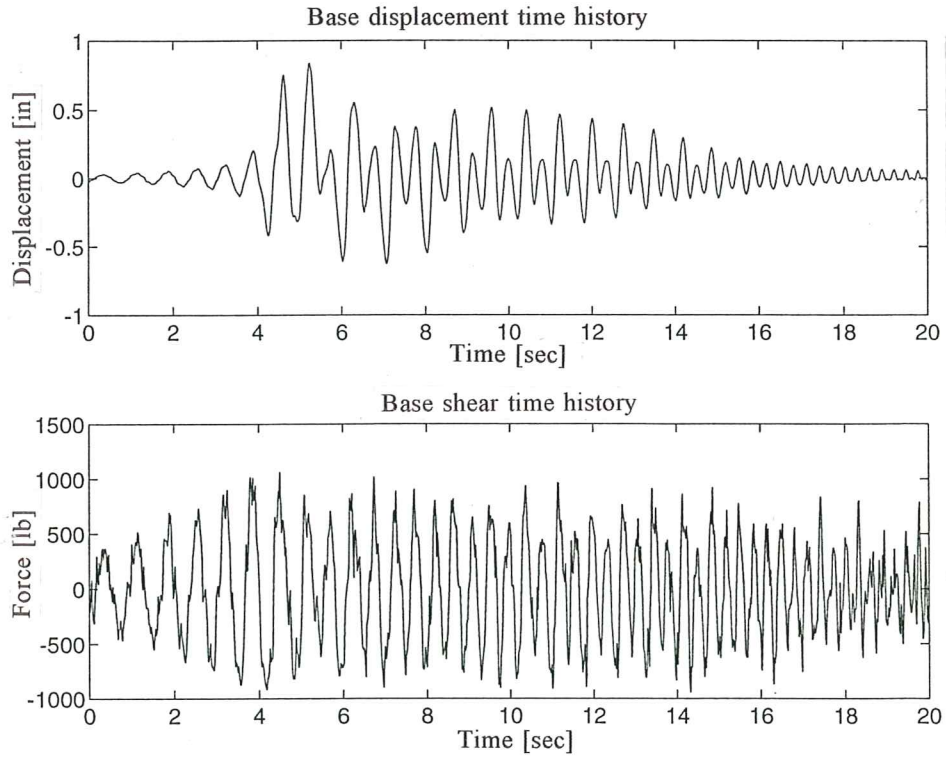

Fig. 31b. Base displacement time history and base shear time history for the base isolated model subjected to a sweep frequency signal. Range [2000 3000].

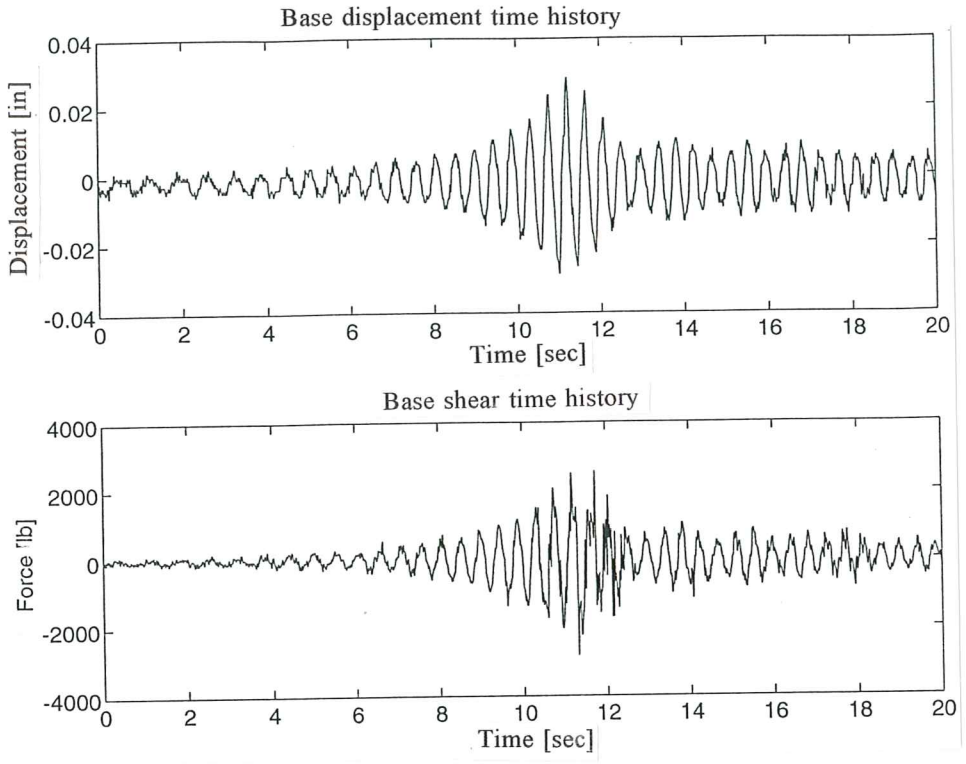

Fig. 31c. Base displacement time history and base shear time history for the fixed base model subjected to a sweep frequency signal. Range [1000 2000].

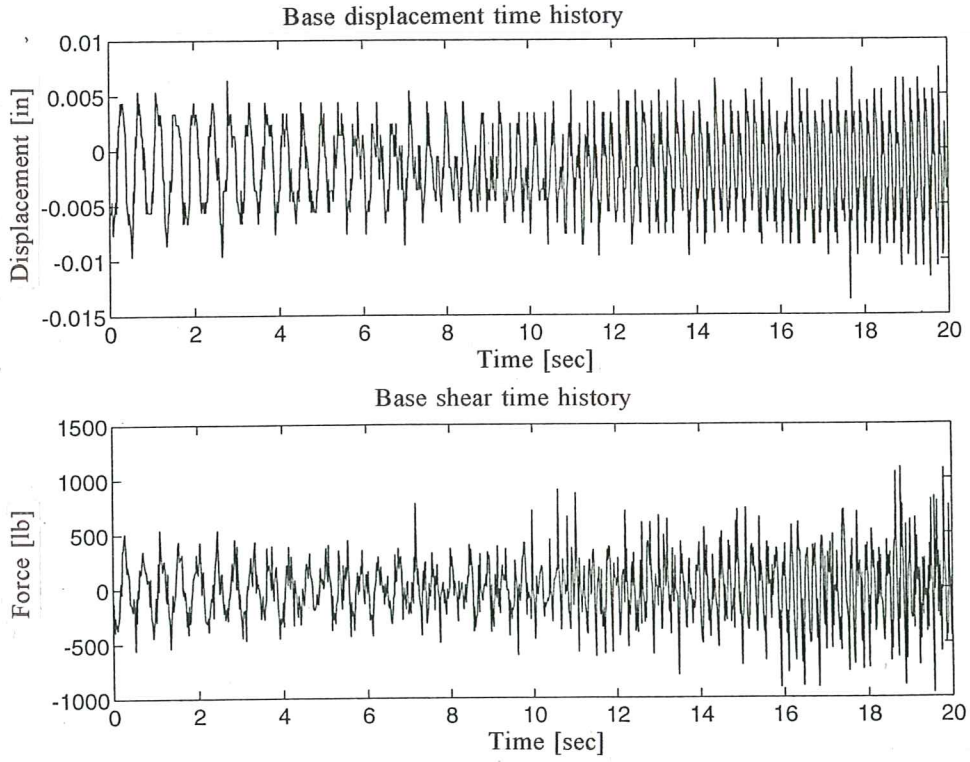

Fig. 31d. Base displacement time history and base shear time history for the fixed base model subjected to a sweep frequency signal. Range [2000 3000].

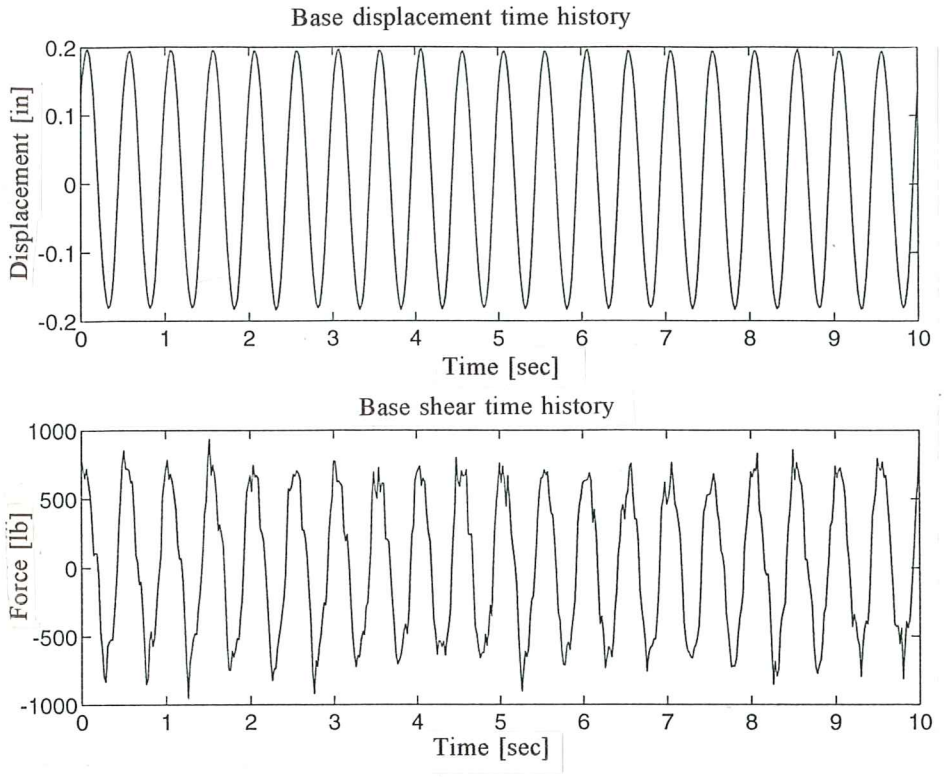

Fig. 31e. Base displacement time history and base shear time history for the base isolated model subjected to a sinusoidal signal (f=2Hz). Range [500 1000].

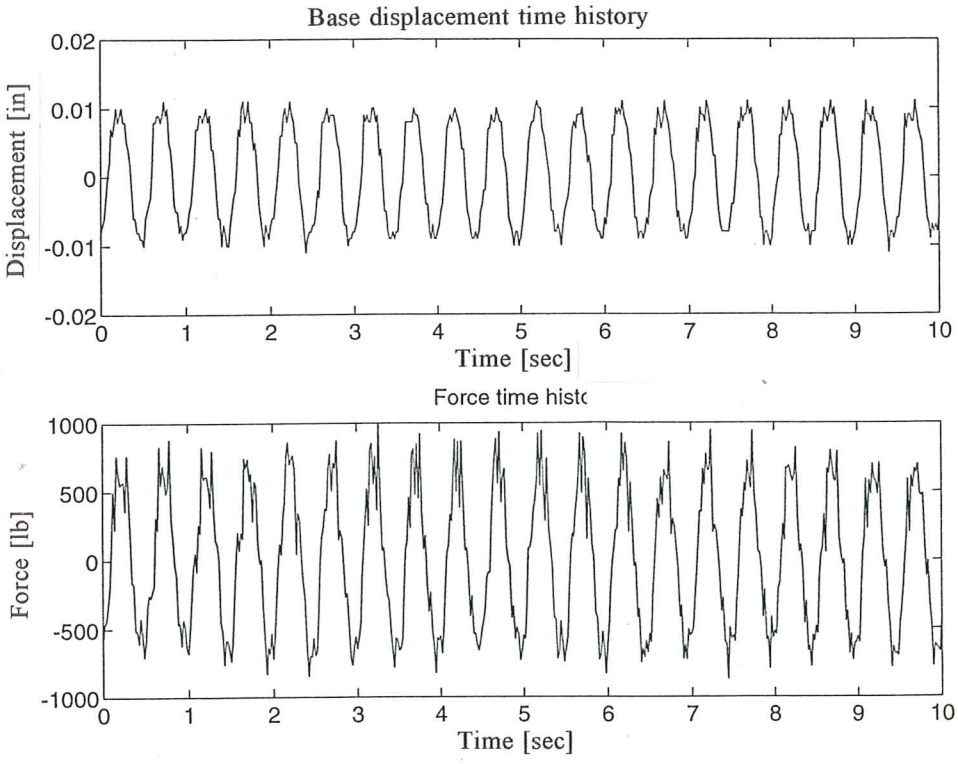

Fig. 31f. Base displacement time history and base shear time history for the fixed base model subjected to a sinusoidal signal (f=2Hz). Range [500 1000].

8.4 DISCUSSION OF RESULTS

The preliminary quasi-static tests performed by the Malaysian Rubber Producers' Association on the Rubber Layer Roller Bearings (RLRB) showed that when the velocity is constant these devices have a behaviour similar to the friction mechanism. Therefore in this case the RLRB belong to the Frictional Isolation System category. This is especially shown in Figures 10, 11, 12, b and c, where the rectangular hysteresis plots with round corners, obtained during the preliminary tests, are typical for a friction system. They illustrate the ability of the system to absorb large amounts of energy during a single displacement cycle.

Frictional isolation systems have two desirable characteristics which makes them better than conventional rubber bearing systems.

First, because the friction force developed at any bearing is proportional to the mass supported by the bearing, there is no eccentricity between the centre of mass of the superstructure and the centre of stiffness of the isolation system. This means that even if the mass distribution in the structure is different from the one assumed in the original design, the effects of torsion at the foundation level are diminished.

The second advantage of frictional systems is their performance over a wide range of input frequencies. Although a structure supported on rubber isolators will have a fundamental frequency much lower than if it were fixed-base, a low frequency ground motion may still drive such a system into reasonance. This makes rubber isolators inappropriate for regions where the major part of the earthquake energy is concentrated in the low frequency range. However, frictional isolators have no characteristic frequency and can effectively dissipate energy over a wide range of input frequencies with no risk of reasonance with the ground motion. This makes frictional systems practical for use in soft soil regions.

The response of frictional isolation systems to low frequency ground motions could be assumed to be linear as a first approximation, probably because there is time for the sliding deformations of the bearings to stop during low frequency acceleration pulse before the next pulse hits. Response to higher frequency ground motions is highly non-linear because the bearings do not stop sliding before the next acceleration pulse hits, and the displacement at the end of each pulse is not predictable.

The non-linearity of the friction system causes a wide range of frequencies and partecipating modes, as shown in the frequency responses of the complete systems to the signal utilised in the series of tests (see Figures 14÷28). In this case the transition between the rigid and the sliding phases leads to an approximate bilinear force-displacement relationship for the friction systems.

Moreover, due to the high value of the normal stress of contact roller-rubber, these isolators fit better in the case of not too high vertical loads.

As a conclusion it is also remarkable to note that the larger intensity earthquake excites the frictional isolators more than the lower intensity signal. This demonstrates that the performance of the RLRB devices improves as the severity of the ground motion increases, realising a powerful seismic isolation system.

REFERENCES

[1] M. James, "Vibration of Mechanical and Structural Systems", New York: Harper and Row Publisher, 1989, p.180.

[2] Clark, P.W. and Kelly, J. M., "Experimental Testing of the Resilient-Friction Base Isolation System"; *Report N. UCB/EERC-90/10, Earthquake Engineering Research Center*, University of California at Berkeley, July 1990.

APPENDIX

Photographs of the shaking table and the whole experimental set-up are showm in this appendix.

Photo n. 1 shows a detail of the isolation system realized with steel balls and two rubber pads, as described in Chapter 2.

Photos 2 and 3 show the model building from the longitudinal and the transversal sides respectively. In Photo 2 it is possible to notice the two restoring springs attached to the shaking table and to the base of the model. In Photo 3 it is also shown the actuator connected to the shaking table.

Photo 4 shows a more complete view of the four lower pads of the isolation system already attached to the shaking table.

In Photo 5 it is possible to notice the presence of a steel frame (the grey device) between the base and the shaking table to mantain the zero position of the model at the end of a test

Photo 6 shows the accelerometers and displacement transducers at each level of the structure and connected to a a fixed reference frame.

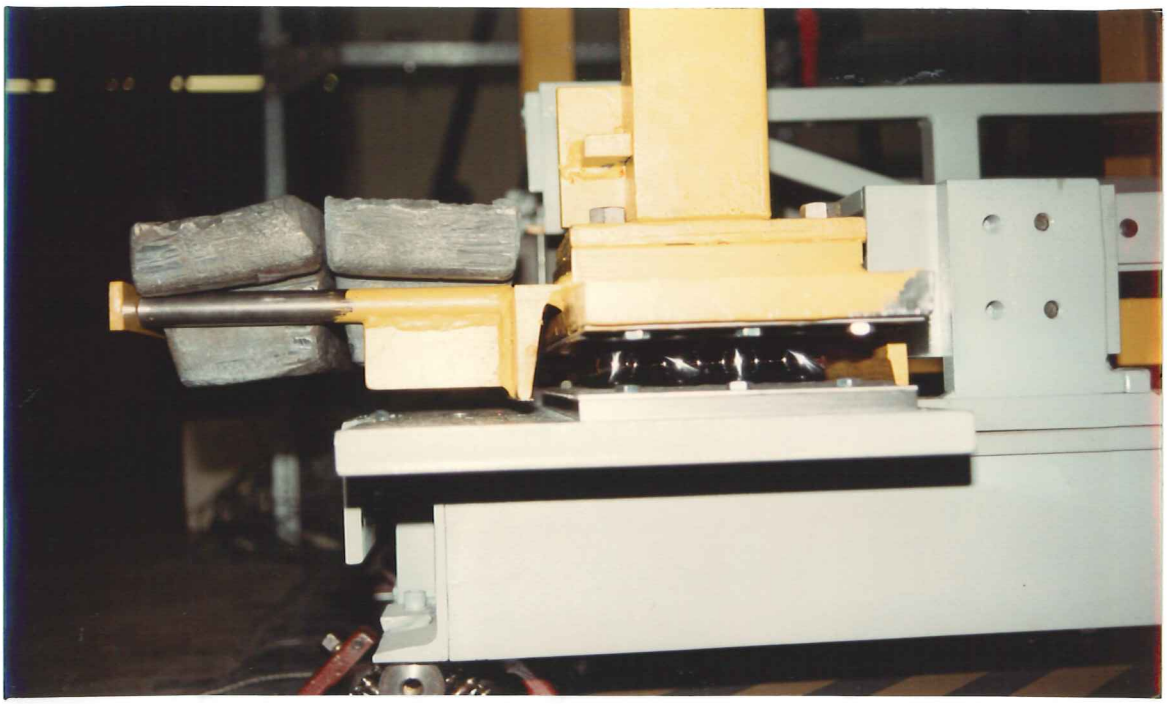

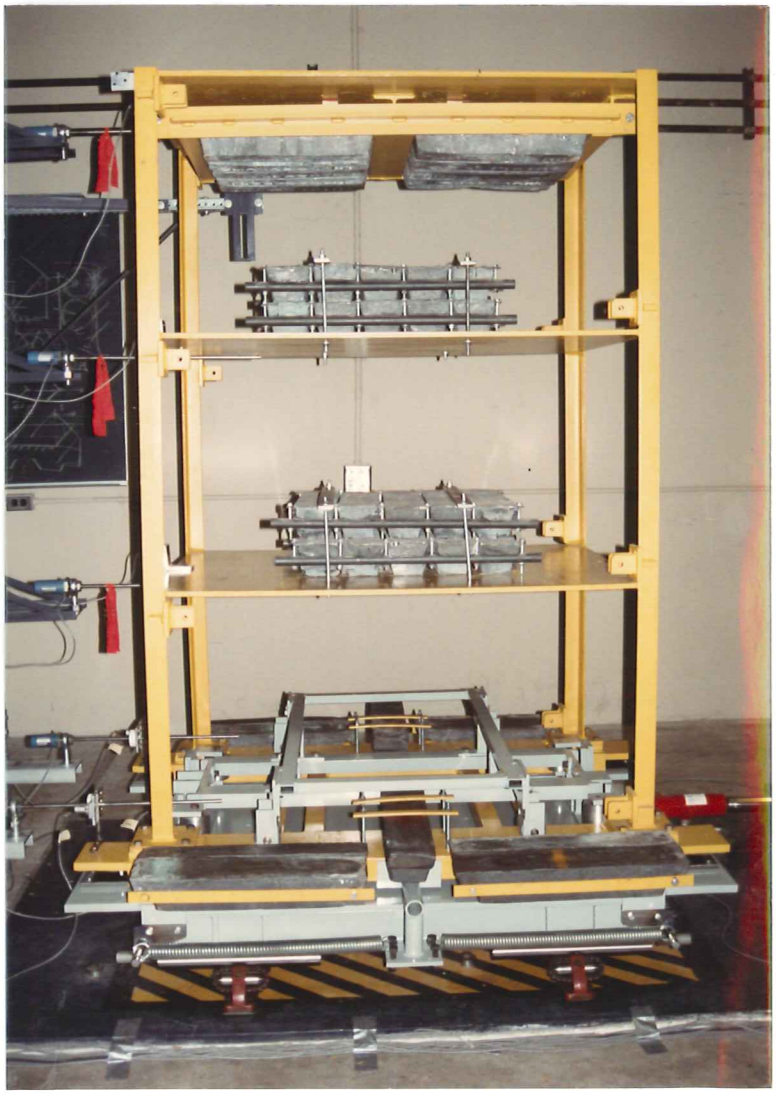

Photo 1. Detail of the isolation device.

Photo 2. Longitudinal section of the model.

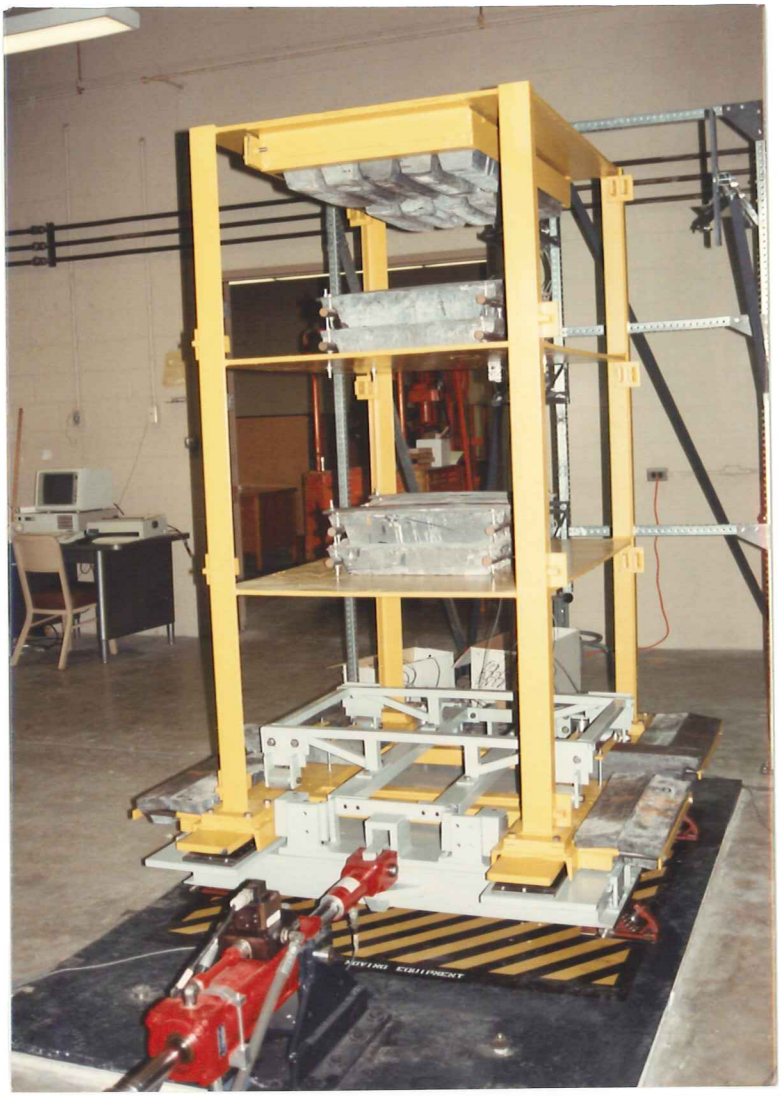

Photo 3. Transversal section of the model.

Photo 4. Steel rollers on the rubber pads.

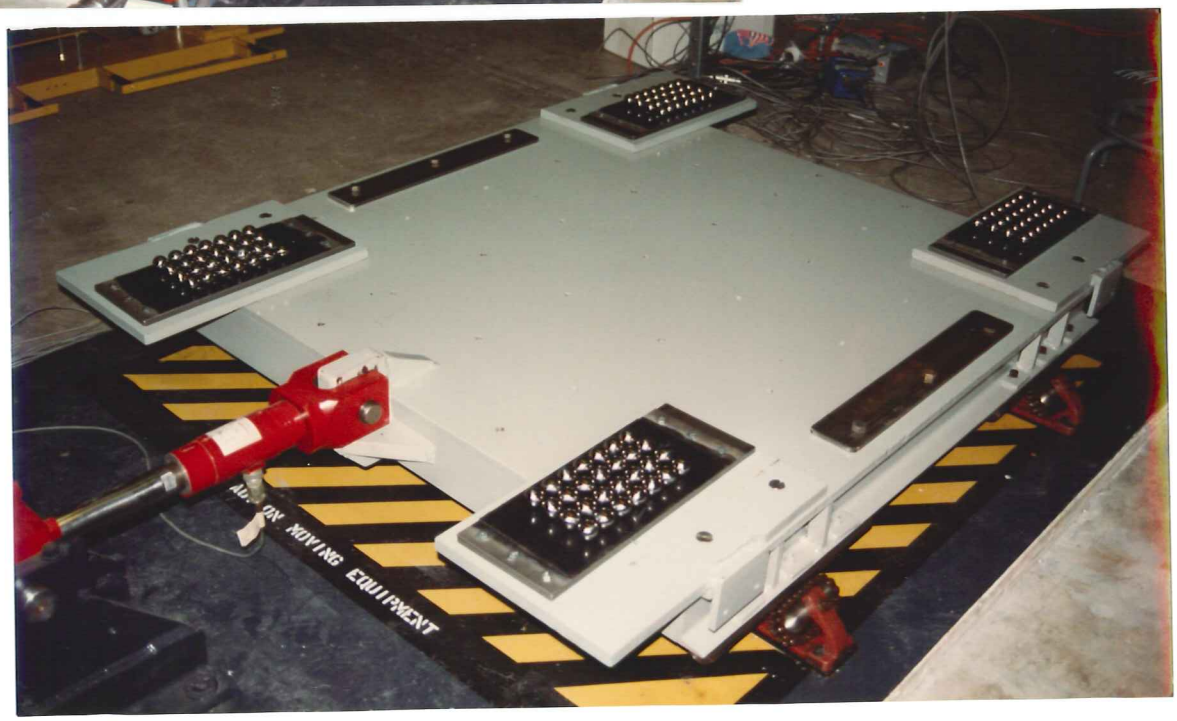

Photo 5. The isolated base of the model frame.

Photo 6. Accelerometers and displacement transducers.

CENTRO INTERNACIONAL DE METODOS NUMERICOS EN INGENIERIA

Lista de monografías publicadas en la Serie de Ingeniería Sísmica

Las monografías pueden adquirirse dirigiéndose al Departamento de Publicaciones del Centro Internacional de Métodos Numericos en Ingeniería, Edificio C1, Campus Norte UPC, c/ Gran Capitán s/n, 08034 Barcelona, telefóno: 93-401.60.37, Fax: 93-401-65-17.

IS-1 *Qualitative Reasoning for Earthquake Resistant Buildings,* Luís M. Bozzo, 149 pp., ISBN 84-87867-36-7, 1993.

IS-2 *Control predictivo en sistemas de protección sísmica de estructuras,* R. Andrade Cascante, J. Rodellar, F. López Almasa, 143 pp., ISBN 84-87867-37-5, 1993.

IS-3 *Simulación numérica del comportamiento no lineal de presas de hormigón ante acciones sísmicas,* M. Galindo, J. Oliver, M. Cervera, 255 pp., ISBN 84-87867-38-3, 1994.

IS-4 *Simulación del daño sísmico en edificios de hormigón armado,* A. Hanganu, A.H. Barbat, S. Oller, E. Oñate, 96 pp., ISBN 84-87867-40-5, 1994.

IS-5 *Edificios con aislamiento de base no lineal,* N. Molinares, A.H. Barbat, 96 pp., ISBN 84-87867-41-3, 1994.

IS-6 *Vulnerabilidad sísmica de edificios,* C. Caicedo, A.H. Barbat, J.A. Canas, R. Aguiar 100 pp., ISBN 84-87867-43-X, 1994.

IS-7 *Análisis de terremotos históricos por sus efectos,* J. R. Arango Gonzalez, 119 pp., ISBN 84-87867-44-8, 1994.

IS-8 *Control activo no lineal de edificios con aislamiento de base,* A.H. Barbat, N. Molinares, J. Rodellar, 124 pp., ISBN 84-87867-46-4, 1994.

IS-9 *Análise estocástica da resposta sísmica nao-linear de estructuras,* Alvaro A.M. F. Cunha, 199 pp., ISBN: 84-87867-47-2, 1994

IS-10 *Definición de la acción sísmica,* A.H. Barbat, L. Orosco, J.E. Hurtado, M. Galindo, 122 pp., ISBN: 84-87867-448-0, 1994

IS-11 *Sismología y peligrosidad sísmica,* J.A. Canas Torres, C. Pujades Beneit, E. Banda Tarradellas, 87 pp., ISBN: 84-87867-49-9, 1994

IS-12 *Riesgo, peligrosidad y vulnerabilidad sísmica de edificios de mampostería,* F. Yépez, A.H. Barbat, J.A. Canas, 104 pp., ISBN: 84-87867-50-2, 1995

IS-13 *Estudios de ingeniería sismológica y sísmica,* J.A. Canas, ISBN: 84-87867-57-X, 13 pp., 1995

IS-14 *Simulación de escenarios de daño para estudios de riesgo sísmico,* F. Yépez, A.H. Barbat y J.A. Canas, ISBN: 84-87867-58-8, 103 pp., 1995

IS-15 *Diseño sismorresistente de edificios de hormigón armado*, L. Bozzo, A.H. Barbat, ISBN: 84-87867-59-6, 185 pp., 1995

IS-16 *Modelo tridimensional de atenuación anelástica de las ondas sísmicas en la Península Ibérica*, J.O. Caselles, J. A. Canas, Ll. G. Pujades, R.B. Herrmann, ISBN: 84-87867-60-X, 119 pp., 1995

IS-17 *Índices de daño sísmico en edificios de hormigón armado*, R. Aguiar ISBN: 84-87867-43-X, 99 pp., 1996

Los autores interesados en publicar monografías en esta serie deben contactar con el editor para concretar las normas de preparación del texto.